THE PHYSICAL AND CHEMICAL CHARACTERIZATION OF SOLUBLE BORATE GLASS NETWORKS INTENDED FOR TRANSIENT EMBOLIZATION OF THE GENICULATE ARTERY

by

Remington Manchester

Submitted in partial fulfillment of the requirements
for the degree of Master of Applied Science

at

Dalhousie University
Halifax, Nova Scotia
Month 2021

Table of Contents

List of Tables

List of Figures

Abstract

Geniculate artery embolization (GAE) is for individuals suffering from osteoarthritis. In particular, GAE is indicated for patients that are resistant to conservative therapies but are not yet indicated for a total knee arthroplasty. Due to the infancy of the procedure, there exist no microspheres tailored to the clinical requirements of GAE. Pre-market research has established that the ideal microspheres for GAE should be both degradable and imageable. To address these considerations, 16 borate glasses modified with K_2O and SrO were investigated as candidates for use in GAE. Glasses were characterized to determine composition-structure-property relationships in addition to dissolution behaviour, imageability, and response to sterilization. The glasses exhibit tailorable dissolution rates and in certain embodiments are imageable on CT without confounding MRI. A preferred composition was selected and processed into microspheres, then recharacterized. This preferred composition has been deemed suitable for further development as a potential product for GAE.

List of Abbreviations and Symbols Used

%	Percent
$\Delta\chi$	Delta Chi
ΔT	Melt/Glass Stability
°	Degree
°C	Degree Celsius
^{11}B MAS NMR	^{11}Boron Magic-Angle Spinning Nuclear Magnetic Resonance
B	Boron
B_2O_3	Boron Oxide
B3	Three-fold Coordinate Boron
B4	Four-fold Coordinate Boron
BCS	Bovine Calf Serum
cAMP	Cyclic Adenosine Monophosphate
CCL2	Chemokines Chemokine (C-C motif) ligand 2
CIRSE	Cardiovascular and Interventional Radiological Society of Europe
COX	Cyclooxygenase
CT	Computed Tomography
DAMPs	Damage-associated molecular patterns
DMEM	Dulbecco's Modified Eagle's Medium
DoM	Design of Mixtures
DSC	Differential Scanning Calorimetry
ECIO	European Conference on Interventional Oncology
ECM	Extracellular Matrix
EMEA	European Medicines Evaluation Agency
FDA	Food and Drug Administration
FGF-1	Fibroblast Growth Factor 1
g	gram
GAE	Geniculate Artery Embolization
GEST	Global Embolization Oncology Symposium Technologies
HIF-1α	hypoxia-inducible factor-1α
HU	Hounsfield Units
IPM/CS	Imipenem/cilastatin sodium
IR	Interventional Radiologist
K_2O	Potassium Oxide
kGy	Kilogray
KOA	Knee Osteoarthritis
kVp	Peak kilo Voltage
MAE	Mixed Alkali Effect
MAEE	Mixed Alkaline Earth Effect
MAS	Magic Angle Spinning
MD	Molecular Dynamic
min	minute
mL	Milliliter
MMP	Matrix Metalloproteinases
mol	Mole
mol%	Mole Percent

MOS	Margin of Safety
MRI	Magnetic Resonance Imaging
mRNA	Messenger Ribonucleic acid
$NaBH_4$	Sodium Borohydride
NBO	Non-Bridging Oxygen
NF-κB	Nuclear Factor Kappa Light Chain Enhancer of Activated B Cells
NGF	Nerve Growth Factor
NMR	Nuclear Magnetic Resonance
NSAIDs	Nonsteroidal Anti-Inflammatory Drugs
O	Oxygen
OA	Osteoarthritis
OARSI	Osteoarthritis Research Society International
PGD_2	Prostaglandin D_2
PGE2	Prostaglandin E2
PSD	Particle Size Distribution
QoL	Quality of Life
RA	Rheumatoid Arthritis
rpm	Revolutions per Minute
s	second
SD	Standard Deviation
SEM	Scanning Electron Microscopy
SrO	Strontium Oxide
TAE	Transarterial Embolization
T_e	Extrapolated End Temperature
T_f	Extrapolated Onset Temperature
T_g	Glass Transition Temperature
TKA	Total Knee Arthroplasty
T_m	Midpoint Temperature
T_{p1}	Crystallization Onset Temperature
TRA	Toxicological Risk Assessment
VAS	Visual Analog Scale
VEGF	Vascular Endothelial Growth Factor
WHO	World Health Organization
WOMAC	Western Ontario and McMaster Universities Osteoarthritis Index
XRD	X-Ray Diffraction
λ	Wavelength
μm	Micron
ρ	Density

Acknowledgments

To begin, I would like to thank Dr. Daniel Boyd for his tireless and continued support throughout this degree. You have made this entire journey enjoyable even in times of uncertainty and even if I could go back in time, I would choose to do this degree the exact same way. Thank you for always taking the time to answer my tireless emails and questions, and always making yourself available even when you yourself were busier than humanly possible. With your help, I have become a stronger scientist, scholar, and most importantly writer. Thank you for pushing me to think outside of the box and encouraging me to take on challenges that I did not even think I would be able to accomplish.

In addition to Dr. Daniel Boyd, I would also like to thank my committee members Dr. Robert Abraham, Dr. Mark Filiaggi, and Dr. Brendan Leung. I know this was not the most conventional year and there were many unforeseen challenges but your continued guidance, expertise, and encouraging words made this an enjoyable process and enabled me to get to where I am today. Thank you for always challenging me with your questions and comments and encouraging me to consider all angles in my research. Your support and guidance have enabled me to conduct my work with confidence.

I would also like to thank Dr. Kimberly Brewer, Dr. Elena Tonkopi, and Dr. Ulrike Werner-Zwanziger for providing their time and aid because without you this thesis work would not be completed at this present time. Thank you for also providing me with your insight, expertise, and guidance so that I could successfully complete this work. Thank you for always being available to answer my questions and going above and beyond to help me through this degree. I would also like to thank ABK and IR Scientific for sharing their resources and time by providing access to their lab equipment so that these experiments could be successfully carried out.

I would especially like to thank Dr. Alicia Oickle and Dr. Tsanka Todorova. Thank you for your constant support, company, and insights throughout this journey and for always being there to answer any of my questions and challenge my assumptions. You have helped me become a better scientist. I would also like to thank Joel, Meghan, and Lindsey for allowing me to bounce my ideas off you and always being there for me in academia and life.

I am also grateful for and would like to thank my family. Even though you are on the other side of Canada, you always make the time to answer my calls (good and bad) and help me put things into perspective when I lose sight of the bigger picture. Your encouragement has made this degree possible, and I cannot put into words how much your unwavering support and love mean to me.

Lastly, I would like to thank the financial assistance of NSERC Discovery Program and Innovacorp ESCF for supporting this work.

Halifax, June 2021
Remington Manchester

CHAPTER 1

1.0 Introduction

The primary objective of this work was focussed on characterizing and understanding fundamental composition-structure-property relationships in alkali and alkaline earth containing borate glass networks. In addition to modelling and understanding specific physical and chemical characteristics, particular focus has been paid to understanding the dissolution behaviour, multimodal imageability, and effects of sterilization *(ionizing radiation)* on network characteristics and performance. Subsequent to this analysis, one formulation was selected as an exemplary composition and subjected to processing as microspheres. The microspheres were recharacterized against previously established network properties to ascertain the suitability of the compositions for flame processing, and to further establish any changes that may occur in the physical and chemical characteristics of the network as a result of this additional processing step. Chapter one of this thesis is intended to provide the reader with some background information relating to osteoarthritis *(and specifically knee osteoarthritis)*, its existing treatments, emerging treat-to target vectors, and then GAE as a treatment to manage osteoarthritis pain. The design criteria for a microsphere indicated for GAE *(as established through one-to-one interviews)* is also presented and is followed by an overview of borate glasses and a justification for the present compositions under investigation. Chapter 2 provides a brief discussion on the overarching objectives of this thesis work, and chapter 3 provides a copy of our paper submitted to the Journal of Non-Crystalline Solids and encompasses an exploration of the role of alkali and alkaline earth cations on the composition-structure-property relationships in borate glass networks. Chapter 4 is a second paper submitted to Discover Materials and further investigates the compositions for their dissolution behaviour and imageability in order to permit the selection of a preferred composition. This chapter also addresses the effects of spheroidization on network properties in addition to characterizing the preferred composition's dissolution behaviour in physiologically representative media and for suspension time. Lastly, chapter 5 addresses final conclusions, limitations of this thesis work, and future studies to be considered.

1.1 Osteoarthritis

Today, osteoarthritis (OA) affects 1 in 8 Canadians and will effect 1 in 4 Canadians within thirty years [1]. In global terms, OA is a common joint disease which affects >303 million people [2] and is considered a serious and debilitating condition [3]. OA is an established contributor to chronic pain [4] and drastically reduces the quality of life (QoL) for patients across many areas, including reduced mobility, independence, and mental health [5]. Regrettably, there are limited pain management therapies available, and existing therapies are ineffectual for the majority of patients [6]. Specifically, present data suggest that *ca.* 47% of patients achieve any benefit from conservative therapies (i.e. education, weight-loss, exercise, nonsteroidal anti-inflammatory drugs (NSAIDs), and opioids) [7]. Aside from the health impacts of the disease, there are substantial socio-economic impacts arising from the condition. Currently (and just within Canada), it is estimated that savings of $488 B (over 30 years) could be realized if adequate pain management strategies were realized [1]. However, pain management is significantly underfunded. From 2005-2006 the Canadian Institutes of Health Research spent the equivalent of $4.30 per individual with arthritis. This is in stark contrast to the $12.83 spent per individual with diabetes and the $138.60 per individual with cancer [8]. Despite this underinvestment, and on the basis of health and socio-economic impacts, it is regarded as essential that adequate pain management therapies are realized and implemented to (i) improve QoL for patients living with OA and (ii) to alleviate the economic burden of treating patients suffering from the disease.

1.1.1 A Serious Disease: Knee Osteoarthritis (KOA)

In order to fully support and establish the definition of a serious disease it is instructive to first examine some illustrative epidemiological data. For example, MacDonald *et al.* [9] published data that is reflective of *"a nationally representative"* sample comprising 4,565 Canadians (>20 years old) [9]. Of this sample 37% (i.e. 1,755 respondents) had a physician diagnosis of OA [9]. Of the 1,755 respondents, 29.4% had knee pain alone [9]. By applying the incidence of those with knee pain (29.4%) to the 4.5 Million individuals who had an OA diagnosis in 2011, it can be estimated that approximately 1.3 Million individuals with an OA diagnosis experience knee pain. Additionally, 38.5% [9] of individuals who experienced knee pain used prescription medications, while 66.2% used non-prescription medications to manage their symptoms (Table 1.1) [9]. By extrapolating both the data from MacDonald *et al.* [9] and the prevalence of OA in 2011 [1], it can be estimated that in 2011, approximately 1.4 million Canadians, 20 years or older, were using prescription or non-prescription medications to treat and manage their KOA pain. Contrastingly, the Arthritis Alliance of Canada, based on 2011 population demographics, estimates

that 13% of the population is affected by the disease, equivalent to 4.5 million Canadians [1]. Discrepancies between the data presented by MacDonald *et al.* [9] and the Arthritis Alliance is associated with methodological variations. In the former, respondents self-selected thereby introducing potential bias into the results. In the latter, *"clinical, survey and administrative data from cohorts of patients living with a diagnosis of OA"* [1] was utilized along with published literature. Irrespectively, these data provide an 'envelope' for the likely range for people affected in Canada. Similar statistics are available for the United States, which suggests that 15.1 million individuals, 25 years or older had symptomatic KOA and 8.6 Million individuals had advanced symptomatic KOA [10].

Table 1.1: Percentage of individuals experiencing KOA pain and associated forms of treatment. Data reflects the Canadian, excluding territories, household population, in 2009, for individuals 20 years or older with an OA diagnoses. Adapted from [9].

Site of Joint Pain	Prescription Medication		Non-Prescription Medication	
	%	Confidence Interval %	%	Confidence Interval %
Knee	38.5	31.8 - 45.7	66.2	59.4 - 72.4

Despite the information presented above, there remains limited information quantifying the true burden of KOA, with limited sources in the literature estimating the current number of individuals affected and/or who have symptomatic KOA [10]. Additionally, there is inadequate information quantifying the type and duration of treatment(s) individuals are undergoing to manage KOA pain. Thus, the numbers presented (Table 1.2) represent an estimate of the population(s) affected by KOA and the number of individuals who use prescription / non-prescription medication to manage their KOA. However, it can be assumed, based on the prevalence of KOA (with a new diagnosis of OA every 60 s [1]), that the numbers presented in Table 1.2 are much larger today.

Table 1.2: Estimated number of individuals with knee, or knee and hip, pain and using prescription/non-prescription medication to treat OA pain (2009). The numbers are extrapolated from the 2014 study by MacDonald *et al.* [9].

Pain Location	Estimated Individuals in Canada	Prescription Medication Treatment	Non-Prescription Medication Treatment
Knee Pain	1.3 Million	500,500	860,600

The data in Table 1.2 provides insight into the population of individuals affected by KOA pain and undergoing conservative treatments to manage OA (Canada only). It is important to recognize that the

majority of these patients (>50% [7]) will experience ineffectual long-term treatment and/or *"treatment related adverse events"* [11] when using existing conservative therapies. The data (Table 1.1 and 1.2) provide the appropriate framing for the definition of a serious disease and further support that there is a largely unmet need in regard to available KOA treatments [12].

KOA is recognized by international agencies and institutions (e.g. U.S Food and Drug Administration (FDA), Osteoarthritis Research Society International (OARSI), and World Health Organization (WHO)) as a 'serious disease'[11-13]. Variable definitions exist for this term; however, FDA defines it is as follows:

> *"… a disease or condition associated with morbidity that has substantial impact on day-to-day functioning. Short-lived and self-limiting morbidity will usually not be sufficient, but the morbidity need not be irreversible, provided it is persistent or recurrent. Whether a disease or condition is serious is a matter of clinical judgement, based on its impact on such factors as survival, day-to-day functioning, or the likelihood that the disease, if left untreated, will progress from a less severe condition to a more serious one" [14].*

Despite the fact that this is a serious disease, there is no *"proven strategy for reducing progression from early to end-stage OA"* [11], and furthermore, there is no therapy that reduces and/or prevents the requirement of a total knee arthroplasty (TKA) [11]. KOA not only negatively impacts individual QoL [15, 16] but equally constitutes a large economic burden [17, 18] on the national and global scale as individuals require treatment to manage their pain, and the disability that results, due to progression of disease. In the US it has been estimated that the lifetime direct medical costs of an individual treated for OA with conservative care such *as "physical therapy, knee braces, acetaminophen, and NSAIDs [non-steroidal anti-inflammatories]"* [19] was $212,700 per person [19]. Additionally, individuals undergoing corticosteroids injections and "guideline-concordant care" [19] incurred a lifetime cost of $228,600 per person. When one considers the epidemiological burden of the disease and then factors in individual costs, the illustration of economic impact becomes self-evident.

Furthermore, a large contributor to the KOA economic burden appears to be the duration of time which patients switch between / use conservative therapies to manage their KOA pain. It has been established that individuals with KOA *"spend nearly 50% of their post-diagnosis life expectancy"* [19] (on average 13.3 years) undergoing / switching between conservative treatments to manage OA pain (Fig. 1.1). Even more crucial is that only 54% of the total overall KOA population in the US were estimated to have received a TKA [19]. These data demonstrate that the majority of KOA patients will continue to use inadequate conservative therapies throughout their lifetime to manage their KOA pain. Additionally, these

data highlight that the majority of patients will spend *ca.* 19 years in-between and/or using various conservative therapies to manage their KOA pain, prior to receiving a TKA if they a deemed eligible to receive a knee replacement.

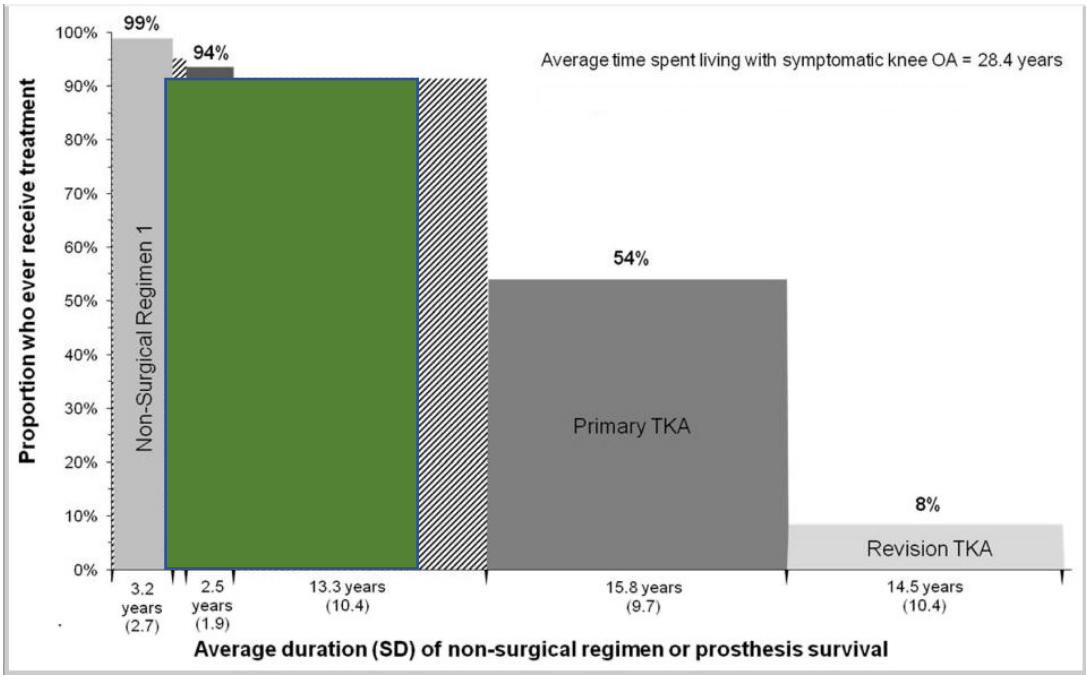

Figure 1.1: Percentage of patients who receive treatment for symptomatic KOA. Non-surgical regiment 1 and 2 consists of conservative therapies and guideline-concordant care. The green block represents occasional usage of analgesics between treatments. Adapted from [19].

An additional crucial perspective that this data offers is the estimated average wait-time to receive a TKA (i.e. 13.3 years) [19]. As recognized by the FDA and OARSI patients are forced to manage their KOA pain and symptoms without adequate and/or safe long-term therapies. As a result, there remains a largely unmet medical need that requires urgent attention at national and international levels.

1.1.2 Treat-to-Target Therapies

To address this challenge, treat-to-target therapies for KOA have become established in the literature. The primary goal of treatments for OA should be to inhibit the pathological structural changes or *"target the underlying pathophysiology"* [12] in order to delay or prevent individuals from requiring TKA [12]. Over the past few decades, much research has focused on a treat-to-target approach in order to find new targets / treatment combinations [20]. These approaches have considered NSAIDs [21], opioids [22], hyaluronic acid intra-articular injections [23], corticosteroid intra-articular injections [24], and tetracyclines [25]. However, prior to discussing the treat-to-target options, it is important to highlight that both exercise and weight loss are considered non-pharmacological first-line treatment options [26, 27].

Both exercise and weight loss are recommended by the American College of Rheumatology/Arthritis Foundation Guidelines to manage patient pain due to OA, based on clinical evidence [28]. Exercise has been shown to reduce patient pain and improve function by strengthening muscles that support the knee joint, such as the quadriceps, and reduce cartilage thinning [28], [29]. Weight loss is essential for overweight and obese patients [28] and reduces the abnormal loading of the joint which can lead to mechanical and/or chemical mediated destruction of the cartilage within the joint [30]. Weight loss has also been shown to have a moderate benefit in reducing pain associated with OA and it has been suggested that patients must ,within a 20-week period, reduce their body weight by 5% in order to have pain relief [31, 32]. However, the impacts of exercise and weight loss are outside of scope for this research and have been comprehensively addressed elsewhere [33]. Accordingly, the following section will provide information on the pharmacological treatment options to manage OA pain via the treat-to-target approach. The sequence of presentation will adhere to the following order: NSAIDS [26], opioids [34], hyaluronic acid intra-articular injections [35], corticosteroid intra-articular injections [36], and tetracyclines [37].

1) Non-steroidal anti-inflammatory drugs (NSAIDs)

NSAIDs are recommended by the American College of Rheumatology/Arthritis Foundation as a treatment option for KOA. Both topical and oral NSAIDs have intended use for individuals with KOA and are a *"mainstay of pharmacologic management of OA"* [28]. Topical NSAIDs are recommended *"prior to [the use of] oral NSAIDs"* in order to minimize systemic exposure [28]. However, they only exhibit short-term efficacy (<4 weeks) for individuals affected by OA [38]. NSAIDs reduce pain by inhibiting cyclooxygenase (COX)1/2 and therefore decrease and/or inhibit the production of prostaglandins such as prostaglandin E2 (PGE2) [21], which is considered to *"be the major contributor to inflammatory pain"* [22]. Prostaglandins, produced in the synovium and bone in OA, sensitize nociceptors in the periphery (i.e. knee) and as a result, individuals experience greater sensitivity to pain [21]. Sensitization of nociceptors (Fig. 1.2) is achieved by the activation of cyclic adenosine monophosphate (cAMP), via the binding of PGE2 to E prostanoid receptors located on the nerve, which results in the phosphorylation of sodium channels, improving the likelihood of the sodium channels opening [22]. Following the opening of sodium channels, a large sodium influx occurs which is capable of depolarizing the membrane and upon depolarization of the membrane potential above a set threshold, an action potential is sent [22]. Sensitization of nociceptors makes it easier for stimuli to trigger an action potential and thereby increases both the patient's sensitivity to stimuli (noxious and non-noxious) and the frequency of the pain signals [21, 22].

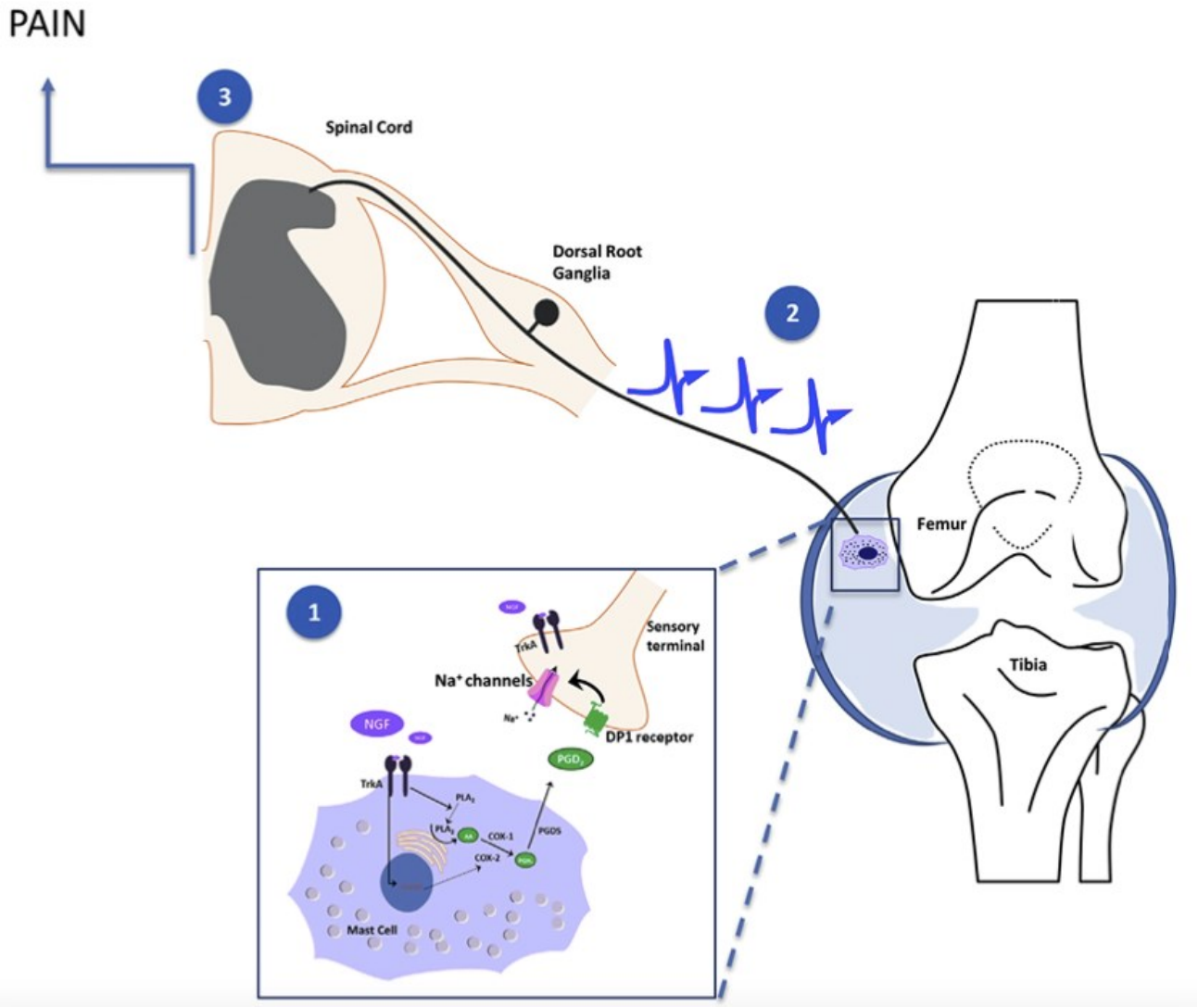

Figure 1.2: Nerve growth factor (NGF) acts on receptors resulting in the production of prostaglandin D_2 (PGD_2) via COX-1 or -2. PGD_2 sensitizes nociceptors which results in hypersensitivity and/or sensitization [39].

Despite the limited efficacy of high-dose and selective NSAIDs, there are additional and substantial concerns associated with their use [40]. Serious adverse effects such as gastrointestinal bleeding, renal toxicity, and cardiovascular side effects have all been recorded in the literature [21, 26, 28]. Within the elderly population, NSAID *"long-term use is a leading cause of drug-related morbidity"* [41] and as individuals age they become increasingly predisposed to the risk of treatment-related adverse effects [41]. Additionally, both the FDA and European Medicines Evaluation Agency (EMEA) agree that COX-2 inhibitors (i.e. NSAIDs) increase the risk of cardiovascular events, specifically thrombotic events such as a stroke or acute myocardial infarction [42]. NSAIDs are also known to have adverse drug interactions with a variety of medications frequently taken by the elderly population, such as anti-coagulants and anti-hypertension drugs (can reduce efficacy and *"increase the risk of acute kidney injury"* [42]) [41]. While

guidelines for the safe use of NSAIDs have been established (with specific cautions for patients who are at a higher risk of toxicity), the suggested dosage/use is not normally compatible with the requirements for chronic pain management [41]. Accordingly, this is of substantial concern as the majority of patients with OA are within these vulnerable age groups and the prevalence of OA increases as age increases [43].

2) Opioids

Non-Tramadol opioids are conditionally recommended against, and Tramadol is conditionally recommended for, individuals with KOA pain who *"have contraindications to NSAIDs, find other therapies ineffective, or have no available surgical options"* [28]. Tramadol is conditionally recommended to treat KOA because of its modest benefits in managing pain for 3 months to 1 year. Furthermore, and perhaps beneficially, Tramadol (and potentially other opioids) are recommended for pain management in patients with contraindications to NSAIDs who are not receiving benefits from other conservative therapies and as such require further / additional pharmacological treatment to manage OA pain [28]. Non-Tramadol opioids are conditionally recommended against due to the risk of toxicity and only a modest benefit established for alleviating patient pain [28]. Despite these recommendations from the American College of Rheumatology/Arthritis Foundation it is important to note that the OARSI regard opioids with uncertainty and suggest opioids have limited long-term usefulness in managing the pain associated with KOA [34, 44].

From a mechanistic standpoint, opioids exert their effects at both the periphery (knee) and the spinal cord by binding directly to opioid receptors (i.e. mu-opioid receptors) on the nerve [22]. Opioids reduce nerve hyperexcitability (which occurs in response to inflammatory mediators or injury) by hyperpolarizing the sensory neuron membrane potential [22], making it more difficult for stimuli to elicit an action potential (*Fig. 1.3*). Despite this clear mechanism, there is varying evidence supporting the safety and efficacy of opioids to treat OA pain [45]. Both Tramadol and non-Tramadol opioids have been shown in a meta-analysis to reduce Western Ontario and McMaster Universities Osteoarthritis Index (WOMAC) pain scores for KOA similarly to NSAIDs [34]. Non-Tramadol opioids have also been shown to demonstrate a small benefit (effect size of 0.28 compared to placebo) in reducing patient pain, however this was paired with an increasing the risk of adverse events [45]. Opioid associated adverse events have been reported as lower gastrointestinal effects (i.e. constipation), nausea and/or vomiting, and respiratory depression [46]. Furthermore, patients using non-tramadol opioids were four times more likely to withdraw from studies due to adverse events and had an increased risk (3x) of experiencing severe adverse events [45].

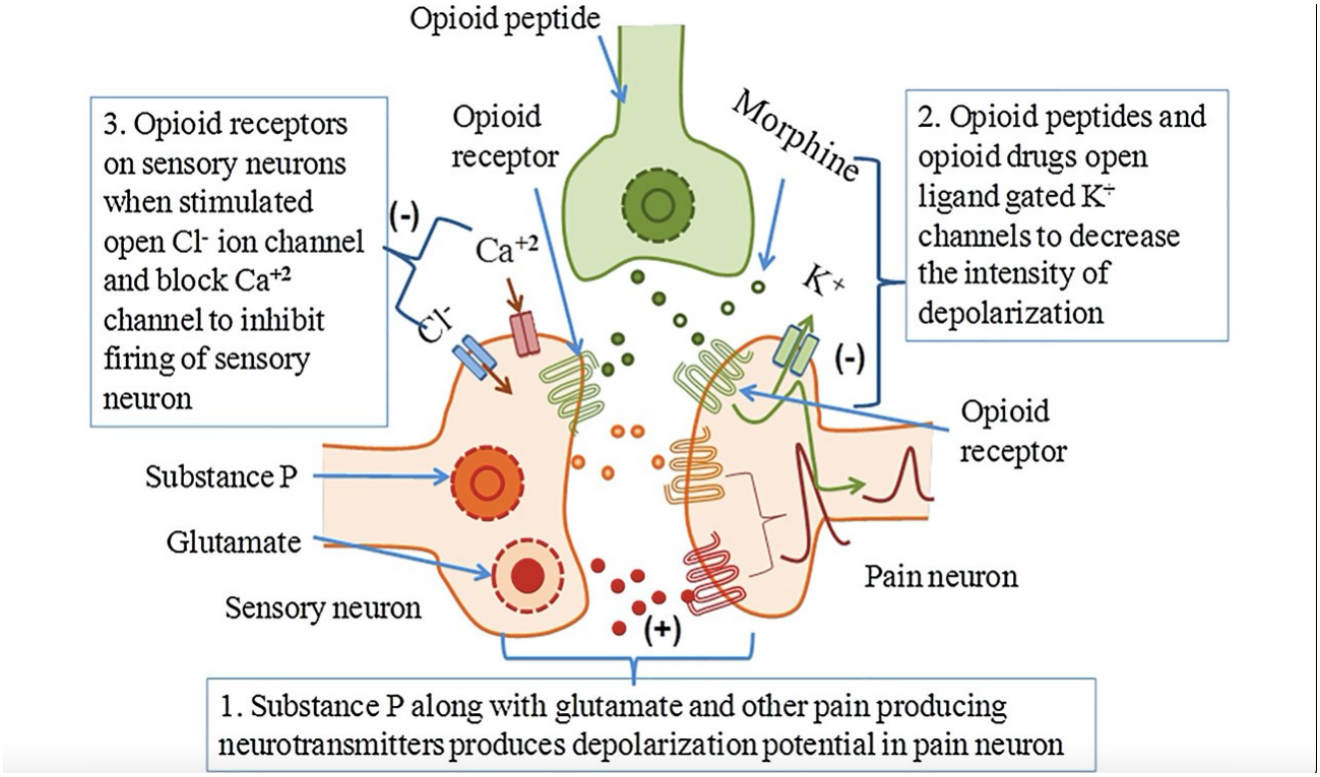

Figure 1.3: Opioids act on both 1st and 2nd order neurons by binding opioid receptors. Opioids hyperpolarize 2nd order neurons and prevent 1st order neurons from signalling [47].

Due to the limited benefit provided by Tramadol on reducing OA pain, it appears that the adverse events associated with Tramadol use may outweigh clinical benefits [45]. In conjunction with serious adverse events, opioids can possess addictive properties that have led to the opioid epidemic [48] and long-term use can also facilitate drug tolerance in addition to opioid-induced hyperalgesia which enables *"a vicious cycle of dose escalation and worsening pain"* [49].

3) Hyaluronic acid intra-articular injections

Hyaluronic acid intra-articular injections are conditionally recommended against by the American College of Rheumatology/Arthritis Foundation as a treatment for KOA [28]. This is the formal position of the College and is based on their review demonstrating *"that [hyaluronic acid intra-articular injection] benefit was restricted to the studies with higher risk of bias"* [28]. Contrastingly, studies with low risk of bias demonstrated the effect size of hyaluronic acid intra-articular injections to *"approach zero"* [28]. This data, coupled with evidence suggesting that hyaluronic acid injections may cause harm to the joint [28], governed the College's decision to only conditionally recommend hyaluronic acid injections as a result.

Mechanistically, hyaluronic acid naturally acts as a shock absorber and lubricant within the joint [23]. Hyaluronic acid also provides cartilage protection by modulating the activity of some immune cells (i.e. inhibit phagocytic activity of macrophages, leukocyte migration, and neutrophil associated cartilage degradation) in addition to reducing the activity/production of both inflammatory mediators and proteases

(i.e. prostaglandins, nitric oxide and MMP's) [50]. Joints affected by OA exhibit a reduction in both hyaluronic acid concentration [23] and molecular weight [51]. In the knee, proteoglycans bind hyaluronic acid, and this complex is what provides the *"compressibility and elasticity of cartilage"* [50] within the joint (that which is lost in OA) [51]. As such, hyaluronic acid intra-articular injections are intended to be used as a method to restore lost hyaluronic acid within the joint and improve the lubrication and shock absorption of the affected joint [23].

Limited studies have reported a *"modest positive effect"* [23] on pain reduction at 24 weeks following treatment with hyaluronic acid. However, further clinical studies, particularly those with low risk of bias, have demonstrated little to no clinical benefit and do not support the use of hyaluronic acid injections for KOA treatment [28]. For example, the findings from Liu *et al.* [52] does not support the efficacy of hyaluronic acid injections to reduce patient pain over a 2-year period. It was demonstrated that the average yearly change in WOMAC pain score for patients treated with hyaluronic acid injections was 0.50 and was not deemed clinically significant [52]. Similarly, two comprehensive reviews concluded no clinically significant reduction in pain for KOA patients treated with hyaluronic acid injections [35, 53]. In fact, one review found an increased risk of serious adverse events such as cardiovascular, musculoskeletal, cancer, and gastrointestinal events associated with the use of hyaluronic acid injections [35]. As a result, hyaluronic acid injections are considered a short-acting therapy with a narrow probability of providing benefit to patients.

4) Corticosteroid intra-articular injections

Corticosteroid intra-articular injections are another form of treatment for which a conditional recommendation by the American College of Rheumatology/Arthritis Foundation exists [28]. Corticosteroid intra-articular injections, specifically glucocorticoid intra-articular injections, are conditionally recommended due to the larger body of quality evidence that supports their efficacy over other forms of intra-articular injections [28]. Corticosteroids are considered anti-inflammatory [54] and are believed to prevent the synthesis of inflammatory mediators and reduce the accumulation of inflammatory cells within the joint [23]. Glucocorticoids, a class of corticosteroid, directly act on nuclear steroid receptors and influences the synthesis of proteins and messenger ribonucleic acid (mRNA) [24, 54] (Fig. 1.4). By binding these receptors glucocorticoids can regulate interleukins [24], cytokines (i.e. *"repress transcription of many genes encoding pro-inflammatory cytokines"* [55]) and enzymes in addition to modifying T (via suppression of dendritic cell function (activate T cells) and / or modify dendritic cells to induce regulatory T cell (immunosuppressive [56]) differentiation [55]) and B cells [54]. Furthermore, corticosteroids are also thought to have a role in inhibiting matrix metalloproteinase (MMP) production and therefore, may have a further role in protecting the cartilage within the joint [25].

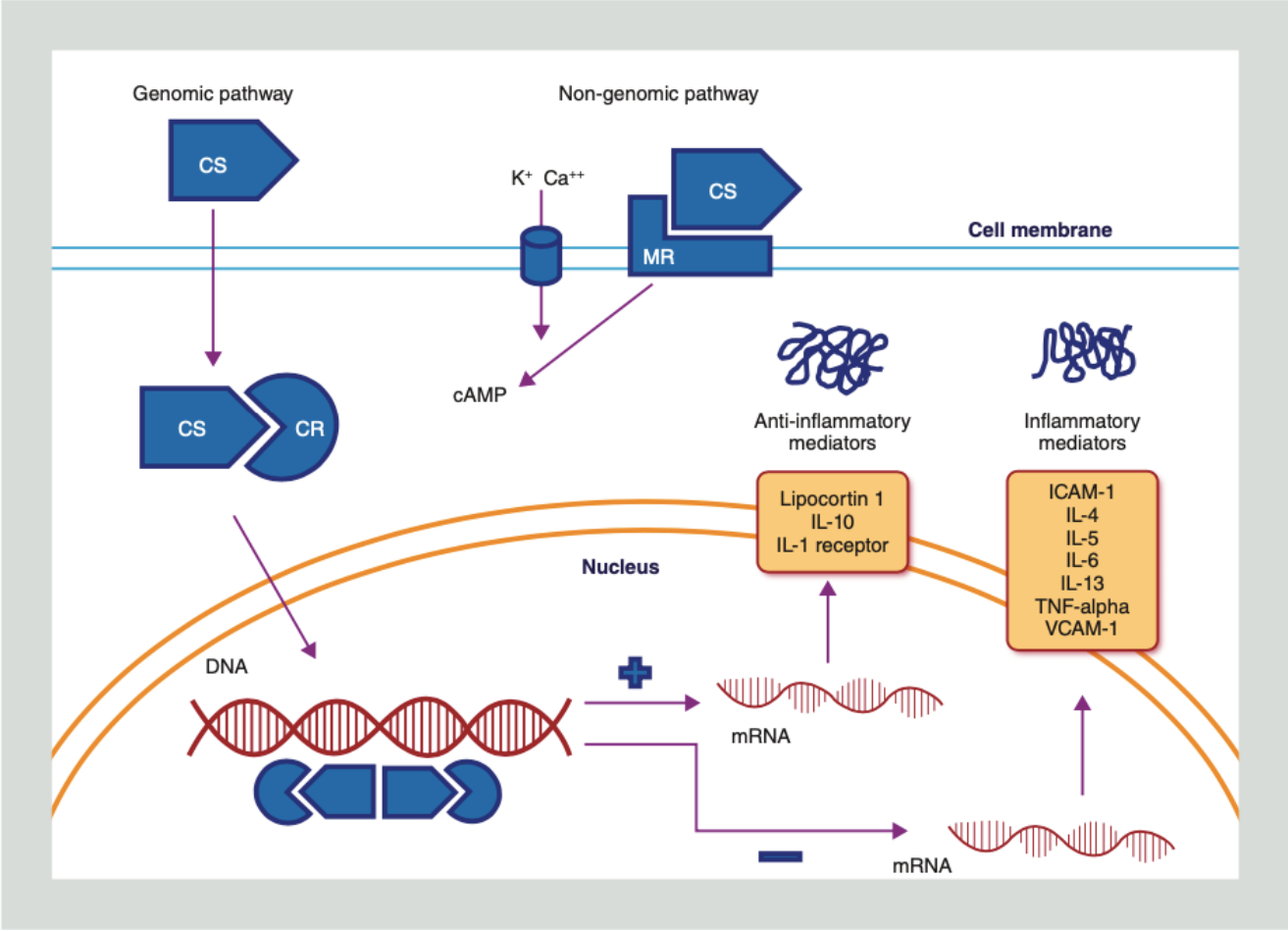

Figure 1.4: Corticosteroids binding their cytoplasmic receptors results in the i) transcription of anti-inflammatory mediators and/or ii) inhibition of gene transcription for proinflammatory mediators. Binding of their membrane receptors (MR) results in secondary messenger signalling and an increase in anti-inflammatory messengers within the cell [24].

A review by Bellamy *et al.* [57] determined that corticosteroid intra-articular injections were effective at reducing patient pain at 2-3 weeks compared to the placebo, however, the effects were short-term and lasted a maximum of 3 weeks. Conversely, other studies have shown that corticosteroid intra-articular injections reduce OA pain for up to 6 months [36]. One study in particular found that corticosteroid intra-articular injections reduced pain by 23.9% at 3 weeks, 26.9% at 6 weeks, 20.7% at 3 months, and 17.1% at 6 months. Interestingly, it was also determined patients with milder forms of OA had a greater response to treatment with corticosteroid intra-articular injections compared to those with severe OA [36]. While intra-articular injections represent a common pain management strategy, there has been evidence suggesting these injections are associated with cartilage volume loss and may potentially contribute to the progression of OA [26, 28, 58]. High doses of corticosteroids, may negatively affect cartilage repair [25]; thus it is recommended patients only receive up to four injections a year [59, 60]. For example, dexamethasone at high doses (>100 micro μM) has been shown to reduce type II collagen levels (a key

component of articular cartilage) and promote extracellular matrix (ECM) degradation [61]. This has also been demonstrated in other corticosteroids at high doses such as hydrocortisone and methylprednisolone, resulting in cartilage degradation, reduced *"chondrocyte viability"*, and reduction in *"cartilage macromolecules"* [61]. Many therapies act to slow down / inhibit cartilage degradation (which is part of the pathophysiological process of OA). As such, a therapy which facilitates cartilage degradation may result in further detrimental pathophysiological changes within the joint, facilitating pain and further symptoms.

It is important to consider, even with a significant clinical benefit, corticosteroid intra-articular injections demonstrate short-term efficacy and require additional injections in order to obtain clinical benefit. Furthermore, the risk of potential adverse events (i.e. chondral toxicity and accelerated progression of OA) should be taken into consideration when undergoing long-term treatments [60] and more evidence is required to understand the adverse events that may arise due to corticosteroid intra-articular injections [62]. Therapies which facilitate processes which contribute to the pathophysiological changes of a disease state (cartilage degradation via corticosteroid use in OA) may exacerbate symptoms and promote / drive further pathophysiological progression, leading to further symptoms and pain for individuals with KOA.

5) Tetracycline

There exists no recommendation/information on tetracycline in the current version of the American College of Rheumatology/Arthritis Foundation Guidelines [28]. Tetracyclines are evaluated in this section due to the clear and well-defined treat-to-target pathway described within the literature, and as such this provides an illustrative example of state of the art internationally.

Tetracycline derivatives are believed to inhibit MMP activity (Fig. 1.5) in a variety of ways such as; i) binding zinc or calcium resulting in a conformation change and loss of function, ii) preventing the activation of the MMP proenzyme, and/or iii) binding zinc at the active site and blocking MMP activity [25]. Tetracyclines negatively regulate MMP production via *"suppression of [the] inflammatory cascade"* [63] and thereby indirectly influence the expression of MMPs [63]. MMPs are recognized to break down cartilage [26] and produce wear particles which can then stimulate the production of inflammatory cytokines [64]. The presence of these inflammatory cytokines results in the further production of MMPs and the continued degradation of cartilage [64]. By inhibiting MMP production / function, the process of further cartilage destruction is intended to be minimized and/or eliminated (Fig. 1.5). Therefore, a reduction in pain and an increase in function should result from treating this target. Doxycycline, a tetracycline-class antibiotic, is the most potent inhibitor of MMP and is also thought to be chondroprotective [25]. Therefore, it has been anticipated that doxycycline would most effectively inhibit

MMP activity and therefore most effectively reduce patient pain. As such, doxycycline represents the most promising tetracycline treatment to reduce / eliminate KOA pain under consideration in the literature.

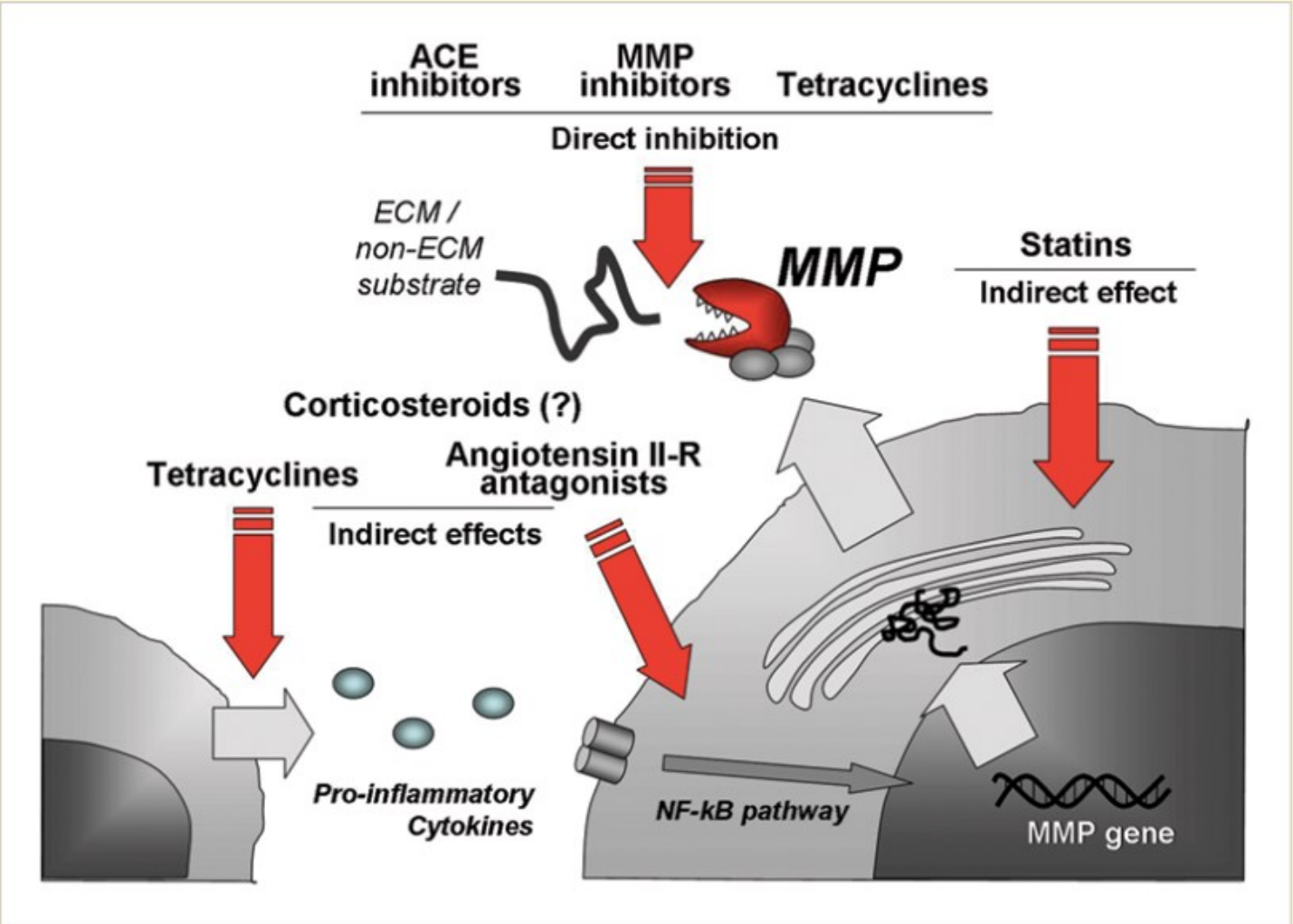

Figure 1.5: Tetracyclines act directly and/or indirectly to inhibit MMP activity and/or production. Tetracyclines can play a role in inhibiting the inflammatory cascade and as a result indirectly regulate the production of MMPs [63].

Despite this clear treat-to-target pathway, a recent Cochrane review showed that doxycycline had minimal to no benefit for managing and reducing OA pain (effect size -0.05) [65]. Further, doxycycline was shown to have no clinically important improvement in physical function (26-29% responded to treatment) compared to placebo, where treatment response was defined *"as a 50% improvement in scores"* [65]. Furthermore, Da Costa *et al.* [65] concluded that, compared to placebo, individuals receiving doxycycline were at an increased risk of both adverse events and dropping-out of the study due to the treatment-related adverse events. As a result, it was concluded that the safety concerns outweigh the potential benefits provided by doxycycline [65]. A second Cochrane review by Nüesch *et al.* [37] had similar findings; demonstrating the effect size of doxycycline on pain to be limited with patients being found to be at a higher risk of dropping-out due to treatment-associated adverse events *("sun sensitivity,*

monilial vaginitis, and nonspecific gastrointestinal complaints"[66]). Thus, it was concluded the symptomatic benefit for patients was minimal to non-existent and doxycycline was not recommended for treating KOA pain [37]. It appears that treatment with doxycycline, much like treatment with opioids, results in an increased risk of patients experiencing adverse events and stopping treatment as a result of same.

These data provide an interesting case in respect to developing treat-to-target vectors for pain management in KOA. The mechanism that tetracyclines (specifically doxycycline) acts on is well developed and there is a clear path describing how this therapy should target and slow down/inhibit structural changes due to OA. More importantly, there appears to be a clear mechanism in which this therapy can potentially eliminate patient pain and improve function. However, the clinical outcomes and the benefit to patients as a result of this treatment do not reflect the hypothesis underlying the treatment. As such, this is a strong example of many treat-to-target therapies that do not necessarily provide symptomatic relief for patients with KOA, and why complementary and alternative strategies in KOA pain management need to be developed and considered.

Treat-to-target is, in theory at least, an ideal method to tackle and manage patient pain. However, in clinical practice the results vary, and the majority of therapies do not have quality conclusive evidence supporting their efficacy and/or they have serious adverse events associated with use (Table 1.3). Additionally, a majority of patients do not respond to these therapies, and evidence suggests that tailored conservative therapies (exercise, education, acetaminophen, physiotherapy, NSAIDs, and tramadol) are effective in only 47% of patients [7]. It is evident throughout the literature that the available conservative therapies are typically ineffectual for the majority of patients [6, 21] and do not provide adequate sustained pain relief [21]. Therefore, it is of the utmost importance that new therapeutic targets are identified that recognize the complexities of the pathogenesis of OA and can break the pain pathways in KOA. In this regard, emerging theories related to the central and peripheral pain mechanisms provide new and exciting avenues for treatment development.

Table 1.3: Summary of data for target of therapy, treatment recommendations, and data supporting efficacy of therapy.

Treatment	Target	2019 American College of Rheumatology/Arthritis Foundation Guidelines [28]	Data support for/against
Topical/oral NSAIDs	• Inhibits COX1/2 and reduces/prevents production of prostaglandins [21].	Strongly Recommended.	• Severe risk of toxicity and adverse events with long-term use [41]. • Topical NSAIDs perform similar to placebo at 2 weeks [38]. • Short-term benefit [38]. • Possible drug interactions (antihypertensives and antithrombotics) [42].
Opioids	• Hyperpolarizes sensitized nerves in the periphery [22]. • Acts on receptors in the periphery and spinal cord [22].	Non-Tramadol opioids are conditionally recommended against. Tramadol is conditionally recommended.	• Small benefit seen for opioid use (tramadol and non-tramadol) in reducing patient pain [28]. • Adverse events have resulted in patient withdrawal and may overcome the therapeutic benefit [45]. • Increased risk of adverse events [45]. • Risk of dependency and tolerance [28, 49].
Hyaluronic acid Intra-articular injections	• Cartilage protective [50]. • Modulate production/activity of proteases, inflammatory mediators, and some immune cell [50].	Conditionally recommended against.	• Mixed evidence in support of efficacy to reduce OA pain [23, 28, 52]. • Risk of Bias in studies supporting efficacy [28]. • Increased risk of adverse events [35].
Corticosteroid Intra-articular injections	• Anti-inflammatory [54]. • Inhibit synthesis of inflammatory mediators [24, 55]. • May inhibit MMP's [25].	Conditionally recommended.	• Data suggesting efficacy in reducing patient pain [36]. • Short-term efficacy [57]. • Evidence suggesting they may contribute to cartilage loss and progression of OA [58].
Tetracycline	• Directly/indirectly inhibits MMP's [25].	N/A	• Minimal to no clinically meaningful reduction in patient pain [65]. • Increased risk of patients experiencing adverse events compared to placebo [37].

1.1.3 The Role of Central & Peripheral Sensitization in OA – The Basis for GAE

Early in OA, pain typically arises during *"movement and loading of the joint"* and is largely regarded as nociceptive pain [4, 5]. It has been suggested that early in OA mechanical stimulation generates intermittent pain mediated *"by fast-conducting myelinated nerve fibers"* [67] and this may provide a potential treatment target [67]. In contrast, for late stage OA, pain is chronic and is regarded as neuropathic pain [21]. In particular, chronic pain exhibits a *"lack of direct correlation between nociceptor activation and the pain experience"* [21] brought upon by central sensitization and there is evidence that this mechanism is significant for patients with OA. In support of this position, previous research has shown that patients with OA have reduced pain thresholds and show signs of allodynia and hyperalgesia [21]; features which are also characteristic of central sensitization [68]. Consequently, there is substantial evidence to support that central sensitization plays a significant role in facilitating OA pain, and by extension, it is believed that understanding the mechanisms which stimulate / maintain peripheral and central sensitization may advance the discovery of new pain management therapies.

In central sensitization, there is a shift from *"high-threshold nociception to low-threshold pain hypersensitivity"* [69]. Central sensitization occurs after prolonged and/or repetitive stimulation from peripheral nociceptors which results in a *"reversible increase of excitability and of synaptic efficacy of central nociceptive pathway neurons"* [70]. This can present (clinically) as allodynia, hyperalgesia [70], and as an enlargement in the total receptive field [4]. Current literature indicates that the mechanisms of central sensitization in OA are plastic and capable of being reversed [21]. For example, after successful joint replacement, there is a reversal in the irregular somatosensory perception (demonstrating plasticity of the system) [21]. Specifically, patients who undergo TKA have a significant reduction in pain. In one study, this was quantified as a reduction in scores from 6.9 ± 0.4 cm to 2.6 ± 0.5 cm on a visual analog scale (VAS) of 0-10 cm (where 10 cm was defined as the maximum amount of pain) [71]. Furthermore, it has been established that after TKA, patients exhibit reduced hyperesthesia (increase in sensitivity) and *"normalized spatial summation of pain"* [71]; re-enforcing that nociceptors in the periphery are important for maintaining central pain [71]. Therefore, not only are the mechanisms that maintain and/or initiate central sensitization important to understand but so too are the mechanisms of peripheral sensitization.

Peripheral sensitization occurs in inflammatory conditions or in injured tissues where chemical mediators can sensitize nociceptor peripheral terminals [72]. Thresholds of these nociceptors are reduced (i.e. become more negative) and there is *"enhanced responses to supra-threshold mechanical or heat stimuli"* [73] which results in abnormal neural signalling to various stimuli. Peripheral sensitization has been shown to have clinical relevance and antibodies blocking nerve growth factors have been shown to provide superior analgesic effects to NSAIDs, however, the mechanisms of peripheral sensitization in OA

remain poorly understood [67]. Peripheral sensitization can subsequently lead to, [73] and maintain, central sensitization (as previously discussed) [21]. As signalling from the peripheral nociceptors increases, the transmission neurons located in the dorsal horn of the spinal cord become increasingly responsive to the input originating in the periphery [5]. The neurons in the dorsal horn, as a result of continual stimulation from the periphery (low-level and/or non-noxious stimuli), have reduced thresholds which results in central sensitization [5]. This information suggests that by eliminating the abnormal signalling from nociceptors at the periphery, there may be plastic changes in the central nervous system which may result in the elimination of the potential mechanism which maintains central sensitization. Therefore, both central and peripheral sensitization provide a potential mechanism in which therapies can target to reduce the overall pain experience for patients with OA in addition to possibly providing effective long-term pain relief.

1.1.4 New Target to Manage Pain in OA: Angiogenesis & Perivascular Nerves

Existing therapies that target pain have been shown to be ineffectual for the majority of patients, including treat-to-target therapies. As a result, there remains a largely unfulfilled need for effective and safe treatments to manage OA pain [12]. A feature that is consistent across all existing treat-to-target therapies is that each therapy only targets one or two mechanisms associated with OA. Current evidence supports that OA is a complex disease and there are many factors which contribute to the progression and symptoms, including pain and functional limitations, of OA [64, 74, 75]. Therefore, based on the available clinical evidence, and in order to provide a successful therapy, many factors that contribute to OA may need to be simultaneously targeted. To date, there is debate over which mechanism(s) of OA contributes most to pain and which mechanism(s) are ideal therapeutic targets [4]. Amongst this debate, angiogenesis and perivascular nerves [76-80] are a new emerging target which are as unique as they are promising. Angiogenesis and perivascular nerves present an exciting opportunity to target and manage patient pain via a multitude of processes. Consequently, this increases the probability of success over other treat-to-target options. By targeting both angiogenesis and perivascular nerves, many mechanisms that are believed to contribute to OA pain are also targeted, including peripheral/central sensitization, inflammation, cell infiltration, and angiogenesis.

This target recognizes that both inflammation and angiogenesis are dependant processes [81]. It has been well established that inflammatory tissues stimulate a hypoxic environment, with hypoxia stimulating inflammation by amplifying nuclear factor kappa-light-chain-enhancer of activated B cells (NF-κB) pathway signalling [82]. Importantly, hypoxic, injured, and diseased tissues, all of which are commonly seen in patients with OA [4, 26], stimulate angiogenesis [78] which also has a suggested role in facilitating pain due to OA. Under hypoxic and inflammatory conditions, pro-angiogenic factors such

as vascular endothelial growth factor (VEGF) and fibroblast growth factor 1 (FGF-1) are released [78] from resident cells of the knee joint (i.e. chondrocytes and macrophages) [76]. Wear particles within the joint are also capable of stimulating the release of cytokines from macrophages and T/B cells which can then stimulate chondrocytes and fibroblasts to release pro-angiogenic factors that further contribute to angiogenesis [83]. Pro-angiogenic factors activate endothelial cells to release enzymes, which degrade the basement membrane and ECM so that endothelial cells can migrate towards the angiogenic stimuli into the tissue and begin forming new vasculature [84]. Angiogenesis has been suggested to contribute to sustaining the pathophysiological changes due to OA and pain through various mechanisms. The expression of adhesion molecules from neovasculature facilitates the migration of inflammatory cells to the site of angiogenesis [85]. New blood vessels are also highly permeable and as such can enable i) oedema formation and ii) inflammatory cells to infiltrate tissue where these new vessels are forming. In this manner, angiogenesis is believed to maintain local inflammation by recruiting/increasing inflammatory cells within the joint [86, 87], indirectly sustaining itself (angiogenesis) through pro-angiogenic factors secreted by the inflammatory cells, and promote hypoxic conditions due to the increased metabolic demand associated with a higher number of cells [82]. Similar mechanisms are identified in rheumatoid arthritis (RA) and are also believed to play a role in the progression of joint destruction [88]. In RA it is believed that the new blood vessels that form are responsible for supplying inflammatory cells with oxygen and nutrients (Fig. 1.6), in addition to providing them with a way into the synovium of the joint [88]. The formation of new vasculature is thought to enable immune cells and cytokines to enter the newly vascularized tissues such as the synovium, as seen in other conditions such as colorectal cancer [89] and thereby contribute to the maintenance of inflammation within the joint [83]. There is clinical support demonstrating an increase in angiogenesis in joints with OA and evidence showing an increase in vascularity in the articular cartilage, meniscus, synovium [87], and subchondral bone [76, 90] as OA progresses. By targeting both angiogenesis and perivascular nerves via GAE, the suggested mechanisms driving pain are eliminated in addition to the sub-mechanisms facilitating / contributing to the pathogenesis / progression of OA such as inflammation, cell infiltration, and hypoxia which may result in significant and sustained pain relief.

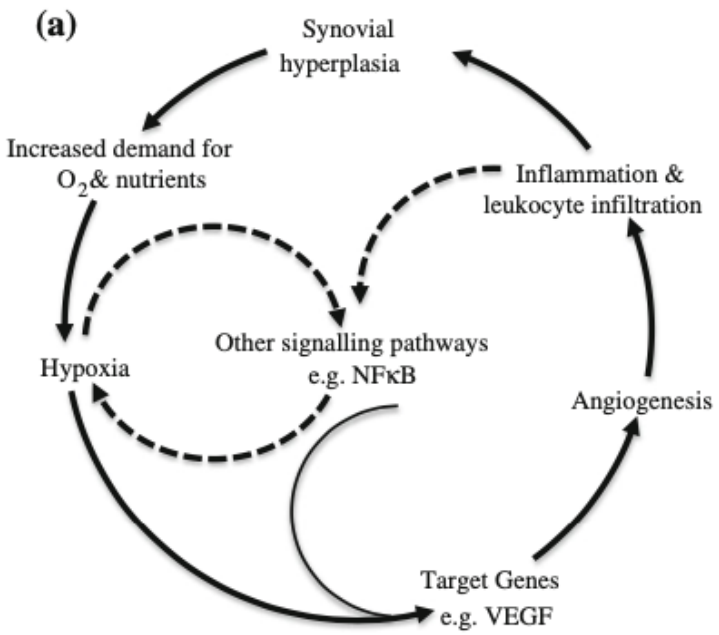

Figure 1.6: How angiogenesis is initiated and promotes inflammation within a joint. Additionally, this figure demonstrates the cyclic nature of RA and describes suggested mechanisms of OA. Adapted from [89].

Crucially, it is understood from other pathophysiological conditions that angiogenesis and nerve growth are highly integrated processes and share many of the same regulatory pathways [76]. Angiogenesis that arises due to pathologic conditions also *promotes "sensory nerve ingrowth along the newly formed blood vessels"* [87], known as perivascular nerves. These nerves grow alongside blood vessels into various structures and tissues which under normal conditions are avascular, (*i.e.* cartilage in adults [91]), or have limited vasculature (i.e. the synovium) and therefore act as a source of pain [87]. Both animal and human studies have shown that blood vessels originating in the subchondral bone are capable of moving into the articular cartilage [21]. It has been demonstrated that these *"growing and damaged peripheral nerves display sensitization"* [91] and likely contribute to the pain experience [91]. In OA, aneural tissues have been shown to be vascularized (such as cartilage [91]) and display increased sensory innervation of the meniscus [92]. In menisci from patients with OA, it has been demonstrated that there is both increased angiogenesis and perivascular nerve growth into the outer region of the meniscus and an increase in angiogenesis in the typically aneural and avascular inner meniscus [92]. It has been well established that the role the meniscus within the knee joint is to provide joint stability and bear the weight of the joint, in addition to protecting articular cartilage [93]. Articular cartilage acts as a lubricated surface, undergoes compressive forces during joint loading [94] and is able to withstand various forces such as shear and tensile forces [95]. Therefore, the presence of nerves in areas that undergo mechanical loading provides opportunity for pain signals to be sent through mechanical stimulation of these nerves and/or

pressure changes within the meniscus, articular cartilage, and subchondral bone. Additionally, these nerves grow and/or multiply in environments that possess numerous ligands (i.e., cytokines) that stimulate pain through direct binding or by inducing peripheral sensitization. As a result there have been efforts throughout the scientific community to understand i) how nerve sensitivity and peripheral sensitization is induced and ii) what specific ligands induce sensitization as this is still an area not completely understood [21]. There is, however, mounting evidence and understanding of potential mediators that induce peripheral sensitization within the knee joint in OA [96]. It can be discerned from the data (Table 1.4), that various factors such as nerve growth factor (NGF), chemokines, cytokines, damage-associated molecular patterns (DAMPs), cell infiltration, and neuromodulators contribute to i) peripheral sensitization and ii) further pathogenesis of OA within the joint.

Numerous factors can contribute to the sensitization of peripheral nerves and ultimately the pain experience of patients affected by OA. By targeting the abnormal vasculature in the knee various components of pain are targeted. When eliminating the abnormal vasculature in the joint, perivascular nerves, peripheral sensitization, and central sensitization are all indirectly targeted. Additionally, by targeting and eliminating the abnormal vasculature, inflammation and other complex factors implicated in progressing and contributing to pain in OA are also targeted such as cell infiltration, inflammation, hypoxia, and angiogenesis. Accordingly, an intervention that could target angiogenesis (eliminate the abnormal vasculature) and perivascular nerves may provide a means to target, inflammation, cartilage degradation, cell infiltration, hypoxia, peripheral / central sensitization, and pain within the joint and thereby dramatically improve treatment options while targeting multiple mechanisms simultaneously.

Table 1.4: Mediators implicated in peripheral sensitization of nociceptors or primary neurons and their mechanism of action/role they play in inducing sensitization.

Source of Sensitization	Mechanism of Action/Role	Source
Nerve Growth Factor (NGF)	• Sensitization through tropomyosin-related kinase A receptor. • Induces hypersensitivity to both heat and mechanical stimuli. • Binding increases nociceptive excitability and increases neurogenic inflammation. • Promote nerve growth.	[96-98]
Chemokines Chemokine (C-C motif) ligand 2 (CCL2)	• Role in maintaining chronic pain. • Upregulation of CCL2 and its receptor associated with mechanical allodynia and its maintenance. • Level of CCL2 in synovial fluid correlate with symptom severity. • CCL2 shown to reduce threshold and increase excitability in dorsal root ganglion neurons.	[96, 99, 100]
DAMPS, ECM, cartilage breakdown products, alarmins, and microscopic inorganic crystals	• Directly excites nociceptors. • Recognized by immune cells and stimulates inflammatory mediator production.	[96, 101]
Cytokines (TNF-α, IL-1β, and IL-6)	• Directly excites nociceptors by promoting an inflammatory environment. • TNF-α changes excitability of nociceptors, increases nociceptor firing and promotes calcitonin gene-related peptide release from nociceptors. • IL-1β reduces threshold of nociceptors, excites nociceptors, and activates voltage-dependent Na^+ currents. • IL-6 shown *in vitro* to mobilize Ca^{2+} in 33% of dorsal root ganglion neurons.	[100, 101]
Cell infiltration	• Macrophages can sensitize/destroy nociceptors. • Mast cells can release NGF.	[96, 102]
Neuromodulators (Calcitonin gene-related peptide)	• Released from nociceptor peripheral terminal and can induce neurogenic inflammation and vasodilation. • Induces hyperactivity of primary neurons.	[96, 103]

1.1.5 Geniculate Artery Embolization

Based on the above mechanisms, a novel and promising treat-to-target approach is gaining clinical traction and has been deployed nationally and internationally for patients with KOA. GAE is a new outpatient procedure indicated for individuals with mild to moderate osteoarthritis who are resistant to conservative pain management therapies and are not yet indicated for a TKA [104, 105]. The duration of the procedure itself varies and has been reported to take approximately 80 minutes [105]. Along with being a relatively quick procedure, it also has a short recovery time and patients can resume daily activities the following day [104]. GAE has been deemed both safe and effective for the treatment of post-knee arthroplasty hemarthrosis [106, 107] and has been preliminarily shown by Okuno *et al.* [104] and Bagla *et al.* [105] to be safe and effective in alleviating patient pain due to OA. Briefly, the procedure is designed to occlude blood flow from within the abnormal vasculature and as a result, targets the abnormal vasculature directly and the perivascular nerves indirectly. GAE is believed to lead to reduced and sustained pain reduction as a result of its targeted approach. GAE is part of a broader set of interventional radiology approaches termed transarterial embolization (TAE). During GAE, percutaneous access to the femoral artery is obtained via an introducer sheath(s) and microcatheter(s). Subsequent to confirmation of microcatheter placement, embolic microspheres are infused and delivered to the target site until hemostasis is achieved (further anatomical detail for the geniculate artery are provided in Appendix E). The reduced blood flow to the abnormal vasculature may result in decreased inflammation and perivascular nerve growth / stimulation within the synovial joint as such eliminating / reducing pain [104, 108]. Clinical data supports the safety and efficacy of the procedure. In particular, data from Okuno *et al.* [104] and Okuno *et al.* [108] have shown a reduction in (i) total WOMAC and (ii) pain WOMAC scores following GAE with long-term pain relief of up to one and two years, respectively. In Okuno *et al.* [104] there was a reduction in both total WOMAC scores (baseline / 48.5, 1 month / 12.5, 4 months / 7.5, and 12 months / 6.0) and total pain WOMAC scores (baseline / 12.1, 1 month / 3.5, 4 months / 1.8, and 12 months / 1.9), for GAE performed with IPM/CS (a degradable embolic agent) as described in Table 1.5.

Table 1.5: Pain scores post GAE. Adapted from Okuno *et al.* [104].

	Treatment	Baseline	1 Month	4 Months	12 Months
Total WOMAC	IPM/CS (n=11)	48.5 ± 9.4	12.5 ± 7.6	7.5 ± 6.4	6.0 ± 8.3
Pain WOMAC		12.1 ± 1.8	3.5 ± 2.4	1.8 ± 2.5	1.9 ± 2.7
Patients receiving NSAIDs		8	3	1	1
Total WOMAC	Embozene (n=3)	43.3 ± 6.8	9.0 ± 4.6	6.0 ± 5.3	-
Pain WOMAC		12.6 ± 2.5	2.7 ± 1.2	1.3 ± 1.1	-
Patients receiving NSAIDs		2	1	0	-

Similarly, in Okuno *et al.* [104] significant WOMAC improvements were reported (Table 1.5) for GAE performed with Embozene (a non-degradable embolic agent). Interestingly, following GAE there is a reduction in the use of supplementary medications for pain relief, such as NSAIDs, reported in the literature. Furthermore, all embolization's in Okuno *et al.* [104] were reported as technically successful (inhibited and/or reduced blood flow to target vessels) and there were no major adverse events reported during this study.

Analogous clinical results (n=20) were reported for GAE in a clinical study conducted by Bagla *et al.* [105]. A reduction in VAS scores at 1 month (22 mm) and 6 months (31 mm) from baseline (76 mm) was demonstrated (Fig 1.7). Additionally, there was a decrease in total WOMAC scores at 1 month (24), 3 months (31) and at 6 months (31) from baseline (61) (Fig 1.8). The mean decrease at 6 months compared to baseline, for both VAS and total WOMAC scores were 44 and 31 respectively (corresponding with an 85% and 80% clinical improvement) and were considered significant [105].

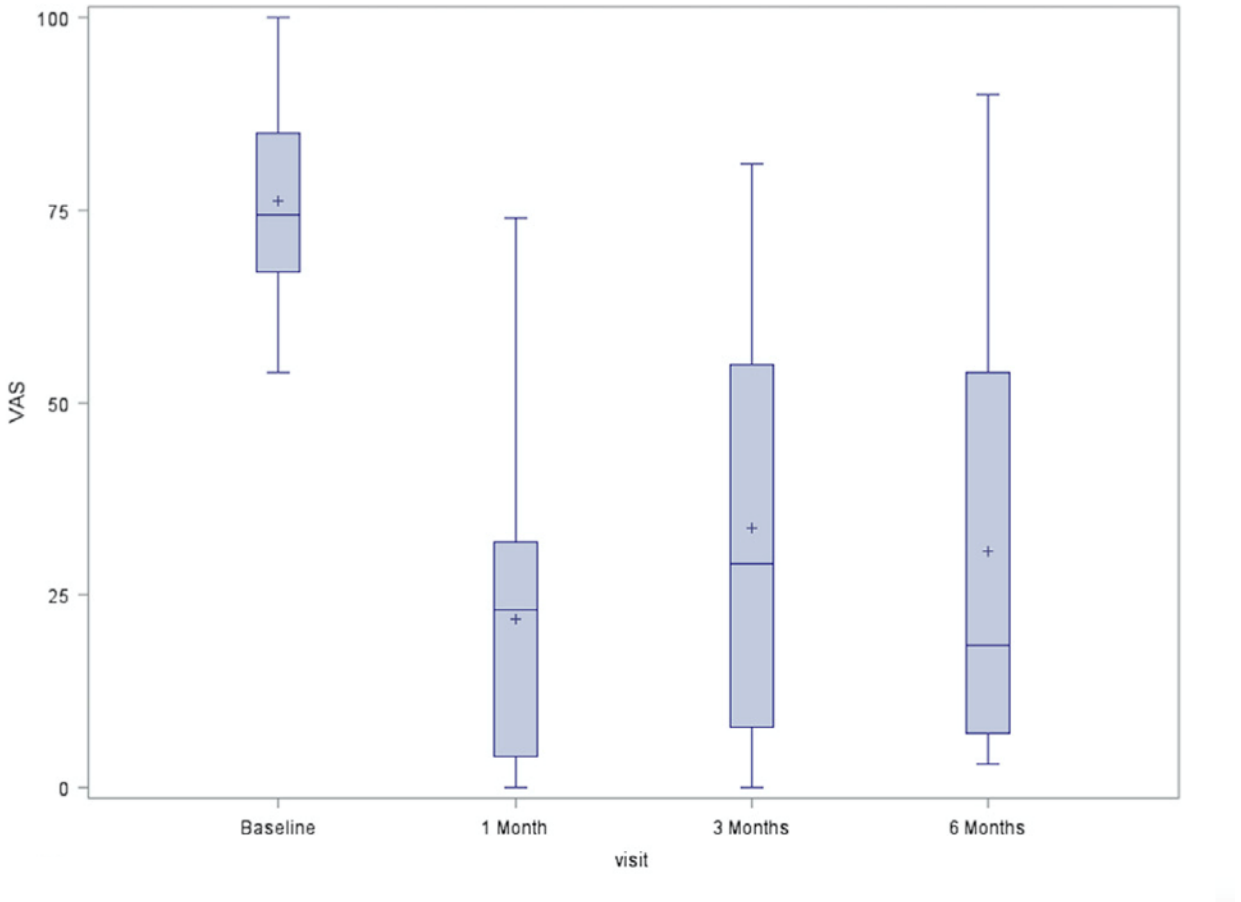

Figure 1.7: Box plot demonstrating VAS scores for patients post GAE at baseline, 1 month, 3 months, and 6 months. Adapted from [105].

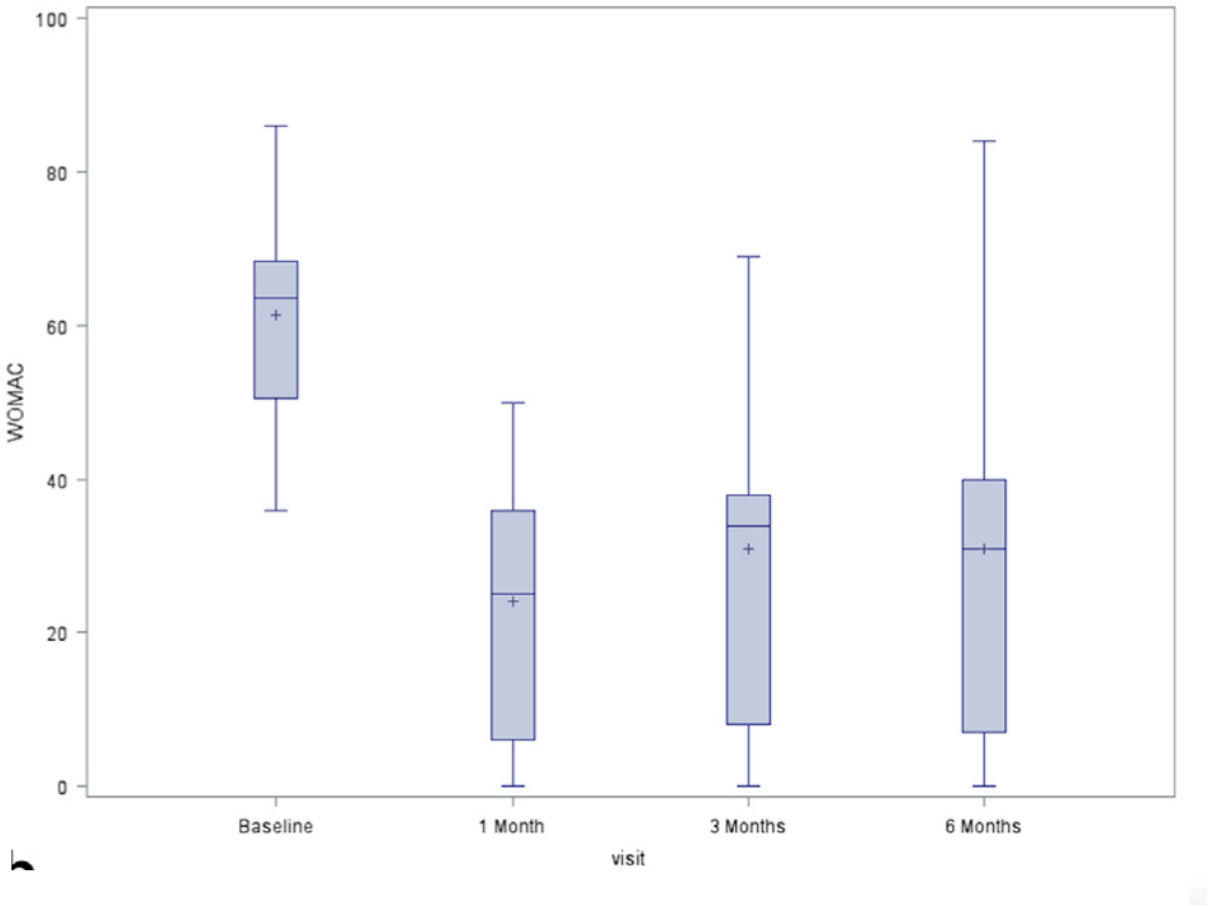

Figure 1.8: Box plot demonstrating total WOMAC scores for patients post GAE at baseline, 1 month, 3 months, and 6 months. Adapted from [105].

The clinical improvement at 6 months for both WOMAC (80%) and VAS (85%) are considered clinically significant [105]. Additionally, and in a similar finding to Okuno *et al.* [104], 65% of patients reported using fewer analgesics on a daily basis following GAE. The observed adverse events were associated with inappropriate particle size distribution (PSD) comprising skin discoloration (resolved within 3 months) and great toe plantar numbness (resolved within 2 weeks). Both adverse events were believed to be the result of non-target embolization due to inappropriate particle size (i.e., <100 μm) [105]. Despite reports of adverse events, both clinical studies by Bagla *et al.* [105] and Okuno *et al.* [104] reported this procedure as both feasible and safe for alleviating patient pain. Furthermore, the duration of pain relief following GAE (one to two years) outlasts conventional therapies that typically provide short-term pain relief (ca. 3 months) and/or result in treatment-related adverse effects (Table 1.6). Thus, it appears that GAE safe and efficacious but also provide sustained pain relief compared to traditional therapies. Based on the breakthrough clinical data, the clinical efficacy of GAE is now being further assessed, and the effectiveness of the procedure is encouraging to patients, regulators, and physicians alike.

Table 1.6. Therapies for KOA and their duration of efficacy in addition to evidence from both clinical studies and the literature to support and/or not support each therapy.

Therapy	Duration of pain relief	Evidence supporting therapy	Evidence not supporting therapy
GAE	• 1-2 years [104, 108].	• Shown to clinically improve pain due to OA [104, 105]. • Shown to have long-term pain relief and reported safe [104, 108]. • Few adverse events that typically resolve on their own [105].	• Few clinical studies published supporting efficacy and safety. • Risk of adverse events [105].
Topical NSAIDs	• Performs similarly to placebo at 2 weeks. • Should only be used short-term [109].	• Diclofenac has been shown to have a clinically meaningful effect on pain [40]. • Short term benefit.	• Risk of serious adverse events with long-term use [21, 26]. • Risk of kidney injury "more than doubles" [110] in individuals >65 years. • Risk of hospitalization due to heart failure is doubled [110]. • Individuals >65 years and those taking NSAIDs long term are considered high risk patients [110]. • Leading cause of "drug-related morbidity" with long-term use [41].
Opioids	• Shown to have a modest benefit for pain management for 3 months-1 year [28].	• Small benefit compared to placebo in reducing patient pain [45].	• Risk of toxicity for non-tramadol opioids [28]. • Patients using non-tramadol opioids have 3x increased risk of experiencing serious adverse events [45]. • Adverse events due to tramadol resulted in significant patient withdrawal from the study [45]. • Use may contribute to opioid epidemic [48].
Hyaluronic Acid Intra-articular injections	• Shown to have benefit up to 24 weeks [35].	• Suggested modest positive benefit on pain [23].	• Mixed evidence supporting efficacy. • Studies with low risk of bias unable to support clinical benefit [28]. • Increased risk of serious adverse events [35].
Corticosteroid Intra-articular injections	• Short-term efficacy of 3 weeks [57]. • Shown to have efficacy up to 6 months [36].	• Shown to reduce patient pain [36, 57] .	• Evidence demonstrating may result in cartilage volume loss and OA progression [26, 58]. • Can only receive a maximum of 4 injections per year [59, 60].

GAE differs from existing treat-to-target therapies by simultaneously targeting multiple mechanisms that contribute to OA pain. Traditional treat-to-target approaches focus on a singular mechanism which contributes to and/or facilitates the progression of OA. As demonstrated in Table 1.6, existing approaches result in short-term efficacy and/or little to no clinical benefit versus GAE. Existing therapies that do provide clinical benefit today typically have treatment-associated adverse events that out-weigh the benefit of the therapy and/or have a suggested role in contributing to the progression of OA. Therefore, GAE provides a unique and exciting approach to target both nerve pain (central and peripheral sensitization) and local pain (at the knee) over the long term for patients living with KOA.

1.1.6 Treat-to-Target: Geniculate Artery Embolization

Reflecting back to emerging pain theories for OA, pain at various stages of OA has been described as neuropathic with emerging evidence and clinical presentation supporting the idea of peripheral and central sensitization driving pain in OA. Nerves, specifically perivascular nerves, are shown to arise due to the pathophysiological conditions in the joint and grow alongside the abnormal vasculature that arises due to angiogenesis. It is understood that both "growing and damaged peripheral nerves display sensitization" [91] and it is believed that nerves may become further sensitized, due to factors in the environment that can stimulate peripheral sensitization. Therefore, it has been suggested that angiogenesis may drive the pain experience in OA, via neo-innervation [91]. Angiogenesis is largely driven by inflammation and the various conditions (Fig. 1.9) within the joint that appears as OA progresses. Inflammation is now recognized to play a vital role in driving the various changes within the joint and facilitate a vicious cycle that furthers the symptoms and physical progression of OA.

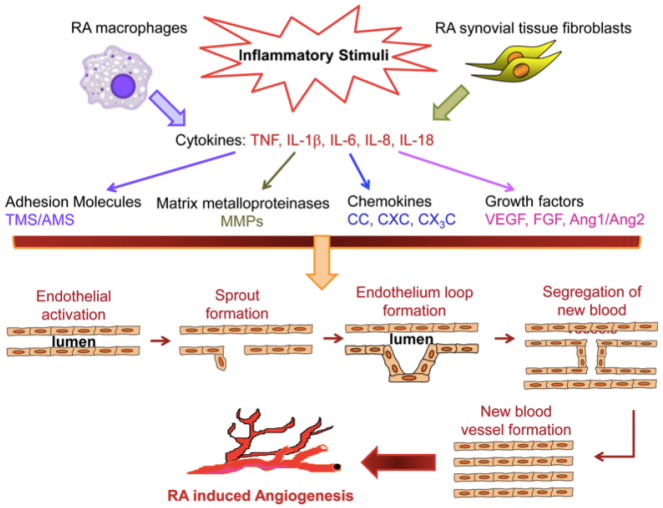

Figure 1.9: Inflammatory stimuli facilitate the production of inflammatory cytokines which then modulates protein expression (MMPs, chemokines, growth factors, and adhesion molecules). These proteins stimulate endothelial cell migration and proliferation which promotes angiogenesis [111].

By embolizing the abnormal vasculature that arises, GAE may disrupt the *"inflammatory cycle"* (Fig. 1.10) and as a result slow down OA progression [105]. However, the mechanisms of GAE remain poorly understood and there is ongoing research to understand the role GAE plays in breaking the pathological cycle of OA. Based on a review of the literature and evaluating the role of the abnormal vasculature in other conditions (such as RA), it appears GAE may target a variety of distinct mechanisms that contribute to pain in OA as opposed to traditional treat-to-target approaches.

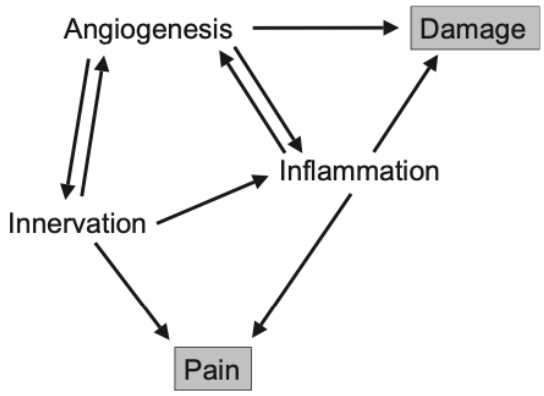

Figure 1.10: Cyclic nature of angiogenesis, innervation, and inflammation in OA and contribution to pain / damage in OA [91].

In RA, the abnormal vasculature plays a role in sustaining inflammation, inflammatory cell recruitment, and cell infiltration into tissue [88, 89]. Inflammation within the joint may be indirectly targeted by elimination of the abnormal vasculature, which may subsequently provide a novel mechanism to control inflammation and eliminate the path whereupon immune cells enter into tissues [83]. By reducing the influx of immune cells into the joint, there may be a reduction of inflammatory mediators being produced in addition to oxygen and nutrient demand from increasing cells which reduces the potential of hypoxia from occurring (Fig. 1.11). Both inflammatory mediators and hypoxic conditions stimulate angiogenesis and by potentially eliminating / reducing the above via embolization the process indirectly eliminates / reduces the pro-angiogenic signals being produced as a result of these environments within the joint (Fig. 1.11). Additionally, by eliminating inflammation and inflammatory mediators within the joint, mechanism which stimulate peripheral sensitization are reduced and may result in overall pain diminution in patients with OA. Both angiogenesis and inflammation stimulate each other and are implicated in facilitating patient pain. As a result of embolization (via GAE), numerous mechanisms that contribute to patient pain and OA progression may be targeted, and this cyclic loop may be broken [91].

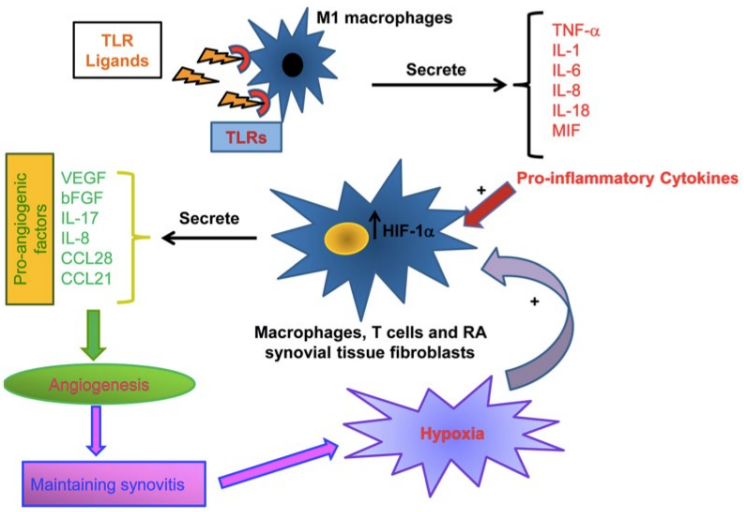

Fig 1.11. Stimulation of toll-like receptors results in the production of pro-inflammatory cytokines / pro-angiogenic factors. Leukocyte migration reduces oxygen within the joint and promotes hypoxia and hypoxia-inducible factor-1α (HIF-1α). Together pro-inflammatory cytokines and HIF-1α stimulate leukocyte production of pro-angiogenic factors, facilitating and maintaining angiogenesis [111].

By eliminating the mechanism(s) which facilitates nerve growth and nerve sensitization, both central sensitization and peripheral sensitization may be indirectly targeted. Embolization of the abnormal vasculature may result in an overall reduction in pro-inflammatory and angiogenic signals, which may result in the complete reduction of nerve sensitizing agents (Table 1.4) and perivascular nerves. In the absence of these nerve sensitizing agents, the mechanism(s) which stimulates peripheral sensitization is reduced and/or eliminated. Both continual peripheral input [70] and peripheral sensitization [73] have been demonstrated to drive central sensitization. By eliminating the opportunity for both peripheral sensitization and constant peripheral stimulation to occur central sensitization may also be eliminated [73]. However, the mechanism(s) which facilitates the sensitization of nociceptors in OA are still incompetently understood [21] and further investigation into these mechanism(s) is required. By reducing inflammation and perivascular nerve growth into tissues, peripheral and central sensitization is also inhibited/reduced. Therefore, GAE appears to provide a unique and multitargeted approach to manage patient pain due to KOA. Irrespective of the underlying mechanism, which will likely be further elucidated over the coming years, the clinical outcomes associated with the procedure are significant and represent an exciting opportunity to effectively manage the pain of KOA for millions of patients.

1.2 GAE Microspheres

1.2.1 Current GAE Microspheres

Current microsphere technologies utilized in GAE are not indicated for the procedure and have been used off-label. Presently, there is no approved or cleared device (i.e., embolic microspheres) for the indication of GAE. The published clinical data which is exclusively related to GAE (excluding GAE for hemarthrosis) utilizes either Embozene and/or imipenem/cilastatin sodium (IPM/CS) as the embolic agent(s).

Okuno *et al.* [104] conducted one of the earliest studies evaluating the safety and feasibility of GAE using IPM/CS. IPM/CS is an embolic agent which, when mixed with contrast media, forms globules (10-70 μm) that behave as the embolic material [104]. Despite supporting the clinical feasibility of GAE there are concerns regarding the use of IPM/CS for the intended purpose. A primary risk concerning the use of IPM/CS is the particle size (10-70 μm) of the globules that form when mixed with contrast media. As identified in a study by Bagla *et al.* [105], when particles <100 μm were utilized as embolic agents in GAE, off-target adverse events (e.g., plantar paresthesia) resulted. As a result, there is disquiet that patients may also experience off-target adverse events due to the small particle size of IPM/CS. Furthermore, IPM/CS is an antibiotic and in GAE is administered in low doses. Use of IPM/CS in GAE has prompted concern regarding the potential to contribution to antibiotic resistance, which is considered one of the "world's most urgent public health care problems" [112]. Inappropriate use of an antibiotic and subtherapeutic concentrations enables bacteria to undergo genetic alterations which can result in resistance to the antibiotic [113]. Additionally, IPM/CS cannot be used for every GAE procedure due to contraindications (i.e. allergy to IPM/CS) [104, 105]. Despite the risks and concerns associated with the use of IPM/CS, it has properties that make it unique from other existing embolic agent technologies in particular, and in respect of GAE, its transient persistence *in vivo* is an attractive property. In particular, IPM/CS has been shown to have a half-life of 10 hrs at 37 ºC in human serum [114]. A substantial benefit of utilizing a degradable embolic agent is that they completely degrade and are eliminated from the body. In this way, there may be a reduced risk of off-target embolization and "permanent alterations in histological architecture, vascular capacitance and / or injury" [115].

In contrast, Embozene is a permanent non-resorbable microsphere [116] and like IPM/CS has been used off label for GAE [104, 105]. Embozene microspheres have a hydrogel core made of polymethyl-methacrylate and a non-degradable ~30 nm thick Polyzene-F (poly-bis[trifluoroethoxy]phosphazene) shell [117]. Embozene is a class 2 medical device (USFDA) [116] and is intended for use in the "embolization of arteriovenous malformations and hypervascular tumors" [116]. Embozene deforms *in vivo* and the percentage deformation is dependent on the location of the target vessel for embolization, as seen in the

deformation difference between the kidney (22%) and uterine vasculatures (10%) [118]. Additionally, when evaluated for conformity to specific manufacturer's specifications, 39% (Embozene 700 μm) and 70.5% (Embozene 900 μm) are inside the indicated size specifications [118]. This data suggests that 61% and 29.5% of the product, respectively, does not satisfy the specific manufacturer's specifications and microsphere size within the dose will vary which may result in off-target embolization due to inappropriate PSD. The ability of Embozene to deform may also result in an increased risk of off-target embolization due to the ability of the microspheres to deform and occlude inappropriate vasculature. However, there are benefits to utilizing Embozene microspheres in TAE / GAE procedures. Embozene microspheres possess a Polyzene-F coating which *"reduces the inflammatory reaction"* [119] in both vessels and the area adjacent to the microspheres. Embozene microspheres have also been shown to reduce the production of *"vascular growth factors"* [119] following embolization. In a study by Stampfl *et al.* [120] Embozene microspheres were shown to have a reduced inflammatory response compared to Embosphere (another commonly used embolic agent for TAE), which was surrounded by a larger quantity of giant cells (formed via multiple macrophages to degrade foreign substances), at 4 weeks. This provides potential benefits to patients as it may reduce pain symptoms following TAE / GAE whilst also reducing the chance for treatment-associated adverse events (i.e., tissue necrosis). Additionally, there are cases where permanent embolic agents are more appropriate than degradable embolic agents such as occlusion of large vessels (i.e. splenic artery), small vessel embolization's where angiographic visualization of a bleeding artery is not possible, embolization of tumors, long-term occlusion is desired, and / or tissue necrosis is the desired outcome [121]. There may also be benefits to utilizing permanent embolic microspheres for GAE procedures as permanent microsphere has been well defined from a physical and chemical standpoint and have well established safety and efficacy attributes [122]. Additionally, permanent microspheres mitigate the risks associated with potentially hazardous degradation by-products and may result in the inappropriate occlusion of the targeted vasculature [122].

However, there is currently an on-going debate surrounding the use of permanent embolic microspheres for GAE and if they are an appropriate material for the indication. From a patient standpoint, the majority of the public prefer degradable materials rather than a permanent material [122]. From a physician standpoint, an initial market research report which consisted of interviews with intervention radiologists (IR) in the US (e.g., California, Nebraska, Illinois, New York, Virginia, South Carolina, and Florida*)* crystallized an overwhelming preference for a degradable microspheres for GAE [123]. Degradable microspheres were preferred over non-degradable microspheres for a variety of reasons, including the ability of the treating physician to repeat the process and re-embolize abnormal vessels for patients that do not achieve a clinically acceptable pain reduction. Additionally, the availability of an

alternative soluble microsphere for GAE would provide the IR community with the opportunity to move away from IPM/CS, which is logistically cumbersome to arrange and mix and is associated with several other side effects and issues as identified earlier and in the literature [123].

It is also important to consider that the embolic agents commonly used in GAE are considered off-label use. Concerns surrounding off-label use is the lack of information regarding both the benefits and risks [124] associated with employing off-label embolic agents for GAE. There is a lack of clinical data to support both the efficacy and safety of the embolic agents being used as a result and there is no regulatory approval process for these products to be used in GAE [124]. Additionally, it is important to note that to date there has been little discussion among leading experts in the field, performing GAE, on what the requirements are for an ideal embolic agent for GAE. This provides a unique and exciting opportunity to explore an embolic agent designed specifically for this procedure.

1.2.2 Ideal GAE Microspheres

To determine user needs and design inputs for an ideal microsphere indicated for GAE (Table 1.7) several one-on-one interviews were conducted with leading experts in the field. Initial interviews were conducted by TL Health (Philadelphia, USA) and followed up with additional interviews conducted on an international basis within the United States (Global Embolization Oncology Symposium Technologies (GEST)), and the European Union (Cardiovascular and Interventional Radiological Society of Europe (CIRSE) and the European Conference on Interventional Oncology (ECIO)). Through these interviews (n=20), and in addition to reviewing existing technologies, it was determined that an ideal microsphere technology indicated for GAE must effectively occlude the abnormal vasculature and in addition:

1) *Shall be* degradable – within 2-72hrs to ensure effective occlusion of the vasculature while balancing both safety (short contact) and efficacy (provide sustained pain relief) [125].
2) *Should be* imageable – on Computed Tomography (CT) and not confound Magnetic Resonance Imaging (MRI) [122, 126].
3) *Shall be* within a pre-determined PSD – of 100-300 μm to reduce risk of non-target embolization [105].
4) *Should* have a density preferably <2.3 g/cm^3– to sustain a suspension in commercially available contrast media (e.g. Omnipaque 350 or Isovue 370) to prevent sedimentation of microspheres and to reduce the risk of retrograde flow [127, 128].[1]

[1] *Should* have a density of >2.3 g/cm^3 and <4 g/cm^3 to permit microsphere delivery if a delivery device is provided.

5) *Shall be* Sterile – Complete sterilization of the medical device as per industry standards using γ-radiation [129, 130].

Table 1.7: The user needs and critical design inputs to establish feasibility for an embolic agent technology for GAE.

Requirement	Degradable	Safe	Effective Pain Relief	Imageable	PSD	Density	Sterile
User Needs	*Shall* degrade and be considered degradable as per ISO10993-1	*Should* have a short contact time	*Shall* effectively occlude vasculature	*Should* be imageable on modalities used within the procedure	*Shall* have particles >75 μm and <500 μm	*Should* be ~isodense with commercially available contrast media	*Shall* be sterile
Initial Design Input(s) for this Phase of the Project	100% mass loss between 2-72 hrs	Safe chemistry, MOS >1, unintended constituents deemed acceptable per ICH3QD [131], and Degradable in <24 hrs	Provide sustained pain relief >1 year, to the patient via occlusion (by achieving hemostasis) of the abnormal vasculature via microspheres	Imageability within the range of 2500-12040 HU on CT [132]	100% of particles within 100-300 μm	<2.3 g/cm^3	γ-radiation between 25-30 kGy as per the appropriate sections in ISO11137 [129, 130]

It is crucial at this stage (feasibility/proof of concept) that the prototype microspheres have a tailorable degradation timeframe to provide flexibility to optimize the embolic technology as it progresses through the development cycle. The user needs for degradation are such that the microspheres, *shall* fully degrade within a range of 2-72 hrs as per Table 1.7. This timeframe was further informed by risk-based evaluations of the intended use and indications for use which considered both safety (low toxicological risk, MOS >1, absence of unintended constituents that are not deemed acceptable as per ICH3QD [131], and short contact time) and effectiveness (pain relief via occlusion of the target vasculature). A degradation time frame of <2 hrs does raise questions of efficacy and not necessarily safety. An embolic agent that degrades in <2 hr may have limited contact time with the vasculature and may result in ineffectual occlusion of the vasculature [133]. As a result, effective pain relief will not be achieved as the mechanism(s) believed to be facilitating pain will remain unobstructed and continue to stimulate / signal pain. Conversely, an embolic agent with longer degradation time frames (weeks to several months) may result *in "a chronic inflammatory response, vessel remodeling, and a fibrotic reaction"* [134] as seen in existing slow

degrading embolic agent technologies (e.g., gelatin sponge particles) [134]. There are also differential endpoints to address based on the microsphere's duration of exposure (time to complete degradation) within the vasculature. As per ISO-10993-1 [125], there are fewer endpoints to address (i.e. recognition of low risk to patient) when considering a microsphere which degrades in <24 hrs; reflecting the higher safety profile for transient materials. Therefore, to balance the concerns regarding safety and efficacy a time period of 2-72 hrs is being established for this phase of the project. A degradable upper limit of *ca.* 72 hrs provides the flexibility to tailor the degradation time frame to best suit the user needs for GAE in addition to identify the most appropriate time which balances both safety and efficacy.

The user needs for imageability are such that the microspheres *should* have imageability within the range of 2500-12040 HU on CT [132] and not confound MRI. Imageability may provide clinically meaningful data to determine both i) the success of embolization and ii) spatial distribution of the microspheres within the target vessels providing potential insights on safety and effectiveness [135]. Traditional embolic agents are not visible and require the use of contrast media to assess the clinical endpoint [135]. The ability to visualize embolic microspheres on CT provides practitioners with the capacity to visualize the microspheres during GAE and post-procedural follow-ups. This may also address safety considerations by providing the spatial distribution of the microspheres during and after the procedure *in vivo,* enabling practitioners to determine the source of any off-target adverse events and the location of the microspheres. Additionally, it is critical that these microspheres do not confound imaging on MRI as these scans (specifically R1- and R2-weighted scans) are commonly used as follow-up assessment tools for TAE procedures [115] and GAE [105]. As such, it is important to ensure these microspheres do not perturb the images post-embolization and negatively effect the user's ability to "evaluate treatment efficacy" [115] and / or discern critical structures / pathologies especially if repeat embolization's are required. Conversely, if imageability of the microspheres is not attainable traditional embolic agent imaging methods can be employed *(i.e., imaging with contrast media)*. During delivery of the microspheres in embolization procedures, such as TAE and GAE, contrast media is combined with the microspheres. This blending then provides the "temporal and spatial distribution of microspheres with the target tissue" [126]. Therefore, if imageability of the microspheres is unattainable, delivery of the microspheres *in vivo* will remain feasible. However, they will have limited spatial resolution compared to an imageable embolic agent.

The user needs for PSD is such that the microspheres *shall* have a PSD of 100-300 μm. A study conducted by Bagla *et al.* [105] identified that off-target adverse events *(i.e. skin discoloration and plantar paresthesia)* were resulting due to a PSD of <100 μm being utilized in GAE in patients with KOA. Skin discoloration was attributed to the occlusion of "small cutaneous arterial branches" and plantar paresthesia

was believed to be the result of occlusion of "a branch of the tibial nerve that receives its vascular supply from branches of the popliteal artery" [105]. Therefore, it was suggested by Bagla *et al.* [105] that to overcome this limitation a larger microsphere PSD was required (100 μm) to prevent occlusion of smaller off-target vessels and/or nerves. To resolve the risks and off-targets adverse effects associated with the initial PSD of 75 μm, Bagla *et al.* [105] continued conducting GAE procedures in patients with KOA with a PSD of >75 μm. After switching to a PSD of 100 μm there were "no further post-procedural neurologic changes" [105] observed. Furthermore, it was concluded at GEST that a PSD >300 μm is not preferred for GAE and more suitable for hemarthrosis embolization procedures. In hemarthrosis embolization procedures, a PSD <300 μm was not employed due to "increased rates of skin erythema or necrosis" [136]. Additionally, a PSD <250 μm was associated with cutaneous ischemia and therefore not utilized in this procedure [136]. Therefore, following the attendance of GEST, the consensus between leading experts in the field is that a PSD of 100-300 μm is the safest and most optimal PSD for GAE.

The user needs for density are such that the microspheres *shall* have a density of <2.3 g/cm^3. In order to successfully deliver and suspend the microspheres for GAE, the microspheres must have densities within close proximity to the densities of existing and commonly used contrast medias with densities >2 g/cm^3 (e.g., Omnipaque 350 (2.2 ± 0.1 g/cm^3)). It has been demonstrated within the literature that embolic agents with similar densities to their paired contrast media have reduced sedimentation and reduced aggregation in the catheter prior/during microsphere delivery [128]. Additionally, microspheres with similar density to their paired contrast media display a prolonged suspension time in media which will provide Interventional Radiologists adequate delivery time of the microspheres before being required to re-suspend the microspheres [128]. Conversely, high-density microspheres have been shown to have increased difficulty for both handling and administrating the microspheres, as a result of fast sedimentation [128]. Thus, the microspheres must have a density that is isodense with contrast media to minimize human factors risk in handling the product under clinical conditions. Based on these design requirements, this project will seek to examine the feasibility of soluble borate glasses to act as a transient embolic agent for use in GAE. Glass materials provides a promising avenue for discovery in this regard given their unique and modifiable properties.

1.3 Glasses as Soluble Embolic Agents

1.3.1 Borate Glasses

Borate glasses have unique and tailorable properties that may make them ideal candidates for use as embolic microspheres and are suited to meet the design inputs established in Table 1.7. The most

distinctive and important property of borate glasses is the modifiable degradation properties they possess [137] which make them distinct from silicates.

Boron oxide (B_2O_3) behaves as an excellent glass former and will form glass with a wide variety of network modifiers over an extensive range of compositional ratios [137]. Furthermore, the structure and properties (e.g. density and radiopacity) of borate glasses may be modified with the appropriate selection and inclusion of network modifiers within the molecular architecture of the glass [138]. The unique "extema behaviour" [139] that borate glasses exhibit in response to specific quantities of network modifier(s) (referred to as the borate anomaly) provides an opportunity to further tailor the unique properties of borate glasses to meet the required properties for several indications where degradable medical devices are sought.

The basic structural unit of borate glasses is $BØ_3$ where the boron atom is surrounded by three bridging oxygens (Ø refers to bridging oxygens) in a trigonal configuration [139]. The basic superstructural unit in the borate glass network is the boroxol ring which is comprised of multiple $BØ_3$ structural units and is connected to other boroxol rings by trigonal $BØ_3$ structural units [139]. In addition to the boroxol ring, the borate glass network consists of a variety of superstructural units whose presence is influenced by the availability of basic structural units and the concentration of network modifier(s) within the network [138]. The presence of various superstructural units, in addition to boroxol rings, can further modify the properties and structure of the borate glass by influencing the connectivity and packing within the network. Hence, the dissolution rate of the glass will depend on both the basic structural units and borate species present in the borate network [140]. Consequently, the degradation of borate glass networks may be altered based on the borate species and basic structural units present within the glass network [140]. This unique property of borate glasses provides a basis to potentially tailor the degradation time frames of a particle to meet the 2-72 hrs user need previously established.

Various quantities of network modifier modulate the presence of these basic structural units which also play a role in the final properties and structure of the borate glass. With the addition of network modifiers (0-30 mol%) trigonal $BØ_3$ are converted to tetrahedral $BØ_4^-$ basic structural units [138, 139, 141] as per Fig 1.12. Further addition of network modifier (30-70 mol%) results in a decrease of $BØ_4^-$ structural units and an increase in $BØ_3$ structural units and the formation of non-bridging oxygens (NBO's) [138]. These changes in basic structural units can increase / decrease the degradation of the glass network *(based on the presence and quantity of the basic structural units)* in addition to the ion release and final pH of the solution during/post degradation. The cation from the network modifier itself also plays a role in the modification of the glass properties and connectivity [142] by modifying the network structure further to fulfill the cation's own requirements [141].

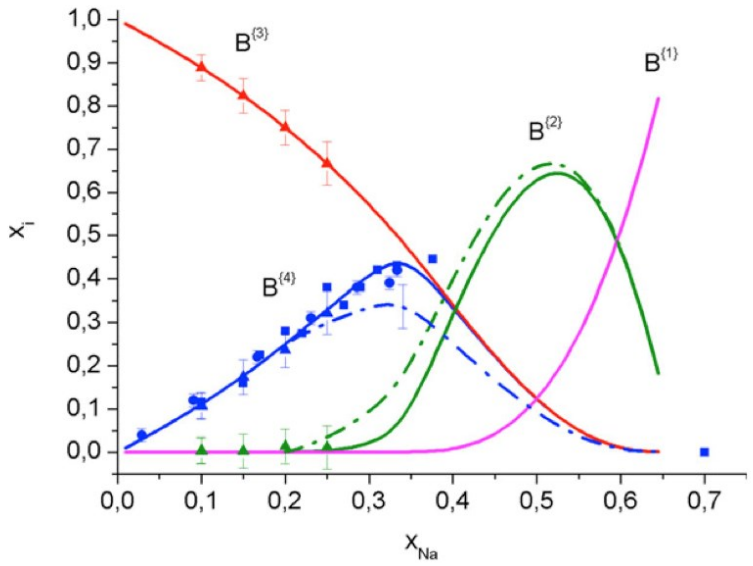

Figure 1.12: Structural units that form in response to specific quantities of network modifier added to the borate glass network. $B^{(n)}$ represents the borate structural units and (n) represents the boron coordination number [138].

Succinctly, the degradation rates of the borate glass network are tailorable based on the i) the structural units present in the glass network and ii) the network modifier added to the borate glass network [142]. From a mechanistic standpoint, degradation of these networks is believed to occur via hydration and hydrolysis. Hydration is believed to play a significant role in modifying the degradation of the borate glass network. George & Brow [140] demonstrate in the following equations (Eqn. 1 & 2) how hydration of the cation from the network modifier influences borate glass solubility (see overleaf):

Eqn 1. $(Na{+}[B\text{Ø}_4]^-)_{glass} + H_2O \longrightarrow (H^+[B\text{Ø}_4]^-)_{glass} + (Na^+ + OH^-)_{sol'n} \longrightarrow (B\text{Ø}_2OH)_{glass} + (Na^+ + OH^-)_{sol'n}$

Eqn 2. $(B\text{Ø}_2O^-Na^+)_{glass} + H_2O \longrightarrow (B\text{Ø}_2OH)_{glass} + (Na^+ + OH^-)_{sol'n}$

The sodium (Na^+) cation (Eqn. 1 & 2) balances the negative charge from the tetrahedral $B\text{Ø}_4^-$ and the non-bridging oxygens [140]. Hydration occurs in equation 1 when water interacts with the alkali and/or alkaline earth borate glass and replaces the cation with the proton from the water. This interaction between the proton and tetrahedral $B\text{Ø}_4^-$ results in "an unstable four-coordinate borate unit" [140], and to achieve a lower energy configuration the tetrahedral $B\text{Ø}_4^-$ converts to trigonal boron (losing a bridging oxygen) with a stable OH^- unit [140]. The rate at which the glass degrades is also dependant on the hydration rate of the

cation from the network modifier [140]. A similar reaction occurs for equation 2 where the proton switches with the cation and a hydroxylated trigonal boron unit forms [140]. Both hydrolysis and hydration play a major role in the dissolution rates of borate glasses with a defined role for the network modifier in the solubility of borate glasses. Cations that form more stable bonds and/or interactions with the boron and/or oxygen atoms result in a slower dissolution rate and therefore a slower degradation rate. Cations that have weaker interactions with the boron and/or oxygen atom results in faster hydration followed by hydrolysis. This further demonstrates why understanding the role the network modifier plays in the borate glass network is critical in order to understand the solubility of the borate glass and the changes in both glass properties and structure.

The other mechanism believed to play a significant role in the degradation of the borate glass is hydrolysis. During hydrolysis (Eqn. 3 & 4), water attacks the bridging oxygen between two trigonal boron units resulting in bond cleavage between the bridging oxygen and the boron atom [140, 142]. Following this, a non-bridging oxygen is formed, and OH^- is added to the boron atom [142] resulting in the production of boric acid (Eqn. 3 & 4) [140]. The following equations (Eqn. 3 & 4) below demonstrate the possible hydrolysis mechanisms of trigonal $B\text{Ø}_3$ structural units in water [140]:

Eqn 3: $(\text{Ø}_2\text{B} - \text{O} - \text{B}\text{Ø}_2)_{glass} + 3\text{H}_2\text{O} \longrightarrow 2\text{B(OH)}_3\text{(sol'n)}$

Eqn 4: $(\text{B}\text{Ø}_2\text{OH})_{glass} + \text{H}_2\text{O} \longrightarrow \text{B(OH)}_3\text{(sol'n)}$

Consequently, glasses with higher percentages of $B\text{Ø}_3$ structural units and structural units with non-bridging oxygens ($B\text{O}\text{Ø}_2^-$ and $\text{BO}_2\text{Ø}^{2-}$) will be more susceptible to hydrolysis and have faster dissolution rates than more interconnected/crosslinked counterparts [143-145]. To meet the required design input of a degradation rate of 2-72 hrs, the percentage of $B\text{Ø}_3$ structural units and non-bridging oxygens will be required to remain at a low concentration within the glass network, as a large concentration of these units will result in a glass that degrades in <2 hrs and therefore not meet the required design inputs. Additionally, a glass with an extremely high percentage of BO_4^- structural units may be too stable and resistant to degradation and as a result, degrade >72 hrs. By understanding the role of the basic structural units within the glass it is possible to tailor the degradative time frame to meet the design inputs and select the optimal quantity of network modifier(s) that will enable degradation in 2-72 hrs. Therefore, significant consideration of the network modifier and contiguous structures must be deliberated in order to anticipate and ensure the degradation time frame is compliant with the user needs and design inputs for an embolic agent technology indicated for GAE.

1.3.2 Modifier Ions

Despite the utility of borate glasses <2% of the published literature characterizes and examines these systems due to their lack of industrial applicability [115]. Of the existing literature which considers borate glasses, binary glass substitutions of alkali [141] or alkaline earth [146] network modifiers are the most highly characterized within the literature [147]. There has been increasing interest regarding ternary glass substitutions, specifically group one and group two substitutions [148], and how they affect glass properties and structure. Existing studies suggest that ternary glass properties cannot be predicted based on binary glass substitutions [115] and this area of borate glass literature is more poorly understood. Due to fewer studies considering and characterizing both group one and two substitutions within a ternary borate glass network, the precise chemical and physical properties of these glass network are less predictable. Therefore, group one and two substitutions within the ternary borate glass network require further evaluation. When considering how to modulate such networks to achieve the desired properties of the ideal embolic agent for GAE, careful consideration of the network modifiers is required in order to produce borate glasses with ideal properties (i.e., degradation and imageability) while balancing toxicological (and other biological response(s)) considerations.

Special consideration regarding the quantity of the network modifiers is required in order to select for optimal and predictable properties of the embolic agent that meet the required user needs and design inputs. The addition of 0-30 mol% network modifier into a borate glass network has been well characterized and understood. However, higher quantities of network modifiers (30-70 mol%) are not completely elucidated and the properties of borate glasses within this range are far less predictable due to the borate anomaly [138]. As such, in order to optimize the degradation and imageability of the borate glasses accurately, this thesis work will focus on glass prototypes within the range of 0-30 mol% network modifier (using both groups one and two substitutions). Additionally, in order to modify and control the degradation of the borate glasses, it is more ideal to remain within the 0-30 mol% network modifier range as the glasses will become more resistant to degradation due to the increasing connectivity of the glass network and tetrahedrally coordinated boron structural units. Larger quantities of network modifier (30-70 mol%) will increase the glasses susceptibility to degradation due to the reduced connectivity within the borate glass network and the formation of trigonal $B\emptyset_3$ structural units and non-bridging oxygens (Eqn. 3 & 4) [115, 138, 143].

The toxicity of network modifier cations and the by-products released from the glass via degradation is also an important consideration when selecting for network modifiers to be used in the embolic agent. It is critical to select network modifiers that do not raise significant questions of safety and are deemed safe for patients. The network modifiers considered must have a toxicological threshold that

can be met when utilized in an embolic agent technology, without raising substantive or additional questions of safety. Likewise, the embolic agent must address and meet endpoints as per ISO 10993-1 (e.g. cytotoxicity, sensitization, irritation, systemic toxicity, subchronic toxicity, genotoxicity, implantation, and haemocompatibility) [125]. To satisfy questions regarding the health risks each candidate element presents, a toxicological risk assessment (TRA) (Table 1.8) was established using international best practise. To assess questions of safety for each candidate element, the safety profile for each element was assessed assuming worst-case scenario of dose and patient exposure. A worst-case scenario dose of 1 g was assumed per knee for a 70 kg patient and assuming technical failure a total of four doses in 3 years. Two degradation time frames were considered (24 and 72 hrs) to meet the compulsory user needs and design inputs. Barium (Ba^{2+}), gallium (Ga^{3+}), zinc (Zn^{2+}), and silver (Ag^{+}) were eliminated as candidate elements after assessment via the TRA (Table 1.8) as the dose for each element exceeded the tolerable daily exposure for both degradation timeframes *(<24 hrs and >24 hrs)*. Of the several candidate elements considered strontium (Sr^{2+}) and potassium (K^{+}) were selected based on their demonstrated safety profile and their anticipated role on imageability and degradation on the borate glass microspheres.

Table 1.8: Selection of modifier ions Sr^{2+}, K^{+}, Ba^{2+}, Ag+, Ga^{3+}, and Zn^{2+} assuming a 1 g dose for a 70 kg individual.

Network Modifier Cation	Degrade <24 hrs daily amount (mg/day)	Degrade >24 hrs daily amount (mg/day)	Tolerable Exposure (mg/day)
Strontium	10.03	6.34	6.02
Potassium	16.99	5.66	N/A
Barium	28.93	9.94	0.14
Silver	46.86	15.62	0.035
Gallium	30.28	10.09	2.058
Zinc	14.2	4.73	0.42

1.3.2.1 Strontium

Sr^{2+} was selected on the basis of being a group two-element, with the highest atomic number, which does not raise significant safety and toxicological concerns. Sr^{2+} has a large daily tolerable exposure (Table 1.8) and does not raise significant questions of safety compared to barium (0.14 mg/day), a potential radiopacifying group two-element**.** Sr^{2+} was selected due to its high atomic number which confers radiopacity to the borate glass so as to increase the probability of synthesizing a prototype that is imageable on CT [115]. Additionally, Sr^{2+} is expected to play a significant role in modifying and stabilizing the borate

glass network against degradation, providing a unique tool to optimize the degradation rate of the borate glass network [115, 137, 148]. Sr^{2+} is expected to reduce the solubility of the borate glass by acting as a cross-linker and increasing the network connectivity of the borate glass network [115, 137]. Sr^{2+} cations have been shown to create ionic bonds between itself and the non-bridging oxygens within the borate glass network [137] which stabilizes the network against hydrolysis [115]. Sr^{2+} has also been previously reported as predominately controlling the degradation rates of borate glasses and as such can be manipulated to optimize the degradation rate [137]. However, the extent to which Sr^{2+} will modulate these properties in the ternary system being investigated in this research is unknown.

1.3.2.2 Potassium

K^+ was selected as a candidate element for consideration in this project on the basis of being a group one-element with the highest atomic number which does not raise toxicological concerns as addressed in the TRA (Table 1.8). K^+ has been deemed to be safe for use in medical devices and humans and has a high toxicological threshold / low toxicological concern. Amongst safety considerations, the high atomic number of K^+ may increase the radiopacity of the ternary borate glass on CT [149, 150]. As a result, the inclusion of K^+ in conjunction with Sr^{2+} may produce an imageable borate glass microsphere.

Another consideration supporting the selection of K^+ was based on the suggested role of K^+ in a ternary borate glass network in conjunction with a group two-element. Group one-elements, such as Na^+, have been shown to increase the solubility of complex sol-gel bioactive glasses [151]. Due to the high reactivity of K^+ in water, it is expected that K^+ will increase the solubility of the borate glass microsphere and as a result, provide a mechanism to modify the degradation rate of the borate glass via the addition of varying quantities of K^+. K^+ is highly reactive in water, more so than Na^+, due to it's larger atomic radii and shielding effect caused by the additional octet of electrons which buffers the single outer electron from the attractive forces in the nucleus. As a result, less energy is required to remove the single outer electron, making K^+ more reactive than Na^+. This phenomenon can be employed to control the degradation rate of the glass microspheres by modifying the quantities of both K^+ and Sr^{2+} in the glass network. Furthermore, there has been no investigation completed on both K^+ and Sr^{2+} together in a ternary borate glass network. Thus, there is scientific interest to characterize how both K^+ and Sr^{2+} will modulate the glass network and its properties, including degradation and imageability.

1.4 Rationale for Design of Mixtures

In this work design of mixtures (DoM) was employed to understand the role of both K_2O and SrO in the glass network within the range of 1-30 mol% respectively, and in the range 69-90 mol% for B_2O_3. An *I-optimal* design [132] was selected to produce models that inform the effect of the modifiers on a variety of responses (e.g., %B3, %B4, density (ρ), and T_g) and provide the flexibility to optimize factors via a response surface optimization to best meet the design inputs for a microsphere technology indicated for GAE. The mixture components were set to establish the 16 glass compositions characterized in this work and the DoM software allows users to generate compositions within a desired range (in this work 0-30 mol%) and explore extremes (0 or 30 mol%) of each component to best understand the effects of the cations in the network. Each component of the mixture (B_2O_3, K_2O, and SrO) had their own criteria in order to generate compositions that contained a maximum total of 30 mol% modifier. Following modeling of the responses, coded coefficients were generated from the models which were used to quantify the relationship(s) and effect(s) of the cations in the network on the responses assessed. For example, a positive coefficient is indicative that the addition of the cation (e.g., +K) to the network will increase the response being assessed. Similarly, a negative coefficient is indicative that the cation has a negative effect on the response (e.g., -K) and that the addition of the cation to the network will reduce the response. For the regression models the coded coefficients generated from components interacting with each other, for example B_2O_3*K_2O, signifies the impact of the cations interacting together in the network. This information can then be utilized to tailor the response to meet the requirements for a particular indication (in this work GAE) via a response surface optimization. Finally, from these models, 3D surface response can be produced to visualize the effects of the cations in the network. These models can then be applied to various applications and fields within science, medicine, and industry to tailor K_2O and SrO borate glasses to a variety of applications.

1.5 The Problem Statement

Based on direct engagements with international users and key opinion leaders in the field of interventional radiology and GAE, provisional user needs and design inputs for a microsphere indicated for GAE have been identified. Borate glasses have been selected as a preferred material to produce the microspheres as they can be modified via the addition of various cations to meet the unique requirements of GAE. However, there remains a large gap within the literature relating to our understanding of the composition-structure-property relationships in complex alkali and alkaline earth borate glasses. These relationships first need to be elucidated to establish the probability of meeting the engineering design challenge using soluble borate networks. This presents an opportunity to i) explore fundamental

composition-structure-property relationships characterizing alkali and alkaline earth borate glass and ii) tailor a unique ternary borate glass to meet the requirements for a microsphere indicated for GAE. To do so, this work will be carried out through three main sets of experiments. The first set of experiments, explored in chapter 3, will aim to characterize the composition-structure-property relationships of K_2O and SrO modified borate glasses in addition to characterizing their dissolution behaviour and imageability on CT and MRI (where both dissolution and imageability are shown in chapter 4) followed by the effects of sterilization on the glass network. The following experiment, explored in chapter 4, will consider all inputs and generated data from this work in addition to a TRA to inform the selection of a preferred composition which best meets the requirements of a microsphere indicated for use in GAE. The preferred composition will then subsequently be subjected to processing as microspheres. In the last set of experiments, also addressed in chapter 4, the microspheres will be compared to the previously established characteristics of the preferred composition to determine if any modifications in properties occurred during processing. The microspheres will then be further characterized to assess dissolution behaviour in physiologically representative media and suspension time to inform clinical feasibility.

Chapter 2

Overarching Thesis Objectives

The overarching objective of this thesis work was to examine a variety of borate glass compositions modified with both K_2O and SrO to establish which composition(s) best fulfills the user needs and design inputs for a microsphere indicated for GAE. To achieve this, 16 borate glass compositions were produced, characterized, and screened using DoM to facilitate the selection of one or more compositions for subsequent and future analysis as an embolic agent. The specific, overarching objectives are listed below for this thesis:

- The first objective of the first experiment was to synthesize and characterize 16 glass compositions modified with both K_2O and SrO to elucidate the role for both K_2O and SrO on the composition-structure-property relationships within the borate glass network.
- The second objective of the first experiment was to screen the compositions for dissolution time *(in both 100% contrast media and saline)*, and imageability *(on CT and MRI)*, in addition to the impact of γ-radiation on the glass network. This work was conducted to screen out compositions that do not meet the requirements for a microsphere indicated for GAE and inform the selection of a preferred / optimized composition(s).
- The objective of the second experiment was to select a preferred glass composition(s) *(from one of the 16 compositions characterized in experiment one)* which best meets the pre-established requirements for a microsphere indicated for GAE. If a preferred composition was not identified from one of the existing 16 compositions, then a response surface optimization would be conducted (via DoM) to produce a new composition(s) for synthesis and subsequent recharacterization as per experiment one.
- The last objective completed in the third experiment was to further characterize the dissolution behavior of the selected / optimized borate glass(es) in physiologically representative media to better understand the dissolution behavior *in vivo.* Additionally, the suspension time of the glass(es) was assessed to determine their compatibility with existing embolic agents on the market.

Chapter 3

Mixture designs to investigate the role of alkali and alkaline earth cations on composition-structure-property relationships in ternary borate glass networks

R. A. Manchester[a], T. Z. Todorova[b], U. Werner-Zwanziger[c], D. Boyd[a,b,d]

[a]*School of Biomedical Engineering, Dalhousie University, Halifax, NS, Canada*

[b]*Department of Applied Oral Science, Faculty of Dentistry, Dalhousie University, Halifax, NS, Canada*

[c]*Department of Chemistry, Dalhousie University, Halifax, NS, Canada*

[d]*Department of Diagnostic Imaging and Interventional Radiology, QE II Health Sciences Centre, Halifax, NS, Canada*

[This document (doi: https://doi.org/10.1016/j.jnoncrysol.2021.120982) was completed by Remington Manchester with the supervision and guidance of Dr. Daniel Boyd. All the experiments were conducted by Remington Manchester (particle size distribution (PSD), density, molar volume, and the recharacterization of the glasses following sterilization) and/or in collaboration with other departments at Dalhousie University or external companies (^{11}B MAS NMR, x-ray diffraction (XRD), differential scanning calorimetry (DSC), and sterilization). Dr. Tsanka Todorova provided critical support throughout this work and aided in the data collection for both density and molar volume in addition to reviewing the manuscript. Dr. Ulrike Werner-Zwanziger from the Chemistry Department at Dalhousie University provided critical support and review of the manuscript regarding data and information surrounding ^{11}B MAS NMR. XRD measurements and data collection were conducted by IR Scientific. DSC measurements and data collection were conducted by ABK Biomedical. Nordion conducted the sterilization of all 16 compositions examined in this work. Remington Manchester, as first author, wrote the entirety of the manuscript and incorporated critical inputs from all co-authors. All co-authors were provided the opportunity to review and provide inputs into the final manuscript.

In this chapter, both objectives of the first experiment are encompassed excluding any imaging (CT and MRI) or dissolution data. The first objective of experiment one focuses on the synthesis, characterization, and modelling of all 16 borate glass compositions to better understand the role of both K_2O and SrO on the borate glass network. As such, the following experiments were conducted to meet the first objective in experiment one: PSD, XRD, ^{11}B MAS NMR, density, molar volume, DSC. To meet the second objective of experiment one, each composition was sterilized and then subsequently recharacterized (PSD, XRD, ^{11}B MAS NMR, density, molar volume, DSC) to assess the impact of sterilization on the glass network.

Prior to experimentation hypotheses were generated for both objectives contained within experiment one. As such, the hypothesis pertaining to the data collected and objectives in this work are listed below:

- ^{11}B MAS NMR will demonstrate increasing ratio of B4 to B3 coordinated boron structural units upon the addition of SrO or K_2O (from 0-30 mol%). As such Sr and K will have a coded coefficient >0 in the design of mixtures statistical processes.
- Glasses with high mol% SrO (mol% SrO > K_2O) will have larger densities than glasses with high K_2O due to the higher density of Sr (2.64 g/cm^3 [152]) compared to K (0.862 g/cm^3 [153]). Therefore, Sr is expected to have a coded coefficient that is >0 and >K in the design of mixtures statistical processes.
- High SrO glasses (mol% SrO > K_2O) will have higher glass transition temperature (T_g) than high K_2O glasses, due to the ability of Sr^{2+} cation to increase the network connectivity and create ionic

bonds with non-bridging oxygens within the network which will be evident when comparing T_g. As such, Sr is expected to have a coded coefficient >0 and >K for T_g in the design of mixtures statistical processes.

- Following sterilization, glasses with high mol% SrO are expected to experience minimal/no change in density due to the shielding effect Sr^{2+} cation provides to the glass via its cross-linking ability.
- Following sterilization, glasses with high mol% K_2O are expected to experience an increase in density due to the small cation size of K^+ enabling bond bending and conversion of B4 to B3 structural units in response to the high-energy gamma-rays.]

3.1. Abstract

Sixteen borate glass compositions, modified with K_2O and SrO, were established using a design of mixtures approach and were subjected to chemical and physical characterization (^{11}B MAS NMR, density, and glass transition temperature (T_g)). The analysis intended to establish the influence of K_2O and SrO on the composition-structure-property relationships for borate glass networks. The effects of γ-radiation on the glass networks were also examined to determine the impact that sterilization may have on the glass properties. Structural analysis showed that both K_2O and SrO influenced the fraction of three- and four-fold coordinated boron groups independent of the cation. Thermal analysis of the glasses revealed that SrO significantly increases the glass transition temperature while both SrO and K_2O have comparable impacts on glass stability. These data suggest that Sr^{2+} cations cross-link the networks. Contrastingly, K^+ appears to stabilize B4 structures. All sixteen compositions retained their chemical and physical characteristics following sterilization.

3.2. Introduction

Binary alkali borate glasses have been well examined and characterized in the literature, specifically where the alkali modifier content ranges from *ca.* 0-30 mol%. Within this range, it is understood that the percentage fraction of four fold coordinated boron groups (% B4) in the network, along with glass transition temperature (T_g), and density (ρ) all increase in a predictable and linear fashion based on the quantity of alkali element in the network [138, 141, 154, 155]. The literature also establishes that the % B4 structural units within a borate network is dependent on the alkali cation itself, with larger alkali cations maximizing the % B4 units at lower mol% values. These observations are critical from a glass design standpoint since there is a direct correlation between % B4 and the linear increase in T_g and ρ in the range *ca.* 0-30 mol% alkali modifier [154-156]. For example, Zhong and Bray [156] have established that the increase in T_g, seen in alkali borate glasses, is attributable to an increase in the % B4 and thereby, an increase in the network cross-linking via 3-dimensional bonding. Similarly, alkaline earth borate networks parallel this linearity in structure and properties (i.e. % B4 and T_g) associated with alkali earth networks in the range *ca.* 0-30 mol% [146, 157]. Despite these similarities, differences in alkali versus alkaline earth networks do exist. For example, alkaline earth cations with increasing field strength are associated with a decrease in % B4 compared to lower field strength alkaline earth cations at the same mol%, whereas in alkali borates the opposite trend is observed [146]. Furthermore, and unlike alkali modified networks, alkaline earth networks typically have higher T_g values which is associated with the possible cross-linking role alkaline earth cations may play within borate networks [157].

In contrast to simple binary alkali borates, the phenomenon of the mixed alkali effect (MAE) is manifested as a departure in linearity when assessing structure and properties such as % B4 and T_g. To illustrate the MAE, Vegiri *et al.* [158] examined ternary Li-Cs-B oxide glasses and showed a departure from linearity in the fraction of B4 units being formed with the addition of mixed alkali elements in the range of 0-30 mol%. These changes are believed to occur due to a difference in i) ion size and ii) ion field strength, which results in cations occupying different sites within the network and modifying the structure accordingly [158]. Kamitsos *et al.* [159] supports these observations, and reported an increase in the formation of non-bridging oxygens (NBO) and a reduction in B4 units with the addition of two dissimilar alkali cations. This is in contrast to the linear increases in B4 structural units seen in binary alkali borate glasses with the addition of alkali content up to *ca.* 30 mol%. More recently, Kojima [155] has reinforced these observations by reporting that the % B4 units is lower in mixed alkali glasses than in some of their corresponding binary borate glasses. Furthermore, Kojima [155] correlated composition and structure with T_g and showed that T_g *decreases* to a minima at *ca.* 20 mol% for Li and Cs borate glass ($0.28\{(1-y)Cs_2O$-$yLi_2O\}$-$0.72B_2O_3$) where y=0.2. Despite the predictability and linearity of binary alkali borate glass,

especially with respect to T_g (in the range up to *ca.* 30 mol%), the addition of dissimilar alkali cations to the borate network results in deviation in T_g from all linearity and predictability as seen in binary borate glasses. Similarly, a phenomenon referred to as the mixed alkaline earth effect (MAEE) is known to occur in borosilicate and aluminosilicate glasses. Similar to the mixed alkali effect (MAE), the MAEE is manifest as a significant deviation in linearity of glass properties. It was recently elucidated in the literature that the mechanism governing this phenomenon may be associated with a "shift in [the] angle around oxygen in the cation-oxygen-cation bond in the glass network" [160]. Ding *et al.* [160] further attributes the deviation in linearity to the variation in mixing energies that arises due to the dissimilar cation sizes which impact the "most energetically favorable structural configuration" [160] and therefore, overall glass properties and structure. Collectively these data demonstrate the complexity of borate glasses even within highly characterized ranges of network modifier. What is less clear in the literature is the effect of mixing alkali and alkaline earth elements in borate networks. As a result, there is benefit in systematically evaluating and establishing the fundamental impacts of mixed alkali and alkaline earth cations on borate glass networks from a chemical and physical standpoint. This knowledge is fundamentally important as the applications for borate glasses have increased, especially in medical, biomedical, and industrial applications [161-164]. Within some of these applications (e.g. medical and biomedical), sterilization of these glasses is required to eliminate pathogens [165] and minimize the risk of infections [166]. Accordingly, there is also a need to establish the effects of sterilization on the physical and chemical properties of such networks.

To the best knowledge of the authors, there is a lack of theoretical and experimental data on ternary borate glasses, where K_2O and SrO are used as glass-network modifiers. Accordingly, the primary objective of the current study is to investigate the chemical and physical properties of ternary high borate glass networks with potential for biomedical and industrial applications.

3.3. Materials and methods

3.3.1. Material design and synthesis

The compositions of each glass were established using Design-Expert Software (Version 12.0.9). A design of mixtures *I-optimal* quadratic model was utilized based on three components *(B_2O_3, K_2O, and SrO)* and included five replicates for a total of 16 'runs' *(i.e., compositions)*. The design constraints based on mol% for each component are provided in Table 3.1 and yield 16 glass formulations as identified in Table 3.2.

Table 3.1: Mixture Components and Design Constraints Summary.

Name	Units	Minimum	Maximum	Coded Low	Coded High
B_2O_3	Mol %	69	90	+0 ↔ 69	+0.724138 ↔ 90
K_2O	Mol %	1	30	+0 ↔ 1	+1 ↔ 30
SrO	Mol %	1	30	+0 ↔ 1	+1 ↔ 30
		Total =	100.00	**L_Pseudo Coding**	

Table 3.2: Glass compositions for the 16 prototype glasses by weighed out mol%. Within the table there are five replicate compositions consisting of 1 and 13, 4 and 8, 5 and 7, 6 and 12, and 9 and 10.

Glass Identified	B_2O_3	K_2O	SrO
BKSA 1*	**69.00**	**30.00**	**1.00**
BKSA 2	**75.79**	**8.74**	**15.47**
BKSA 3	**90.00**	**8.28**	**1.73**
BKSA 4†	**83.55**	**15.45**	**1.00**
BKSA 5‡	**69.00**	**15.53**	**15.47**
BKSA 6ˆ	**69.00**	**1.00**	**30.00**
BKSA 7‡	**69.00**	**15.53**	**15.47**
BKSA 8†	**83.55**	**15.45**	**1.00**
BKSA 9¤	**79.37**	**1.00**	**19.63**
BKSA 10¤	**79.37**	**1.00**	**19.63**
BKSA 11	**69.00**	**8.24**	**22.76**
BKSA 12ˆ	**69.00**	**1.00**	**30.00**
BKSA 13*	**69.00**	**30.00**	**1.00**
BKSA 14	**82.72**	**8.93**	**8.35**
BKSA 15	**90.00**	**1.00**	**9.00**
BKSA 16	**73.91**	**20.40**	**5.69**

Glasses were synthesized using a melt quench technique previously described in the literature [115]. Analytical grade boric anhydride, strontium carbonate, and potassium carbonate reagents (Sigma-Aldrich, USA) were weighed out, in accordance with Table 3.2 *(precision of two decimal places)*. Components were then homogenized in a mechanical blender (twin shell dry blender, Patterson-Kelly, USA) for one hour and then transferred to 100 mL Pt crucibles (XRF Scientific, Montreal) and placed in the furnace (Carbolite RHF 1600, UK). The thermal process had two steps: Firstly, samples were placed at room temperature and subjected to a 25 °C/min ramp rate up to the first dwell temperature of 600 °C where they were subsequently held for 60 mins. Thereafter a 20 °C/min ramp rate was applied to achieve a final dwell temperature of 1200 °C for 60 mins. The melt was quenched between two stainless steel plates and the resulting glass was then broken into small particles, using a hammer and mortar and pestle technique, and sieved to obtain particles <300 μm using ASTM E-11 compliant sieves (Superla Sieve™, Newark Wire Cloth Company). Each glass was then placed in labelled glass vials and housed in vacuum desiccators for subsequent analysis.

3.3.2. Particle size distribution

To determine particle size distribution (PSD) a Malvern Mastersizer 3000 laser diffraction particle size analyzer was used per the manufacturer's instructions. Each composition, with particles sieved <300 μm, was suspended in deionized water to obtain an obscuration value for the suspension between 5-8 %. Blue (λ = 470 nm) and red (λ = 632.8 nm) lasers were then used to measure the glass suspension. Each composition suspension was measured five times, and the PSD data was reported as the mean diameter Dx90, Dx50, and Dx10.

3.3.3. X-ray Diffraction (XRD)

1.5-2 g of each glass composition (<300 μm) was used for x-ray diffraction analysis using a Bruker D2 Phaser in order to establish (i) that the materials were amorphous (ii) free from identifiable crystalline species and (iii) where applicable to determine percent crystallinity of each glass. To conduct the experiment a Lynx-Eye XE 1D detector (linear array) was used. Each composition was pressed into a hollow steel wafer and scanned between $10\ ° \leq 2\theta \leq 60\ °$ with a step size $2\theta = 0.03$ and a step time of 2 s.

3.3.4. ^{11}B MAS NMR

^{11}B magic angle spinning (MAS) NMR spectra was determined using a 16.4 T Bruker Avance NMR spectrometer (^{11}B Larmor frequency= 224.67 MHz) using a 2.5 mm HX probe head operating in

single resonance mode. Solid $NaBH_4$ was then used to calibrate the ^{11}B parameters and also utilized as an external chemical shift reference (-42.1 ppm relative to $BF_3{\cdot}Et_2O$). All samples were spun at 20 kHz MAS frequency adding between 40 - 64 scans. For all compositions (<300 μm) and experiments, the ^{11}B NMR was accumulated using a 0.53 μs pulse which corresponds to a 15 ° pulse angle in a nearly cubic environment of $NaBH_4$. Spin lattice relaxation times were then determined via saturation recovery separately for threefold coordinated boron groups, B3, and B4 groups and ranged from 4.5 to 8.7 s. Five times of the slowest value in each sample was used to determine the pulse delay. The boron background was removed by subtracting the spectrum of the used empty rotor. After baseline correction with a spline function, the integral values are determined for the B3 and B4 groups. For alkali (R) modified glasses with the composition xR_2O - $(1\text{-}x)B_2O_3$ with up to about 30% alkali modifier [167], the theoretical B4 fraction, N_4, was estimated as $N_4=x/(1\text{-}x)$ for each O/B ratio.

3.3.5. Density and molar volume

An AccuPyc 1340 helium pycnometer (Micromeritics, USA) with a 1 cm^3 insert chamber was calibrated and used to determine the density of each glass composition per manufacturer instructions [168]. 0.9-1.0 g frit was used for all 16 compositions. The results were then reported as the average ± standard deviation (SD) (n = 3). To calculate the molar volume of each prototype the equation V=M/p was used, where M is the molecular weight and p is the density of each sample [168].

3.3.6. Differential scanning calorimetry (DSC)

A simultaneous thermal analysis DSC 404 F1 Pegasus with Auto-Sampler (Netzsch-Geratebau-GMBH, USA) was used to analyze each glass composition via DSC. Approximately 20-60 mg was weighed for each composition (<300 μm) and placed into PtRh crucibles and heated at 10.0 (K/min) from 30 to 1100 °C (Standard Test Method for Assignment of the Glass Transition Temperatures by Differential Scanning Calorimetry, ASTM E1356, 2014). Proteus Thermal Analysis (Version 8.0.2) was used to determine the extrapolated end temperature (T_e), extrapolated onset temperature (T_f), inflection temperature (T_i), midpoint temperature (T_m), and crystallization onset temperature (T_{p1}) and was reported as the average ± SD for each glass microsphere to assess for glass transition temperature (T_g) [169]. The equation "$T_{p1} - T_g$ = glass stability" was used to determine the glass stability and composition 14 was excluded from the model.

3.3.7. Sterilization and chemical/physical recharacterization

Each glass composition used to establish density, % B3, % B4, B3:B4 ratio, and % crystallinity (sections 2.2.2-2.2.4) was then subjected to a standardized sterilization regime. All 16 glasses were sent to Nordion and sterilized with γ-radiation per ISO11137:2017 and exposed to a dose range of 25-30 kGy [170]. The samples were then recharacterized as per sections 2.2.2-2.2.4 in order to establish the impact of sterilization on the networks.

3.4. Results

3.4.1. Material synthesis

All compositions (Table 3.2) were successfully synthesized. Of the 16 compositions, 15 of the compositions had no apparent phase separation or crystallization, however, composition BKSA15 formed a white opaque material which was subsequently found to be amorphous on XRD.

3.4.2. Characterization of materials

3.4.2.1. Particle size distribution

Each glass was processed to meet the particle size distribution (PSD) of <300 μm. The data in Table 3.3 depicts the Dx10, Dx50, and Dx90 for each composition and is provided for repeatability and reproducibility purposes.

Table 3.3: Particle size distribution and % crystallinity for all 16 BKSA glass compositions.

	PSD			XRD
BKSA	**Dx(10) (µm)**	**Dx(50) (µm)**	**Dx(90) (µm)**	**% Crystallinity**
1	114	193	309	1
2	120	185	280	1.2
3	128	213	345	3
4	132	223	366	4.7
5	98	194	351	1
6	92	199	373	1.1
7	116	186	286	0.4
8	127	217	354	3.1
9	118	203	335	1.2
10	118	195	302	1
11	120	203	333	1.2
12	121	210	364	1
13	109	192	333	1.9
14	137	225	362	2.2
15	115	213	367	3.5
16	129	215	346	0.2

3.4.2.2. X-ray diffraction (XRD)

All synthesized materials were classified as amorphous and were free from identifiable crystalline species (Table 3.3). The % crystallinity across the compositional design space ranged from 0.2 to 4.7 % and a linear model with statistical significance (Table 3.4) was developed to examine the influence of composition on % crystallinity. Examination of the coefficients relating to the model suggest the ranking of factors resulting in an increase in % crystallinity as follows: B>K>Sr. BKSA15 was found to be amorphous (3.5 % crystallinity) despite its white opaque appearance and thick viscosity as it was poured from the crucible which was a noticeable difference to all other glasses produced in this work.

3.4.2.3. ^{11}B MAS NMR

A representative (BKSA16) ^{11}B MAS NMR line spectra is provided in Fig. 3.1A. The peaks represent the B3 (20-10 ppm) and B4 (5-(-3) ppm) in the sample. The general trends observed from the ^{11}B MAS NMR line spectra was an increase in the B3 and a decrease in the B4 fractions with increasing quantities of B_2O_3. The ^{11}B MAS-NMR analysis for % B3 produced a special cubic model with statistical

significance (Table 3.4). The % B3 ranged from 56.6% to 84.5%. An analysis of the coefficients (Table 3.4) demonstrates a ranking of factors (resulting in an increase in % B3) as follows: B>Sr>K>K*Sr>B*K>B*Sr, where B*Sr and B*K reduced the % of B3. The % B4 (Fig. 3.1B), in each glass was determined and modelled across the compositional design space. Analysis of the % B4 produced a statistically significant special cubic model (Table 3.4) with the % B4 ranging from 15.5 % to 43.4 %. An analysis of the coefficients demonstrates a ranking of factors (resulting in an increase in % B4 with increasing modifier content) as follows: K≈Sr>B*Sr>B*K>B>K*Sr, where K*Sr decreased the % of B4. Lastly, analysis of the B3:B4 ratio (Fig. 3.1C) produced a statistically significant (Table 3.4) reduced cubic model within the range of 1.30 to 5.45. An analysis of the coefficients provided a ranking of factors, as follows: B>K>Sr>B*K>B*Sr, where the interactions B*Sr and B*K are decreasing the ratio of B3:B4. Full model details including coefficients are provided in Table 3.4.

Additionally, the experimental fractions of B3 (blue dots) and B4 (orange dots) and the theoretical values based on binary alkali borate glasses (colour matching lines), were plotted against the O:B ratio for the weighed in sample compositions (Fig. 3.1D). The experimental points for the K_2O and SrO modified glasses with similar O:B ratio fall onto each other within error limits. The error bars are derived from a 2% error in determining the relative fractions % B3 and % B4 from the NMR data (vertical axis) and 2% uncertainty in the sample composition to account for compositional changes during the heating process, the latter being a conservative allowance. The experimentally obtained data points do not fall along the theoretical lines, however, the error bars do intercept the theoretical line.

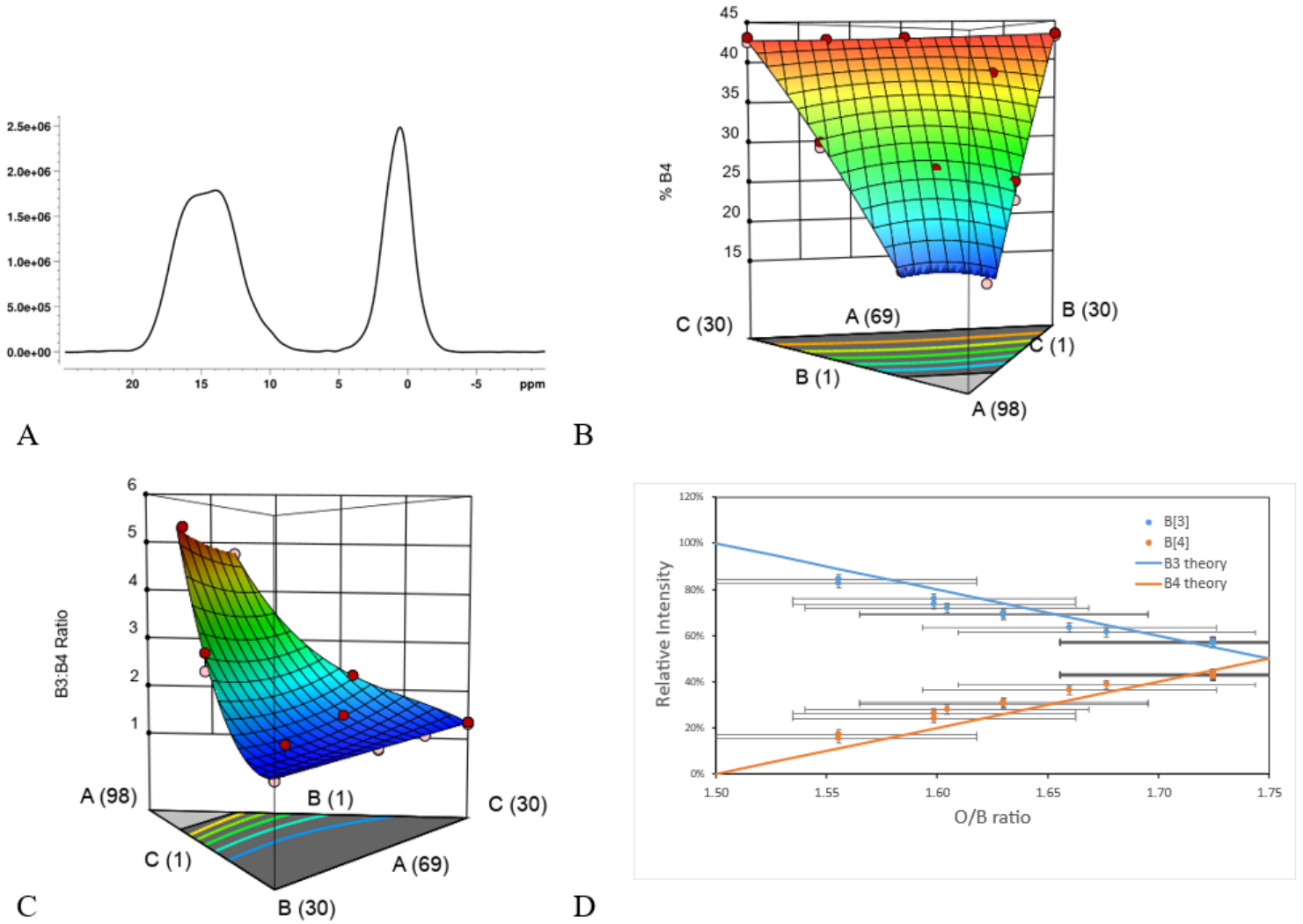

Figure 3.1: (A) Representative ^{11}B MAS NMR spectra for the networks examined (BKSA16). (B) Contour plot depicting the % B4 within the glass network at varying mol% of B_2O_3, K_2O, and SrO. (C) Contour plot depicting the ratio of B3:B4 structural units within the glass network at varying mol% B_2O_3, K_2O, and SrO. For each contour plot the X1, X2 and X3 axes are labelled 'A': the quantity of B_2O_3, 'B': the quantity of K_2O, and 'C': the quantity of SrO. (D) displays the experimentally obtained concentration B4 (orange dot) and B3 (blue dot) versus B:O ratio for each composition. The orange line represents the theoretical B4 values, and the blue line represents the theoretical B3 values seen in binary borate glasses [167].

3.4.2.4. Density and molar volume

From the density analysis, a linear model with statistical significance was produced (Table 3.4) with density values ranging from 2.05 g/cm^3 to 3.00 g/cm^3 (Fig 3.2A). Analysis of the relating to this model coefficients (Table 3.4) indicate the ranking of factors (leading to an increase in density) were as follows: Sr>K>B. From the molar volume analysis, a statistically significant linear model (Table 3.4 and Fig 3.2B) was also established. The molar volume values ranged from 26.71 cm^3/mol to 35.18 cm^3/mol. The analysis of the coefficients for molar volume is as shown B>K>Sr.

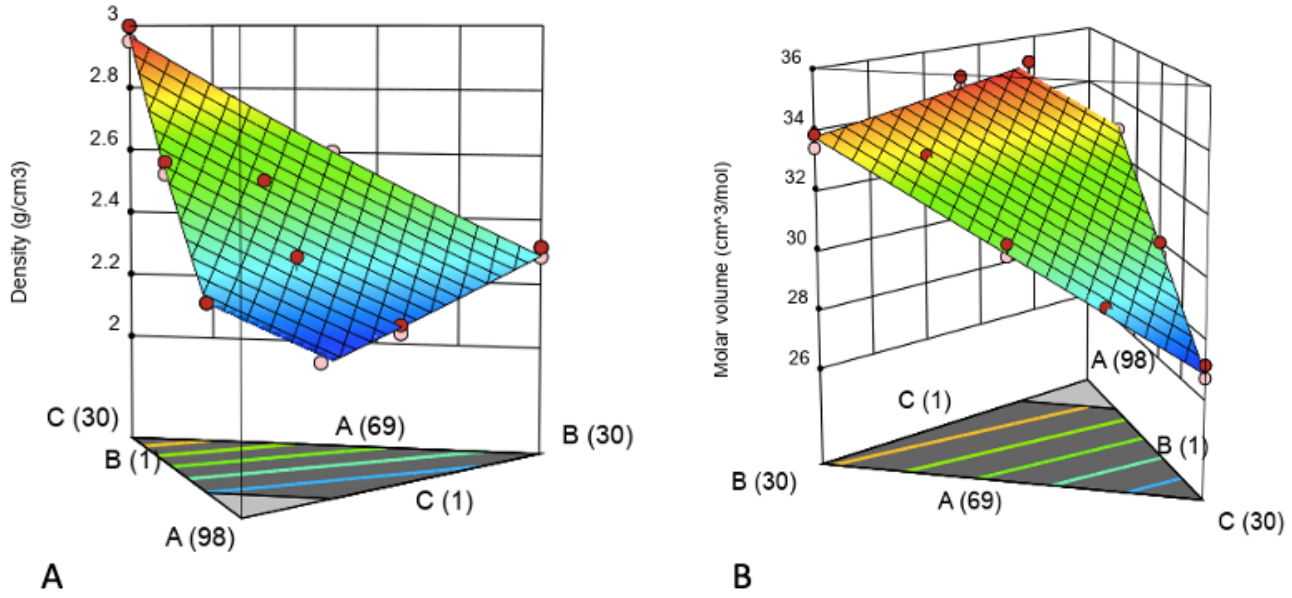

Figure 3.2: (A) Contour plot of density for the design space. (B) Contour plot depicting the molar volumes of each BKSA glass series. For each contour plot the X1, X2 and X3 axes are labelled 'A': the quantity of B_2O_3, 'B': the quantity of K_2O, and 'C': the quantity of SrO.

3.4.2.5. Differential scanning calorimetry (DSC)

Analysis of the T_g onset values for each glass produced a reduced cubic model with statistical significance (Table 3.4, Fig. 3.3A), with T_g values (ºC) ranging from 369.2 ºC to 618.5 ºC. Analysis of the coefficients relating to this model indicate the ranking of factors (where positive coefficients represent a greater increase in onset temperature) were as follows: Sr>K>B>B*Sr>B*K>K*Sr, where K*Sr resulted in a decrease in temperature onset (Table 3.4). Analysis of the T_g inflection values also produced a statistically significant reduced cubic model (Table 3.4, Fig. 3.3B), with values ranging from 381.6 ºC to 660 ºC. Analysis of the coefficients relating to this model indicate the ranking of factors (resulting in an increase in inflection temperature) were as follows: Sr>B>K>K*Sr>B*K. Of note, B*K and K*Sr resulted in a decrease in inflection temperature. Interestingly, in figure 3.3B there is a maximum in T_g approximate

to the minimum (*ca.* 2 mol%) and maximum (*ca.* 24 mol%) mol% for strontium, instead of a gradual increase in inflection temperature as the mol% of Sr increased from 1-30 mol%. Analysis of the T_g final values produced a reduced cubic model with statistical significance (Table 3.4, Fig. 3.3C), with temperature ranging from 393.5 ºC to 633.7 ºC. Analysis of the coefficients relating to this model indicate the ranking of factors (resulting in an increase in final temperature) were as follows: B*Sr>Sr>K>B>B*K>K*Sr, where K*Sr resulted in a decrease in final temperature. From the glass stability analysis, a reduced quadratic model (Fig. 3.3D) with statistical significance (Table 3.4) is shown and the stability values ranged from 99.3 ºC to 238.6 ºC. An analysis of the coefficients (increasing glass stability) demonstrates the following ranking of factors B*Sr>K*Sr>Sr>B>K.

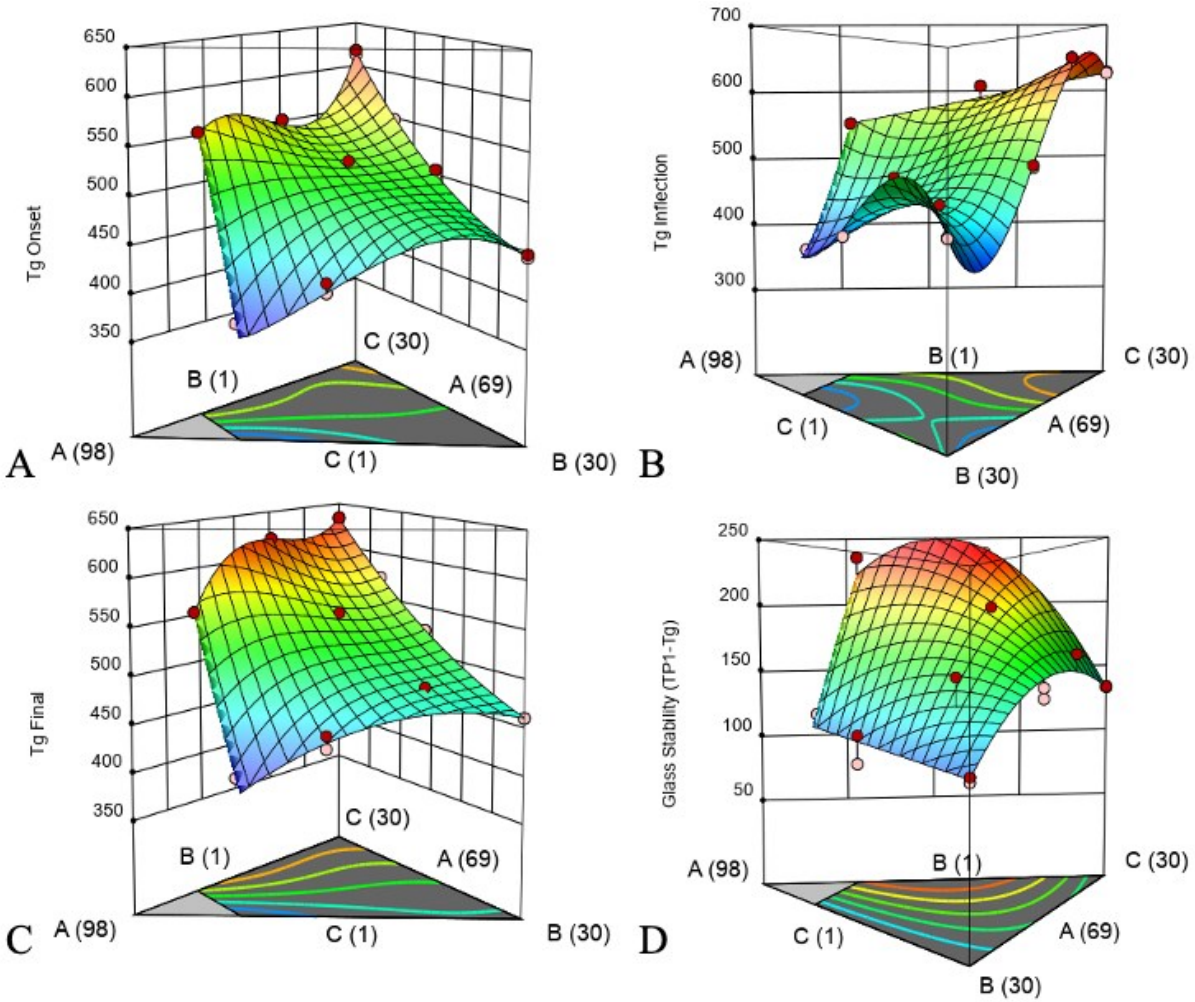

Figure 3.3: (A) Contour plot for T_g onset temperature. (B) Contour plot for T_g inflection. (C) Contour plot for T_g final. (D) Contour plot of glass stability. For each contour plot the X1, X2 and X3 axes are labelled 'A': the quantity of B_2O_3, 'B': the quantity of K_2O, and 'C': the quantity of SrO.

Table 3.4: The L_Pseudo components coded equations for each response (^{11}Boron MAS NMR, XRD, Density, Molar Volume, and DSC) generated within the Design of mixtures design space. The summarized ANOVA with the R^2, $R^2_{adjusted}$, $R^2_{predicted}$, Prob > F and C.V% are also contained within the table.

Response	Regression Models	ANOVA				
		R^2	$R^2_{adjusted}$	$R^2_{predicted}$	Prob > F	C.V. (%)
^{11}Boron MAS NMR						
% B3	$+95.90B_2O_3+56.65K_2O+57.30SrO-5.53B_2O_3*K_2O-9.20 B_2O_3*SrO+0.6582K_2O*SrO$	0.9966	0.9943	0.9869	440.47	1.11
% B4	$+4.10B_2O_3+43.35K_2O+42.70SrO+5.53B_2O_3*K_2O+9.20B_2O_3*SrO-0.6582K_2O*SrO$	0.9966	0.9943	0.9869	440.47	2.13
B3:B4	$+9.71B_2O_3+1.36K_2O+1.35SrO-9.92B_2O_3*K_2O-10.54B_2O_3*SrO$	0.9929	0.9894	0.9737	281.16	5.87
DSC						
Onset	$+353.68B_2O_3+444.80K_2O+616.26SrO+24.51B_2O_3*K_2O+305.33B_2O_3*SrO-116.94K_2O*SrO$	0.9952	0.9911	0.8963	239.03	1.37
Inflection	$+523.52B_2O_3+456.01K_2O+628.40SrO-239.19B_2O_3*K_2O-93.08K_2O*SrO$	0.9757	0.9594	0.9186	60.13	3.21
Final	$+280.96B_2O_3+460.04K_2O+632.90SrO+249.49B_2O_3*K_2O+635.93B_2O_3*SrO-83.30K_2O*SrO$	0.9985	0.9972	0.9889	752.00	0.7866
Glass Stability	$+121.69B_2O_3+110.19K_2O+133.29SrO+489.76B_2O_3*SrO+146.38K_2O*SrO$	0.9521	0.9329	0.9102	49.65	7.82
Density	$+0.6829B_2O_3+0.8275K_2O+1.09SrO$	0.9941	0.9932	0.9911	1103.44	1.06
Molar Volume	$+35.38B_2O_3+33.77K_2O+26.85SrO$	0.9879	0.9860	0.9817	531.13	1.00

3.4.2.6. Sterilization and chemical/physical recharacterization

The impact of sterilization (Table 3.5) on density, molar volume, % crystallinity, % B3, % B4, and B3:B4 was assessed for all BKSA glasses (BKSA1-16). No substantial changes were identified in any of the chemical or physical attributes of the networks (i.e., density, molar volume, % crystallinity, % B3, % B4, and B3:B4) following sterilization. The responses for density ranged from 2.0532-2.9978 g/cm^3 and 2.0703-3.0236 g/cm^3 pre- and post-sterilization, respectively. The responses for molar volume ranged from 26.71-35.18 cm^3/mol and 26.48-34.89 cm^3/mol pre- and post-sterilization, respectively. The responses for % crystallinity ranged from 0.2-4.7 % and 0.7-11.7 % pre- and post-sterilization, respectively. All glasses were considered to be amorphous both pre- and post-sterilization with no identifiable crystalline species and meeting the definition of an amorphous material. The responses for % B3 ranged from 56.6-84.5 % and 56.3-83.6 % pre- and post-sterilization, respectively. The responses for % B4 ranged from 15.5-43.4 % and 16.4-43.7 % pre- and post-sterilization, respectively. Lastly, the responses for B3:B4 ranged from 1.3041-5.4516 and 1.2883-5.0976 pre- and post-sterilization, respectively.

Table 3.5. The density, molar volume, XRD, and % B4 values pre- and post- sterilization for all 16 glass compositions.

	Response							
	Density (g/cm^3)		Molar Volume (cm^3/mol)		XRD (%)		% B4	
BKSA	Pre	Post	Pre	Post	Pre	Post	Pre	Post
1	2.28	2.30	33.85	33.58	1.0	1.5	43.1	43.7
2	2.53	2.55	30.48	30.27	1.2	1.6	36.5	36.4
3	2.05	2.07	35.18	34.89	3.0	9.6	15.5	16.4
4	2.11	2.15	34.98	34.32	4.7	6.3	24.1	23.6
5	2.57	2.62	30.64	30.06	1.0	0.7	42.6	42.5
6	2.95	3.02	27.14	26.48	1.1	0.7	42.5	42.4
7	2.60	2.65	30.23	29.74	0.4	1.6	43.0	42.7
8	2.13	2.13	34.57	34.57	3.1	11.7	26.4	26.7
9	2.59	2.60	29.57	29.39	1.2	1.4	31.1	31.0
10	2.55	2.57	29.99	29.59	1.0	1.6	30.4	30.1
11	2.76	2.78	28.79	28.52	1.2	0.8	42.8	42.5
12	3.00	2.99	26.71	26.75	1.0	1.0	43.1	43.0
13	2.31	2.34	33.41	33.09	1.9	3.7	43.4	43.4
14	2.32	2.36	32.15	31.57	2.2	3.6	28.0	27.9
15	2.21	2.22	32.93	32.86	3.5	6.9	17.3	17.0
16	2.32	2.33	32.97	32.89	0.2	1.2	38.7	38.5

3.5 Discussion

Binary borate glasses (with either alkali or alkaline earth modifiers) have been shown throughout the literature to demonstrate predictable linear responses for % B4 and T_g with alkali or alkaline earth additions up to 30 mol%. However, upon addition of two or more dissimilar cations, as seen in mixed alkali and mixed alkaline earth borate glasses, these properties deviate from linearity [160, 171, 172] compared to binary borate glasses within the same compositional range. Despite our understanding of the changes that occur in the presence of two or more dissimilar cations there is limited literature characterizing the impact of blended alkali and alkaline earth cations in a borate glass networks. Furthermore, there is limited literature assessing the impacts of sterilization on the chemical and structural properties of borate glass networks. With the widespread use of borate glasses in a variety of fields, some applications may require sterilization of glass networks. Consequently, there is potential that the chemical and structural characteristics of the glass may be altered following sterilization. Therefore, the goals of this study are to characterize the role that blends of alkali and alkaline earth modifiers may have on the physical and chemical characteristics of K_2O and SrO substituted borate glasses. Additionally, this work intends to establish the effects of γ-radiation on the glass networks and their associated properties.

It is largely accepted within the binary borate glass literature that the addition of either an alkali or alkaline earth modifier (0-30 mol%) will result in a reduction in the % B3 and an increase in the % B4 units in the glass network [155]. Based on the trends observed for binary alkali borate glasses, the theoretical B4 values can be calculated by x/(1-x) *(where x is equal to the mol% network modifier)* at each O:B ratio [173]. In this work, our data were plotted against the theoretical fractions of B4 and B3 for binary alkali borate glasses (Fig. 3.1D). The experimental data points generated in this work follow the anticipated trend from the literature. The B3 and B4 values of the K_2O and SrO modified glasses with identical O:B ratio fall on top of each other. This indicates that within our experimental constraints, the cation character does not influence the B3 and B4 fractions, as long as the of cation charge concentration remains the same. The ^{11}B MAS NMR spectra demonstrate a decrease in the B4 and an increase in the B3 fractions in response to increasing B_2O_3 (69-90 mol%) which is also in accordance with observations from the literature. In agreement with the observed independence of the cation character, the coefficients generated by the Design-Expert software for the ^{11}B MAS NMR data (Table 3.4) show that both K_2O and SrO have nearly identical coefficients for the % B4 (and % B3) and therefore have the same effect on the % B3 and % B4. This is in contrast to available literature on binary borate glasses from which we expected to maximize the % B4 when comparing alkali modifiers with alkaline-earth modifiers at the same mol% even at low concentrations [146, 154-157]. The deviations in the % B3 and B4 values represent a complex

matter and revealing the precise network former-modifier interactions in multicomponent borate glasses remains problematic due to uncertainties associated with the atomistic and mechanistic basis behind glass structural changes. As shown in Tokuda *et al.* [174] the MAE/MAEE affects not only the transport related properties such as ion conduction, but also the non-transport physical properties such as T_g and density. However, the physical origins of the MAE on non-transport properties in oxide glasses are not yet clarified and several theoretical studies based on thermodynamic approaches have been proposed [175-177]. However, full agreement on the structural origin of MAE/MAEE in borate-based glasses remains to be established. One possible explanation for the equal influence of K_2O and SrO on the % B3 and % B4 observed in this work may be that when the cation charge concentration remains constant, the O:B ratio remains constant. Negatively charged B3 groups with terminating oxygens are not expected in this composition range and so B4 groups are the only negative charge bearing groups that compensate the (two) K^+ and/or Sr^{2+} charges. Although there are number of experimental techniques such as neutron diffraction, NMR, and Raman spectroscopy used to investigate the short-range order in oxide glasses, when considering borate-based networks most of these studies largely discuss the composition dependence of % B4 while de-emphasizing the effects of the other borate structural unit fractions, which becomes increasingly important at higher concentrations of the network modifiers. In fact, other major processes that can affect the B:O ratio and result in non-linear deviations of the B3 and B4 values such as ion mobility, phase separation or solubility remains poorly investigated. Thus, the borate network is only one aspect of the structure while the network-modifying cations also play a critical role and further atomistic and experimental studies are required to clarify the MAE/MAEE effect on the glass behaviour.

When assessing the influence of K_2O and SrO on the thermal characteristics of the networks, it can be seen (Table 3.4) that SrO plays the largest role on increasing both the T_g onset and inflection in addition to being the largest driver for increasing glass rigidity. The significant role SrO has on T_g is further reinforced as the coefficients for B*Sr also largely drive the increase for T_g onset and T_g final. These findings are consistent with the thermal data from our previous work which demonstrates that when introduced to the glass network, SrO increases T_g and this was suggested to occur due to the cross-linking role Sr^{2+} may play within the glass network [115, 137]. Furthermore, within the literature it has been established that glass stability and T_g are dependent on the structural units present in the glass network and more specifically on the % B3 and B4 [178]. Conversely, in view of the data from T_g and NMR together, SrO similarly increases both the % B3 and B4 within the glass network despite an increase in the % B4 typically being attributed to the increase in T_g. Nonetheless, SrO drives an increase in T_g onset, inflection, and final in addition to glass stability (Table 3.4). Therefore, it can be suggested that Sr^{2+} is increasing the

rigidity of the glass network but does not change the local boron coordination (as reflected in the NMR data). It may also be speculated that Sr^{2+} is closely interacting with several oxygen atoms within the network and through cross-linking of neighbouring boron groups increases the glass stability [137, 146, 157].

Interestingly, K^+ cation also appears to play a large role on glass stability despite (i) similarly increasing both the % B3 and B4 in (ii) having a smaller positive influence on T_g onset, inflection, and final (Table 3.4). This result may be reconciled when looking to the literature describing the role of alkali modifiers in zeolite networks. In Fild *et al.* [179], the addition of alkali ions to zeolite networks stabilizes B4 units by compensating for B4 negative charges. Additionally, in Hwang *et al.* [180] alkali cations (i.e., Na^+) were shown to protect B4 units from converting to B3 and in de Ruiter *et al.* [181] boron loss *(from the network)* was reduced when sodium ions were present. To reconcile the role for K^+ cation on glass stability it may be suggested that K^+ behaves similarly in the borate glass network as compared to the zeolite network and stabilizes the B4 units present by charge compensation; therefore, increasing the stability of the glass despite having similar positive effects on the % B3 and B4.

When comparing the glass stability data for both K_2O and SrO, it is observed that K^+ plays an important but less influential role than Sr^{2+} on both T_g and glass stability. From the existing literature, this result may not be completely unexpected as alkaline earth metals have been shown to have a greater effect on glass properties compared to alkali metals in borate glass networks [137]. Additionally, network cross-linking has been shown to play a greater role on T_g *(as suggested for Sr^{2+})* compared to the "degree of borate polymerization manifested by N_4" [182]. This result further supports the hypotheses that both Sr^{2+} and K^+ play differential stabilizing roles within the glass network where K^+ may primarily stabilize / balance the B4 units and Sr^{2+} may act as a cross-linker.

In conjunction to T_g, glass density and molar volume were also assessed (Fig. 3.2). The trends for density in this study are consistent with the findings in the literature which demonstrate that glass density depends on i) the quantity of network modifier [178] and ii) the atomic mass of the cation [183]. As seen in Mascaraque *et al.* [183] where glasses containing Na^+ had a higher density than glasses containing lithium, which was attributed to the higher atomic mass of Na^+. In this study, Sr^{2+} has the greatest positive coefficient for density (Table 3.4) compared to K^+ and B which can largely be attributed to the greater atomic mass of Sr^{2+} over both K^+ and B. Unlike density, molar volume is generally regarded to be dependent on cation radii size [184] and network modifier quantity [185]. However, there are some ambiguities within the literature, and it is important to consider that a multitude of factors influence and contribute to variations in molar volume. As seen from our data (Table 3.4), Sr^{2+} has the smallest positive

coefficient for molar volume after K^+ and then B. Based on the experimental data, molar volume agrees with the density data (Fig. 3.2B).

The effects of γ-radiation on the K_2O- and SrO- borate glass networks were also assessed in this work. Previous studies have demonstrated that sterilization (i.e., γ-radiation) of borate glasses can impact both the structural and chemical characteristics [186, 187] as seen in El-Alaily and Mohamed [188] were glass density increased, which was attributed to compaction of the glass network, in response to increasing radiation (fast neutron- or γ-radiation). Additionally, in Kaur *et al.* [189] increasing Ba^{2+} content (0-20 mol%) in borosilicate glasses reduced the conversion of B4 units to B3/NBO's in response to increasing doses of γ-radiation, indicating that borate glasses can be made more resistant to the effects of sterilization with the addition of network modifier. As demonstrated, sterilization may modify glass properties and as a result these properties may be modified and no longer meet the required parameters. Subsequently, there is a requirement to further characterize the effects of sterilization on the borate glass network from a fundamental standpoint in order to recognize the impact of sterilization on glass composition-structure-property relationships. From our data (Table 3.5), it appears that sterilization did not largely impact glass density, molar volume, % crystallinity, % B3, % B4, or B3:B4 ratio. Accordingly, it can be concluded that sterilization at 25-30 kGy did not affect the chemical and physical properties of the K_2O- and SrO- borate glasses. Thus, utilization of any of these 16 glass compositions in an application where sterilization is required will not alter the chemical or physical characteristics of the glass network and therefore, these glasses will retain the original parameters required/selected for prior to sterilization.

3.6 Limitations

There are limitations of note related to the present study. Firstly, and due to the DoM screening nature of this work, a post-firing compositional analysis was not completed to verify the final glass compositions. However, the absence of the post-firing verification does not interfere with the data in this study as the elements used are not highly volatile and our previous work has demonstrated that similar glasses are "within 5-8% of the calculated theoretical composition[s]" [137] post-firing. The superstructural units in this work were also not evaluated and future work conducting Raman spectroscopy to elucidate superstructures would be beneficial. Lastly, there is no existing x-ray and/or molecular dynamic models characterizing a ternary alkali and alkaline earth borate glass that can be used to confirm the suggested role of K_2O and SrO within the glass network. As a result, the roles suggested for both K^+ and Sr^{2+} by the authors are hypothesized based on the existing literature and further studies are required to fully elucidate the role which K_2O and SrO play in the borate glass network.

3.7 Conclusions

The results of this study demonstrate the impact of K_2O and SrO on the composition-structure-property relationships of borate glass networks containing up to 31 mol% blended alkali and alkaline earth modifiers. Data from the ^{11}B MAS NMR suggests that both K_2O and SrO modulate the % B4 in a similar manner to binary alkali, or binary alkaline earth networks. SrO has been shown to have a large impact on T_g, with SrO and K_2O having similar effects on glass stability, despite both having similar influence on the % B3 and % B4. These results indicate that both K^+ and Sr^{2+} may stabilize the glass network through differential mechanisms not established by the ^{11}B MAS NMR data which has been hypothesized by the authors to be a cross-linking role for Sr^{2+} and a stabilizing role for K^+. Lastly, both trends for density and molar volume are consistent with what is seen in the binary borate glass literature and the properties of the glass network were determined to be unchanged following sterilization.

Chapter 4

Dissolution Behaviour and Imageability of Ternary Borate Glasses for use in Geniculate Artery Embolization

R. A. Manchester[a], T. Z. Todorova[b], E. Tonkopi[c], B. Kelly[d], J. Gosse[d], C. Davis[d], K. Brewer[a,d], M. Shymka[e], & D. Boyd[a,b,c,]

[a] *School of Biomedical Engineering, Dalhousie University, Halifax, NS, Canada*

[b] *Department of Applied Oral Science, Faculty of Dentistry, Dalhousie University, Halifax, NS, Canada*

[c] *Department of Diagnostic Radiology, Dalhousie University, Halifax, NS, Canada*

[d] *BIOTIC, IWK Health Centre, Halifax, NS, Canada*

[e] *School of Medical Sciences, Dalhousie University, Halifax, NS, Canada*

[The work in this letter, under the supervision of Dr. Daniel Boyd, was completed by Remington Manchester. In this work all dissolution and suspension time experiments were conducted by Remington Manchester and the imageability data was obtained in collaboration with other departments at Dalhousie University. Dr. Tsanka Todorova provided critical support and inputs during the collection of the dissolution data, suspension time data, and during the review of the manuscript. Dr. Elena Tonkopi from the department of Diagnostic Imaging and Interventional Radiology at Dalhousie University provided critical support and observations surrounding collection of the CT imaging data and during review of the manuscript. Dr. Kim Brewer and her colleagues from BIOTIC (Jessica Gosse, Christa Davis, and Brianna Kelly) provided critical support and observations surrounding collection and interpretation of the MRI data in conjunction to reviewing the manuscript. Mikayla Shymka provided a draft version of the introduction for this manuscript in addition to the toxicological risk assessment used in this work. Remington Manchester, as first author, wrote the entirety of the manuscript and incorporated critical inputs from all co-authors. All co-authors were provided the opportunity to review and provide inputs into the final manuscript.

In this chapter, the second objectives of the first experiment are encompassed in this work (excluding sterilization) in addition to both the second and third experiments. The second objective of experiment one focuses on the characterization of the dissolution behaviour and imageability of all 16 borate glass compositions to screen out compositions which do not meet the design inputs for an embolic agent indicated for GAE. The experiments in the second objective of experiment one consists of CT and MRI imaging in addition to a mass loss screen at 2 hrs. The objective of experiment two was to select a preferred/optimized composition(s) which best correlates with the design inputs for an embolic agent indicated for GAE by considering inputs from this work as well as the data obtained in experiment one. The objective of experiment three was to further characterize the preferred/optimized composition(s) in physiologically representative media to characterize the dissolution behaviour of the glass *in vivo* in addition to the suspension time of the particles to inform future experiments. Below are the hypothesis pertaining to the data collected in this work and for both objectives in experiment one:

- Glasses with high mol% K_2O, due to the reactivity of K^+ in water, are expected to have a coded coefficient <0 and <Sr for residual mass at 2 hrs. As a result, glasses with high mol% K_2O are expected to have lower residual mass at 2 hrs.
- Glasses with high mol% SrO will achieve higher CT radiopacity than high mol% K_2O glasses due to the greater atomic number of Sr^{2+} which confers radiopacity and as such, Sr will have a coded coefficient >0 and >K for increasing glass radiopacity on CT at 70 and 120 kVp.]

4.1. Abstract

Sixteen borate glass compositions comprising K_2O and SrO were screened, using a design of mixtures approach, to model compositional effects on dissolution, CT imageability, and MRI relaxivity (R_2). Based on the characteristics of each network, together with dose determination and toxicological risk, the composition identified as BKSA16 was selected as a preferred composition for pre-clinical evaluations related to geniculate artery embolization (GAE). Accordingly, BKSA16 particles were subjected to a flame spheroidization process and recharacterized, including the evaluation of residual mass at 72 hrs in physiologically representative media along with clinical determinations of suspension time (ease of use). For both the irregular particles and microspheres residual mass was present at 72 hrs in physiologically representative media. Additionally, both the microspheres and irregular particles achieved suspension times deemed to be acceptable for clinical use. The collective data confirms that BKSA16 microspheres have a range of beneficial features (specifically both degradable and imageable) suited to GAE.

4.2. Introduction

Osteoarthritis (OA) is a common, chronic, and debilitating condition affecting the synovial joint [190]. Substantial limitations with existing treatments have driven intensive research intended to identify new therapies using a 'treat-to-target' approach [20, 21, 28]. One emerging treat-to-target option is known as geniculate artery embolization (GAE) [104, 105, 108]. GAE was developed for patients who are resistant to conservative therapies and not yet indicated for a knee replacement [104]. GAE is a transcatheter based clinical intervention *(ca. 80 minutes)* that targets abnormal angiogenesis [104] which facilitates the growth of new unmyelinated sensory nerves inducing pain signalling and sensitization [21, 92]. Based on this mechanistic understanding, and the treat-to-target nature of GAE, it has been clinically demonstrated to provide substantial pain relief for patients [105, 108].

GAE requires embolic microspheres to generate vessel occlusion. However, at this point in time, there exists no microspheres designed to meet the demands of this clinical intervention. The ideal embolic microspheres for GAE should possess several features including, in the first instance, the ability to degrade *in situ*. It has been determined that degradable microspheres (i) ameliorate clinical risks by ensuring no long-term presence in the body, (ii) facilitate vessel recanalization post treatment(s), and (iii) allow flexibility for repeat embolization procedures if necessary [122, 127, 191]. Furthermore, patients have an overwhelming preference for technologies which are eliminated from the body on completion of such treatments. Coupled with degradation, it is considered beneficial to have microspheres that exhibit certain imageability characteristics. For example, it may be beneficial to have microspheres with intrinsic x-ray attenuation characteristics *(for intraprocedural imaging),* while also exhibiting appropriate MRI relaxation characteristics *(so as not to confound follow-up imaging on MRI)* [115]. The expanded selection criteria for an ideal GAE microsphere can be described as (i) ensuring no residual mass remains in situ after *ca.* 72 hrs, with (ii) a particle size distribution (PSD) of 100-300 μm, (iii) a density of <2.4 g/cm^3, and (iv) preferably a suspension time of $\geq$2 mins.

The purpose of this work is to characterize the dissolution behaviour and imageability of 16 borate glasses, and to identify a preferred composition which best addresses the ideal design features of an embolic microsphere for GAE.

4.3. Methods

Sixteen glass compositions *(including five replicates for statistical purposes)* were established (Table 4.1) using Design-Expert Software (Version 12.0.9) based on an *I-optimal* approach (Manchester *et al.* 2021). Each composition was synthesized using a melt quench technique and subjected to baseline

characterization (density, x-ray diffraction (XRD), ^{11}B MAS NMR, and differential scanning calorimetry (DSC)) as described elsewhere (Manchester *et al.* 2021). Samples were stored under desiccated conditions prior to experimentation.

Table 4.1: BKSA compositions (with five replicate compositions 1 and 13, 4 and 8, 5 and 7, 6 and 12, and 9 and 10) by mol% as characterized in Manchester *et al.* 2021.

Glass Identified	B_2O_3	K_2O	SrO
BKSA 1*	**69.00**	**30.00**	**1.00**
BKSA 2	**75.79**	**8.74**	**15.47**
BKSA 3	**90.00**	**8.28**	**1.73**
BKSA 4•	**83.55**	**15.45**	**1.00**
BKSA 5+	**69.00**	**15.53**	**15.47**
BKSA 6†	**69.00**	**1.00**	**30.00**
BKSA 7+	**69.00**	**15.53**	**15.47**
BKSA 8•	**83.55**	**15.45**	**1.00**
BKSA 9▪	**79.37**	**1.00**	**19.63**
BKSA 10▪	**79.37**	**1.00**	**19.63**
BKSA 11	**69.00**	**8.24**	**22.76**
BKSA 12†	**69.00**	**1.00**	**30.00**
BKSA 13*	**69.00**	**30.00**	**1.00**
BKSA 14	**82.72**	**8.93**	**8.35**
BKSA 15	**90.00**	**1.00**	**9.00**
BKSA 16	**73.91**	**20.40**	**5.69**

Symbols represent replicates.

Dissolution experiments for each glass were conducted in two stages. Firstly, glasses were subjected to screening, using sterile saline as the dissolution media, to identify chemistries with desirable mass loss characteristics. Individual Corning® 15 ml centrifuge tubes were weighed in triplicate with 10 mL saline (0.9% Sodium chloride, Baxter, Illinois, USA). 0.1 g of each glass composition (100-300 μm) was placed in falcon tubes (n=3 per composition for each media) and then in a shaking incubator (120 RPM and 37 °C for 2 hr) then immediately centrifuged (3.0 RCF/ 4.4 RPM) for 15 mins. The supernatant

was decanted from the pellet and the pellet (in the original test tube) was dried (50 °C for 96 hrs) then weighed to determine the average residual mass. The preferred glass (BKSA16) was subjected to residual mass experiments in physiologically representative media using a mass: volume ratio of 0.1g (glass) to 10 mL of 10% bovine calf serum (BCS)/90% Dulbecco's Modified Eagle Medium (DMEM) (Sigma Aldrich, USA). Residual mass was determined after 72 hrs using the same conditions as described for the screening stage.

Each composition was imaged on a clinical CT scanner Somatom Definition AS+ (Siemens Healthineers, Erlangen, Germany) at 70 and 120 kVp using 400 mAs, pitch=0.5, and 1 mm slice thickness [115]. Both full and half strength Omnipaque 350 (Iohexol; 350 mg of non-ionic iodine per mL, GE Healthcare Ireland, Cork, Ireland) were used as controls. Radiopacity measurements was reported as Hounsfield Units (HU) ± standard deviation (SD) [115].

MRI susceptibility was established for each composition by dispersing the materials (100-300 μm) in a non-aqueous gel made with 1% Evonik Intelimer IPA 13-1 NG polymer in peanut oil (2, 4, 6, 8, 10% w/w, n=5). The gels were then loaded in 5 mm tubes and exposed to magnetic stirring, horizontal rotation, and heating before cooling on ice to solidify the gel. Each composition was measured at room temperature using Agilent 3T preclinical MRI to obtain R_2 (CPMG) MRI relaxometry measurements. A linear regression analysis and extrapolation to 100% volume fraction was used to provide values for the particles [115].

Irregular BKSA16 particles (100-300 μm), were subjected to flame spheroidization using a propane oxygen flame to transform the morphology of the glass frit to a microsphere (described elsewhere [192]). After processing the glass microspheres were packaged dry clean containers and sterilized using gamma irradiation (average dose 30 kGy, Nordion, Ontario, Canada).

Scanning Electron Microscopy (SEM) was conducted on BKSA16 microspheres (BKSA16M). A Hitachi S4700 Cold Field Emission scanning electron microscope (with an Oxford Analytical 80 mm SDD detector for energy dispersive x-ray spectroscopy) was used to image the microspheres with a condenser lens 1 set to 3, an emission current of 20 mA, and accelerating voltage of 10 kV. Prior to imaging the specimens, they were placed on aluminum stubs and coated with gold-palladium (20 nm) to prevent product contamination [191].

Following spheroidization of BKSA16 from irregular particles (BKSA16I) to microspheres (BKSA16M), the samples were recharacterized (density, XRD, ^{11}B MAS NMR, and DSC) as previously described in Manchester *et al.* 2021**.** The data pre- (Manchester *et al.* 2021) and post-spheroidization was compared to determine the impact of spheroidization on the material.

The suspension time of BKSA16 microspheres was qualitatively determined using accepted methods from the relevant clinical literature [193]. Succinctly, 0.1 g of glass (100-300 μm) placed into sealed 15 mL tubes with 10 mL of Omnipaque 350 (n=3). Once added, a timer was started, and the tubes were inverted (10x) to create a suspension. Subsequently, the falcon tubes were held upright, placed against a black background and monitored until the suspension fell below 2/3 of the total volume [193]. The time was then averaged for three runs to determine the average suspension time.

4.4. Results

Average residual mass at 2 hrs as assessed in saline is presented in Fig. 4.1A. From these data a cubic model with statistical significance was established (Table 4.2). The average residual mass at 2 h ranged from 7% to 108% (where a value >100% represents a residual mass greater than the initial mass used). The ranking of factors that facilitate an increase in the final residual mass are B>K*Sr>Sr>K>B*Sr>B*K, where B*K and B*Sr result in a decrease in the final residual mass.

CT radiopacity at 70 kVp (Fig. 4.1B) produced a statistically significant reduced quadratic model (Table 4.2). CT Radiopacity (70kVp) ranged from 212 to 5249 HU. Analysis of the coefficients at 70 kVp (Table 4.2) resulted in the following ranking of factors that lead to an increase in radiopacity: Sr>K>B>B*Sr>K*Sr. CT radiopacity at 120 kVp (Fig. 4.1C) produced a statistically significant reduced cubic model (Table 4.2). CT Radiopacity (120kVp) ranged from 161 to 3600 HU. Analysis of the coefficients at 120 kVp (Fig. 4.1C) ranked the factors driving an increase in radiopacity as: Sr>K*Sr>K>B>B*Sr>B*K. Notably, interactions B*K and B*Sr resulted in a reduction in CT radiopacity.

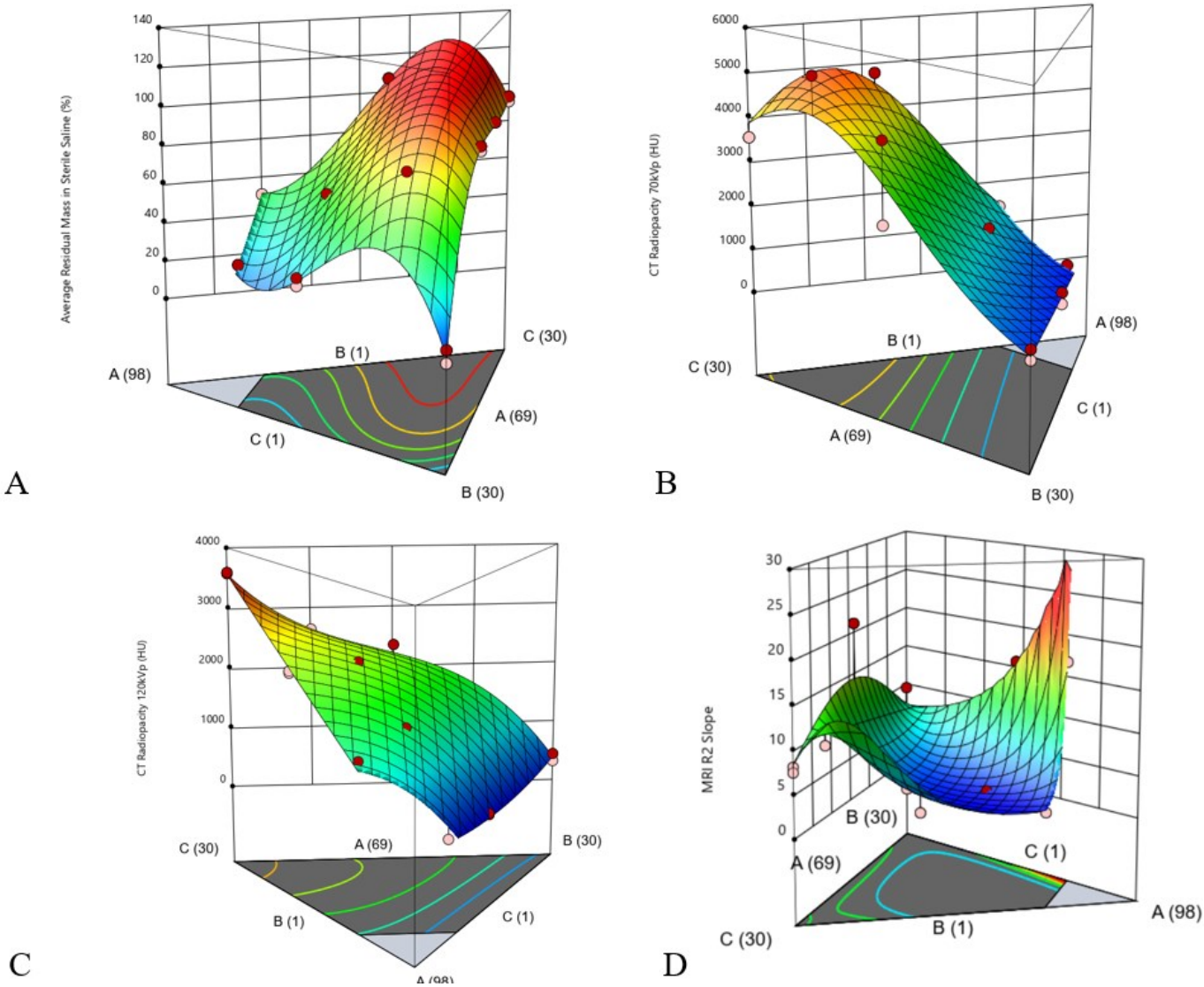

Figure 4.1. Contour plots of responses for (A) average residual mass at 2 hrs in sterile saline, (B) radiopacity at 70 kVp. (C) CT radiopacity at 120 kVp, and (D) MRI R2 slope. The x-axes are labelled as 'A': mol% B_2O_3, 'B': mol% K_2O, and 'C': mol% SrO.

Analysis of the R_2 slope for MRI (Fig. 4.1D) provided a statistically significant reduced cubic model (Table 4.2) with values ranging from 1.298 to 21.12. Analysis of the coefficients for the R2 slope (Table 4.2) resulted in the ranking of factors for increased slope (i.e., higher relaxivity) as follows: B>K*Sr>Sr>K>B*K>B*Sr (where B*K and B*Sr decrease slope).

Table 4.2: Model equations and model statistics for each response per Figure 1 and data for density, XRD (% crystallinity), ^{11}B MAS NMR (B[3]: B[4]), and DSC (T_g onset and inflection) pre- (Manchester *et al.* 2021) and post-spheroidization of BKSA16.

Model Statistics

Response	Regression Models	R^2	$R^2_{adjusted}$	$R^2_{predicted}$	Prob > F	C.V. (%)
Average Residual Mass (2 hr screen)	$+143.19B_2O_3+10.37K_2O+92.92SrO-196.32B_2O_3*K_2O-161.39B_2O_3*SrO+139.83K_2O*SrO$	0.9978	0.9944	0.9479	299.46	4.02
CT 70 kVp	$+5.58B_2O_3+6.24K_2O+8.22SrO+4.82B_2O_3*SrO+3.31K_2O*SrO$	0.9464	0.9269	0.8920	48.53	3.80
CT 120 kVp	$+389.14B_2O_3+401.69K_2O+3568.03SrO-1047.05B_2O_3*K_2O-71.46B_2O_3*SrO+1005.86K_2O*SrO$	0.9940	0.9889	0.9676	165.01	7.73
MRI R2 Slope	$+4.56B_2O_3+1.88K_2O+2.01SrO-2.49B_2O_3*K_2O-10.62B_2O_3*SrO+2.41K_2O*SrO$	0.8247	0.6713	0.2596	5.38	26.56

BKSA16 Pre- and Post-Spheroidization

BKSA16	Density	% Crystallinity	B[3]: B[4]	T_g Onset (°C)	T_g Inflection (°C)
Irregular Particle (BKSA16I)	2.322	0.2	61:39	464.5	475.1
Microsphere (BKSA16M)	2.301	5.9	68:32	428.5	437.2

BKSA16 was processed into microspheres and morphology was confirmed via SEM imaging (Fig. 4.2A). Imaging confirmed the absence of irregular particles, surface contamination or other adverse findings. For completeness, and to account for any changes in the chemical and physical properties arising from microspheres processing, the irregular particles (BKSA16I) and microspheres (BKSA16M) had their basic characteristics compared (Table 4.2).

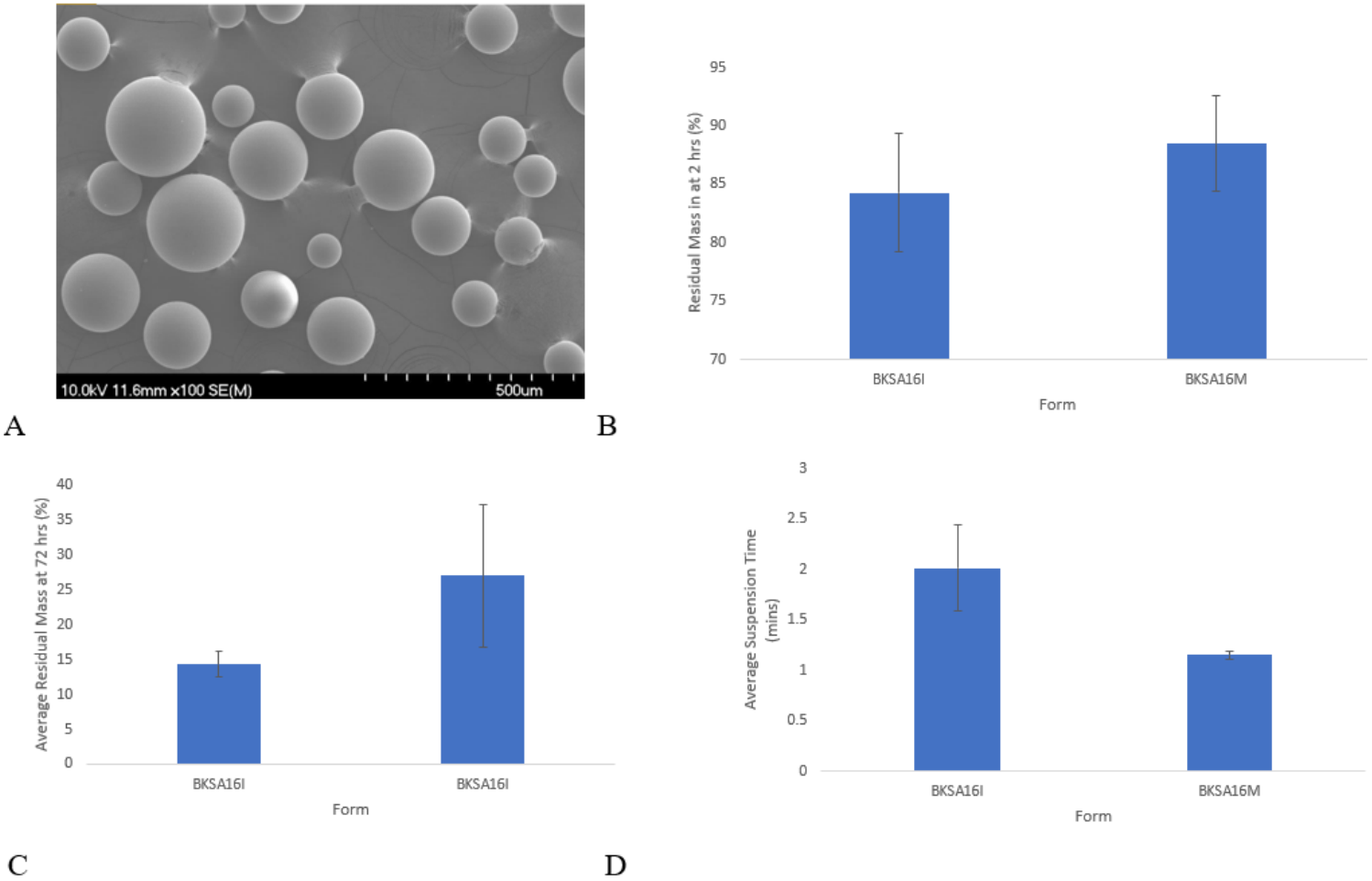

Figure 4.2. (A) SEM image of BKSA16 microspheres (100x), (B) residual mass in saline at 2 hrs for BKSA16I and BKSA16M, (C) residual mass in 10% BSC/90% DMEM at 72 hrs for BKSA16I and BKSA16M, and (D) suspension times for BKSA16I and BKSA16M.

BKSA16I and BKSA16M were compared based on residual mass in saline after 2 hrs (Fig. 4.2B). BKSA16I achieved a residual mass of 84.25 ± 5.04% and BKSA16M achieved a residual mass of 88.44 ± 4.1% after 2 hrs. Average residual mass for the irregular particles (BKSA16I) and microspheres (BKSA16M) were also evaluated in 10% BCS/90% DMEM at 72 hrs (Fig. 4.2C). Notably, BKSA16 had residual mass at 72 hrs in both forms (irregular particles and microspheres). Finally, the average suspension time for BKSA16I was determined to be 2.01 min (run 1: 2.05 min, run 2: 1.20 min, and run 3: 1.58 min). The average suspension time for BKSA16M was determined to be 1.15 min (run 1: 1.11 min, run 2: 1.18 min, and run 3: 1.17min).

4.5. Discussion

Average residual mass in saline (Fig. 4.1A) lead to the elimination of seven compositions (BKSA1, 3, 4, 8, 13, 14, and 15) as they achieved *ca.* <50% residual mass at 2 hrs. This decision was informed from previous work where mass loss *in vitro* was a significant overestimate of *in vivo* dissolution rates [115, 191]. As such these compositions have a low probability of clinical success based on dissolution requirements. It was determined that radiopacity sufficient for clinical use can be achieved in glasses with high mol% SrO (Fig. 4.1B and 4.1C) such as, BKSA6, 7, 9, 10, 11, and 12. These compositions achieve radiopacity comparable to microspheres deemed sufficient for clinical imaging in the literature. For example, Negussie *et al.*, and Ashrafi *et al.*, have established imageable particles as having attenuation values of >3972 HU and 4718 HU respectively [194, 195]. Additionally, Contour™ particles in half strength contrast have reported attenuation values of *ca.* 2500 HU [132]. Similarly, BKSA6, 7, 9, 10, 11, and 12 exhibit CT radiopacity values in the range 3563-5249 HU at 70 kVp. SrO was found to be the largest driver of increased CT radiopacity and responsible for facilitating a larger residual mass following dissolution experiment (Table 4.2). As such control of this critical constituent is an important consideration in materials design. Imageability on MRI was also assessed (Fig. 4.1D) and the compositions were shown to induce minimal R_2 contrast changes and as such, these particles will not confound follow-up R_2-weighted MRI scans in a clinical setting as required [115].

Considering the data from our previous work (Manchester *et al.* 2021) and in conjunction with dissolution and imageability findings, BKSA16 was selected as it best addressed the GAE microsphere requirements, and was further evaluated. While it has low CT radiopacity, BKSA16 also has a relatively low concentration of SrO *(5.69 mol%)* and B_2O_3 *(73.91 mol%)* which facilitates potential increases in the clinical unit dose (from 44 to 55.91 mg (Shymka 2021)) without raising toxicological concerns *(BKSA16 margin of safety (where >1 indicates low toxicological risk) at 44 mg dose: boron=1.27 and*

strontium=1.67 (Shymka 2021)*).* Due to the novelty of the procedure, there currently exists no cleared/approved products with a defined dose and as a result the dosing for this indication remains ambiguous. Nevertheless, on the basis of the existing clinical data which confirm doses within the range of *ca.* 0.2 mL [104, 108], it can be estimated that a probable dose for GAE will be in the range of 44-55 mg (Shymka 2021). For the purposes of this work, a 44 mg dose was established based on the unit dose administered (0.2 ml Embozene particles) in clinical studies [108], a particle size of 100 µm, and a density of 2.3 g/cm^3 (Shymka 2021). Additionally, BKSA16 has a density of *ca.* 2.3 g/cm^3 *(comparable to a range of commercially available contrast media)* which will support adequate suspension, reduced sedimentation/aggregation, and ease of delivery [128]. Finally, BKSA16 has sufficient mass remaining (84.25% at 2 hrs) which should be adequate to support residual mass >2 hrs *in vivo* and thereby, reduce the risk of ineffective occlusion [133]. To overcome the potential issues of low intrinsic CT radiopacity, these particles may be delivered via traditional TAE methods using half strength contrast to safely and effectively image the particles in a clinical setting and as such address this design requirement [196].

Following the selection of BKSA16, the irregular particles were processed into microspheres (Fig. 4.2A) and characterized (Table 4.2). The properties pre/post spheroidization were absent of major differences. As such, the properties of BKSA16 are stable, and these particles can be made into microspheres substantial without alteration of the glass properties. The residual mass in saline at 2 hrs was also compared between the BKSA16 irregular particles (BKSA16I) and microspheres (BKSA16M) (Fig. 4.2B). No major differences in dissolution occurred when comparing the two forms and both forms maintained a residual mass at 2 hrs which will facilitate effective occlusion of the vasculature. The dissolution of BKSA16I and BKSA16M was further assessed in 10% BCS/90% DMEM to provide insight into their dissolution behaviour *in vivo* and both forms were found to have a residual mass of 14.28 and 26.99 % at 72 hrs, respectively (Fig. 4.2C). However, benchtop models have been shown to significantly overestimate mass loss rates in comparison to animal models *(e.g. 100% dissolution ca. 48 hrs and ca. 24 hrs, respectively)* [115, 191]. Thus, it may be appropriate to suggest 100% dissolution will likely occur *in* vivo in <72 hrs meeting the requirements for a microsphere indicated for GAE, however, further animal studies are required to fully characterize the dissolution behaviour of BKSA16 in situ. Lastly, the suspension times of BKSA16I and BKSA16M were assessed and compared to microspheres currently used in TAE procedures (*ca.* 2 mins) [195, 197]. BKSA16I achieved a consistent suspension time with commercially available microspheres used in TAE's procedures and BKSA16M settled out of solution quicker (*ca.* 1.20 min). However, as stated in Johnson *et al.* [198] a shorter suspension time of *ca.* 30 s is still considered sufficient for clinical use, can support the delivery of the particles (with similar handling

when compared to drug loaded DC Bead), and is disregarded as a "clinical concern when sufficient soluble contrast media is used" [198]. As such, BKSA16 is able to sustain a suspension time that is compatible for use clinically. While the data are preliminary and further studies are required, BKSA16 remains a promising candidate for use as an embolic microsphere indicated for GAE.

4.6. Conclusions

Glasses based on B_2O_3, K_2O and SrO were systematically evaluated as potential degradable embolic materials for GAE using a statistical design methodology. Modulation of critical properties across a range of clinical variables were assessed (e.g., dissolution, CT-radiopacity, MRI R_2 relaxivity, and suspension times). Based on the data, one exemplary composition (BKSA16) was processed into spherical form, and no substantive changes to critical properties were observed as a result of processing. BKSA16 is a promising candidate for use as a degradable embolic microsphere indicated for GAE and warrants further development and investigation.

Chapter 5

Conclusions

Osteoarthritis (OA), and more specifically knee OA (KOA), is a debilitating disease that negatively impacts patient quality of life (QoL) and day to day living [15, 16, 199]. Unfortunately, traditional conservative therapies (which use a treat-to-target approach to identify and target potential pain mediators) are beset with limitations such as short-term efficacy, serious adverse effects with long-term use, lack of adequate safety/long-term use data, and/or are ineffectual for managing patient pain [7, 11, 21, 23, 35, 41, 42, 45, 65]. As such, it is critical that adequate pain management therapies are realized and implemented for individuals experiencing pain due to OA, especially those who are resistant to these conservative therapies and are not yet indicated for a total knee arthroplasty (TKA). Fortunately, emerging targets have been identified as a possible means to reduce and/or eliminate patient pain: in particular, the abnormal angiogenesis and perivascular nerves (which are believed to facilitate and be a source of pain [104]) that arise due to the pathophysiology of OA [76, 77, 92]. More recently, a novel treat-to-target procedure known as geniculate artery embolization (GAE) has been developed and works by occluding the abnormal vasculature and thereby indirectly targets the perivascular nerves [104]. Despite GAE being in the early stages of development, the existing clinical studies have deemed the procedure safe [104, 105] and current data suggests the procedure is able to provide sustained pain relief for patients up to two years [104, 108].

Currently, either imipenem/cilastatin sodium (IPM/CS) and/or embozene have been used as the primary embolic agents for GAE. However, these embolic agents are (i) being used off-label, (ii) have limited clinical evidence evaluating the risks and benefits of their use in GAE, and (iii) have not been designed or tailored to meet the unique requirements of GAE. As such, this provides us with an opportunity to develop a specific microsphere technology engineered to meet the unique requirements of GAE. To address these considerations and concerns, initial market research was conducted. As determined through this research [123] there was substantial preference for a degradable embolic microsphere technology for GAE to facilitate repeat procedures and reduce the risks associated with permanent microspheres. From our pre-market research and in conjunction with inputs from our interviews with key-opinion-leaders (n=20), several design inputs were identified for a microsphere technology indicated for use in GAE and are listed as follows (where *shall* is a mandatory requirement and *should* is a conditional requirement that is not required):

1) *Shall be* degradable – within 2-72hrs to ensure effective occlusion of the vasculature while balancing both safety (short contact) and efficacy (provide sustained pain relief) [125].
2) *Should be* imageable – on Computed Tomography (CT) and not confound Magnetic Resonance Imaging (MRI) [122, 126].
3) *Shall be* within a pre-determined PSD – of 100-300 μm to reduce risk of non-target embolization [105].
4) *Should* have a density preferably <2.3 g/cm^3– to sustain a suspension in commercially available contrast media (e.g. Omnipaque 350 or Isovue 370) to prevent sedimentation of microspheres and to reduce the risk of retrograde flow [127, 128].
5) *Shall be* Sterile – Complete sterilization of the medical device as per industry standards using γ-radiation [129, 130].

Based on these requirements, borate glass networks were selected as the material to produce these microspheres due to their unique properties, including the potential to modulate critical properties; specifically, degradation and imageability. As such, the focus of this thesis work was to evaluate borate glass as an embolic agent indicated for use in GAE. To do this, novel borate glasses were characterized to (i) understand how alkali and alkaline earth network modifiers modulate glass properties and (ii) provide insight into ways which the glasses can be tailored to meet the design inputs for a microsphere indicated for use in GAE. Sixteen borate glass compositions modified with both K_2O and SrO were examined within the range of 0-30 mol% and considered to be amorphous (defined as principally amorphous and being substantially free of identifiable crystalline species). From this work, a number of glass properties (namely %B3, %B4, and T_g) were shown to deviate from what is typically seen in binary borate glasses whereas other properties (such as density and molar volume) were consistent with what is observed in the literature. From these observations and in conjunction with both our previous work [115, 137] and the published literature [179], the roles for both the Sr^{2+} and K^+ cation in the network were further elucidated and additional hypotheses for future consideration were developed. It may be hypothesized, based on this work, that the Sr^{2+} may play a cross-linking role in these networks and that K^+ may act to stabilize B4 units in the network. These hypothesized roles reconcile the observations from this thesis work and may provide a rationale for the positive effects of K_2O and SrO on T_g and glass stability (defined as the ability of a material to resist nucleation and crystallization during the manufacturing process) despite having a similar positive influence (at the same mol%) on either the % B3 or % B4s in the network (as reported in chapter 3). The findings from this work highlight that, despite our understanding of binary borate glass systems in

highly characterized ranges (0-30 mol%), the change in properties (i.e., % B4, % B3, and T_g) that arise when two or more dissimilar cations are introduced to the network cannot be anticipated based on existing limited literature. This work also illustrates the complexities of these glasses and demonstrates the need to further characterize alkali and alkaline earth borate glasses even in these highly characterized and believed to be well understood ranges.

Following characterization of the 16 borate glass compositions, the glasses were screened for dissolution and imageability in order to inform the selection of a preferred and/or optimized glass composition(s) that best meets the design inputs for a microsphere indicated for GAE. From the mass loss screen in saline, several compositions were eliminated as candidate compositions. Conversely, all 16 compositions when exposed to contrast media (see in Appendix D) formed a solid complex and achieved an overall mass gain which was highly unanticipated and requires further investigation. Mass loss was initially assessed in full strength Omnipaque 350 as it was anticipated to be the delivery media for these microspheres. Omnipaque 350 maintains a density near isodense with the microspheres and as such would best support microsphere suspension and reduce aggregation/settling [128]. Additionally, this screen would provide insight into the dissolution behaviour of the microspheres during preparation and delivery, prior to arriving to their target location within the vasculature. However, due to these unforeseen complications, further work and considerations will be required in order to determine how best to deliver the microspheres in a manner that will not impede/complicate their delivery. In terms of CT imageability, six of the glasses (BKSA6, 7, 9, 10, 11, and 12) achieved radiopacity within the range (2500-12040 HU [132]) deemed sufficient for clinical use as defined in the literature. For example, DC Bead LUMI™ (a radiopaque microsphere available commercially) exhibits a range from 4268-4767 HU [195] and the reported radiopacity of commercially available Contour™ (in half strength contrast) is *ca.* 2520 HU [132] on CT. Additionally, radiopaque bismuth beads which achieve a radiopacity of ≥3972 HU have also been deemed to have radiopacity which is considered to be *"clinically useful"* [194] and within the range of clinically available imageable beads [194]. Other imageable embolic agents in the literature have reported higher ranges for CT radiopacity as seen in Kehoe *et al*. [126] (benchtop CT radiopacity *ca.* 8000 HU), Kehoe *et al.* [132] (benchtop radiopacity ranging from 3220-12040 HU), and Doucet *et al*. [115, 191] (benchtop radiopacity 6237 HU at 80 kVp and 3798 HU at 120 kVp). As characterized in this work, specific BKSA glasses (with >15.5 mol% SrO) demonstrate radiopacity within the range of 3563-5249 HU. Despite attaining CT radiopacity on the lower end of what is considered *"clinically acceptable",* these glasses exhibit radiopacity that are within the ranges reported for both commercially available microspheres and microspheres deemed 'radiopaque' within the literature. In conjunction with being able

to produce microspheres within the CT imageable range as seen above, the models produced within this thesis work also provide a means in which to improve and tailor the radiopacity of these glasses. From the models generated in this work it is understood that the addition of Sr^{2+} provides increased CT radiopacity to the glasses and as such, these models can be optimized to confer greater radiopacity to the glasses if desired. Additionally, other compositional substitutions (i.e., bismuth [194]) may be possible in order to provide greater radiopacity. In terms of MRI imageability, all BKSA compositions were found to induce minimal R2 or R1 (see appendix F) contrast. This is an important consideration since MRI is a common pre- and post-procedural imaging modality using R1- or R2-weighted MRI imaging [104, 105, 200] and in the case of OA is commonly used as a non-invasive tool to assess joint pathology, pathology of the connective tissues, and lesions [201]. As such, it is critical to produce a microsphere which will not impede imaging contrast on MRI imaging post-embolization and interfere with the physician's ability to assess / visualize the joint [115] especially in cases where repeat embolization's are required. As shown from the data in this thesis work, no singular BKSA composition will interfere with either R1- or R2-weighted MRI scans.

Following the characterization of these novel K_2O and SrO modified borate glasses, a preferred composition was selected. Inputs from the dissolution and imageability screen, composition-structure-property relationship data, user needs/design inputs, and the toxicological risk assessment (TRA) [202] led to the selection of BKSA16 as the preferred composition that best meets the design inputs for a microsphere indicated for GAE. A TRA, published elsewhere [202], was conducted to establish the toxicological risk and margin of safety (MOS) for each composition characterized in this thesis work assuming 100% elemental exposure (B, O, K, and Sr) within 24 hr (i.e., worst case scenario). To do so a dose of 44 mg was assumed based on the unit dose used in Okuno *et al.* [104, 108] (0.2 mL of Embozene), a 2.3 g/cm^3 particle density, and a 100 μm particle size [202]. For BKSA16 both boron (MOS 1.27) and strontium (MOS 1.67) demonstrated a margin of safety >1 (where a value >1 indicates low toxicological risk) indicating that BKSA16 poses a "low toxicological risk to human health" [202] at this dose. Additionally, due to the safety profile of BKSA16, a maximum unit dose of 55.91 mg (supporting a MOS >1) [202] could be given providing users with the ability to increase the unit dose if required.

Following selection of BKSA16 as the preferred composition it was processed into microspheres and the properties (i.e., ^{11}B MAS NMR, density, T_g, and dissolution behaviour) of the microspheres were found to be consistent with those seen for the frit precursor. These data indicate that the properties of this composition are stable and suitable for both production and further characterization. While the deviations in properties are not significant vis-a-vis the design inputs and clinical requirements, they may be

indicative of material changes and should be investigated further. To further characterize BKSA16 and achieve a stronger understanding of its dissolution behaviour *in vivo,* both the irregular particles and microspheres were exposed to 10% bovine calf serum (BCS)/90% Dulbecco's Modified Eagle Medium (DMEM) in order to provide a more adequate and simulated assessment of degradation in situ. Findings from this work indicate that both forms of BKSA16 retain residual mass at 72 hrs. However, from our previous work [115, 191] mass loss achieved *in vitro* (*ca.* 48 hrs [115]) largely overestimates the mass loss seen *in situ* (*ca.* 24 hrs [191]). Additionally, benchtop models provide valuable insight into what may be anticipated to occur *in vivo* however, in many cases (*as is this work*) a variety of factors/conditions seen *in vivo* are not represented in these benchtop studies such as pH changes, fluid dynamics, thrombotic factors, and immune cells which may all contribute to the dissolution of the microspheres. With these considerations in mind and due to the similar chemistries of the BKSA glass series and the glasses assessed in our previous work, it is largely anticipated that similar dissolution time frames will be seen *in vivo*. As such, it is anticipated that BKSA16 will meet the design input for dissolution *in vivo* however, further studies will be required to confirm these results. Lastly, the suspension time of BKSA16 (both irregular particles and microspheres) was assessed to determine its compatibility with existing embolic agents used in TAE procedure. BKSA16I was found to have a suspension time consistent with existing agents *ca.* 2 min whereas, BKSA16M had a slightly shorter suspension time (*ca.* 1.20 min). However, in the literature suspension times of *ca.* 30 s have been reported as sufficient for clinical use [198] additionally, if deployment of the microspheres is done using a delivery device the suspension time of the microspheres will not impact their delivery. As such, both forms of BKSA16 can support an adequate suspension time for clinical use. Overall, the findings and data from this work support BKSA16 as a promising candidate as an embolic agent for use in GAE as it (i) retains residual mass >2 hrs to support effective occlusion of the vasculature, (ii) has a density consistent with commercially available contrast medias to support microsphere suspension, (iii) can be sterilized and made into microspheres without altering glass properties, (iv) can be made to have a particle size distribution of 100-250 μm, and (v) can sustain a suspension time that is sufficient for clinical. Not only do the data from this work identify and support BKSA16's correlations with the design inputs for a microsphere indicated for use in GAE, but they also provide insight into the reproducibility and stability of the glass for industrial and commercial processing.

This thesis work attempted to further describe the role of poorly understood mixed alkali and alkaline earth modifiers in borate glass networks in addition to evaluate the use of borate glass modified with K_2O and SrO for use as an embolic agent indicated for GAE. This work was successful in providing data elucidating the role of K_2O and SrO on the composition-structure-property relationships in a borate

glass network and illustrated how these modifiers may be used to modify/tailor the glasses structure, dissolution, and radiopacity for use in GAE and other scientific or industrial applications. From this work it can be concluded that mixed alkali and alkaline earth borate glasses exhibit non-linear properties (namely T_g and the % B3 and % B4) which deviate from those seen in binary borate glasses in highly characterized ranges (0-30 mol%). This reinforces the complexities of these glasses and highlights that additional work is required to better understand the role of alkali and alkaline earth cations in the glass network with a focus within these highly 'understood' ranges. Lastly, this work successfully identified a preferred composition (BKSA16) that best correlates with the design inputs for a microsphere indicated for use in GAE. While the results from this thesis work are preliminary and further animal, MD, and x-ray studies are required to better understand the role of K_2O and SrO in the borate glass network, BKSA16 remains an exciting candidate composition as an embolic agent indicated for GAE.

Limitations

Within this thesis work there are limitations that require acknowledgement. Firstly, the compositions characterized in this work were not subject to post-firing analysis and as such there may be slight deviations in the theoretical versus post-firing compositions. For future studies, it may be appropriate to conduct post-firing analyses to confirm the compositions being characterized. However, from our previous work post-firing compositions have been shown to be within 5-8% [137] of the theoretical compositions and as such will likely not confound the interpretation of the data in this work. Additionally, the elements/reagents used in this work have low volatility and will likely be within the range of our theoretical calculations as shown in our previous work [137]. Secondly, residual mass could not be assessed in contrast media as an unexpected mass gain occurred as a result of a complex forming in response to each BKSA composition in the contrast media. As a result, it was not possible to assess (i) how the preparation/delivery of the microspheres may impact the residual mass prior to delivery of the microspheres to their target sites and (ii) if delivery of the microspheres in contrast media is possible. Thirdly, there currently exist no molecular dynamic (MD) models or x-ray data characterizing alkali and alkaline earth modified borate glasses. As such, the roles for both K^+ and Sr^{2+} are hypothesized from both the existing literature and data from our previous work. Fourthly, duplicate measurements were used to obtain the imageability data for MRI as each measurement required a large amount of sample which was difficult to generate. From the data, the only statistically significant models were that for R2 slope. While the models produced are beneficial and reliable, using multiple measurements may have enabled the identification of statistically significant models for both R1 and R2* measurements. Fifthly, due to the

absence of any *in vivo* work it is not possible to identify which physiologically representative media (100% BCS or 10% BCS/90% DMEM) is most representative of *in vivo* conditions. As such, no singular media can be identified as a 'more representative media' and *in vivo* work will be required to identify the most appropriate media and inform future benchtop modeling. Second to last, CT imageability was assessed solely on irregular particles and was not recharacterized following spheroidization of BKSA16. Consequently, there may be slight variations in imageability that remain unidentified. However, from our structural and chemical assessment of the BKSA16 microspheres there are minimal differences in the glass properties post-spheroidization and it is likely the imageability of the microspheres will be consistent with the ranges identified in the irregular particles. Lastly, CT imageability was only assessed *in vitro* and there remains no *in vivo* imageability data for any of the BKSA compositions. Therefore, it may be beneficial to obtain these data to identify if BKSA16 has sufficient imageability to inform its spatial and temporal resolution *in vivo* to help govern decisions for future work and applications.

Future Work

This thesis work aimed to explain the role of K_2O and SrO in borate glass networks. Currently, there is a lack of literature characterizing group 1 and 2 cations in borate glasses in addition to an absence of MD models and x-ray work which characterize the role of alkali and alkaline earth cations in borate glass networks. Thus, the roles for both K_2O and SrO were hypothesized based on both the findings in this work and our previous work. Due to the absence of this critical data, it is crucial that both MD models and x-ray work is conducted so that the hypothesized roles of alkali and alkaline earth cations (in this work K^+ and Sr^{2+}) can be fully reconciled. Secondly, only the basic structural units (B3 and B4's) for all BKSA compositions were characterized and remained the primary focus of the structural characterization in this work. Consequently, superstructural units were not assessed for any of the 16 compositions. As such, it would be highly complimentary to this work to characterize the superstructural units via Raman spectroscopy in the BKSA networks. In borate glasses, superstructural units link together to form a continuous glass network [138] and a variety of structural units have been characterized in borate glass networks (i.e., boroxol, pentaborate, and diborate groups) [138]. These groups are made of varying quantities of basic structural units (B3, B4, and/or non-bridging oxygens) and vary with increasing quantities of network modifier [138] which can largely impact the overall glass properties as seen with variations in basic structural units. Thus, Raman work would provide further structural characterization of the BKSA glasses and identify if the presence of two dissimilar cations modulates the superstructural units present as compared to what is seen in binary borate glasses. Thirdly, the dissolution of BKSA16 will need

to be assessed *in vivo* to better understand how this composition correlates with the design inputs for a microsphere indicated for GAE and in parallel provide information assessing which benchtop media (100% BCS or 10% BCS/90% DMEM) is most representative of the dissolution behaviour *in vivo* for future benchtop studies. This work is also required to best inform future decisions and considerations governing the development of this microsphere technology. Fourthly, interactions with all BKSA compositions and contrast media resulted in unforeseen interactions which may impact microsphere delivery when using Omnipaque 350 as the delivery media. The compositions were found to form a complex, and this may block the catheter and/or result in clumping of the microspheres possibly making it difficult to deliver the microspheres. As such, these interactions must be better understood to determine (i) if these interactions can be overcome, (ii) how these interactions may impede delivery of the microspheres, and/or (iii) if another media/delivery vessel would be more appropriate to facilitate ease of microsphere delivery. Lastly, no *in vivo* modelling was conducted in this thesis work. As recommended in ISO10993-1, degradation assessments *in vivo* should "be conducted in an appropriate animal model" [203] for absorbable devices. Additionally, both special and general controls should be addressed as recommended by the FDA to sufficiently inform both the safety and efficacy of novel class II devices indicated for vascular embolization's [204]. As demonstrated in the literature, there currently does not exist an *in vitro* model which can "mimic the complex biological responses to embolization" [191]**.** To investigate the special control criteria recommended by the FDA [204], an *in vivo* model is most appropriate to carry out this work. Hence, future animal studies are critical in order to evaluate the performance characteristics of the microspheres in a clinical setting such as (i) microsphere delivery feasibility, (ii) microsphere delivery time compared to existing agents on the market, (iii) microsphere embolization effectiveness, (iv) microsphere degradation *in vivo* (enabling the identification of a physiologically representative media that is most representative of *in vivo* degradation), (v) device migration, and (vi) vessel recanalization [191, 204]. Not only are these studies critical to evaluate the performance of the microspheres themselves in a clinical setting but also to determine if any foreign body local/systemic reactions, acute complications, and/or toxicities occur due to the presence of the microspheres [191, 204] to inform future work and decisions regarding the microspheres as a medical device.

REFERENCES

[1] *Arthritis Alliance of Canada, The Impact of Arthritis in Canada: Today and Over the Next 30 Years. Arthritis Alliance of Canada.* [Online]. Available: http://www.arthritisalliance.ca/en/initiativesen/impact-of-arthritis

[2] M. Kloppenburg and F. Berenbaum, "Osteoarthritis year in review 2019: epidemiology and therapy," *Osteoarthritis Cartilage,* vol. 28, no. 3, pp. 242-248, Mar 2020, doi: 10.1016/j.joca.2020.01.002.

[3] F. C. Breedveld, "Osteoarthritis--the impact of a serious disease," *Rheumatology (Oxford),* vol. 43 Suppl 1, pp. i4-8, Feb 2004, doi: 10.1093/rheumatology/keh102.

[4] H. G. Schaible, "Mechanisms of chronic pain in osteoarthritis," *Curr Rheumatol Rep,* vol. 14, no. 6, pp. 549-56, Dec 2012, doi: 10.1007/s11926-012-0279-x.

[5] T. Neogi, "The epidemiology and impact of pain in osteoarthritis," *Osteoarthritis and Cartilage,* vol. 21, no. 9, pp. 1145-1153, 2013, doi: 10.1016/j.joca.2013.03.018.

[6] R. E. Miller, J. A. Block, and A.-M. Malfait, "What is new in pain modification in osteoarthritis?," *Rheumatology,* vol. 57, no. suppl_4, pp. iv99-iv107, 2018, doi: 10.1093/rheumatology/kex522.

[7] G. Snijders *et al.*, "Evidence-based tailored conservative treatment of knee and hip osteoarthritis: between knowing and doing," *Scandinavian Journal of Rheumatology,* vol. 40, no. 3, pp. 225-231, 2011, doi: 10.3109/03009742.2010.530611.

[8] "SHI Consulting Life Sciences Strategies. “Canadian Arthritis funding landscape review,” ", Arthritis Alliance of Canada, (2011).

[9] K. V. MacDonald, C. Sanmartin, K. Langlois, and D. A. Marshall, "Symptom onset, diagnosis and managment of osteoarthritis " *Health Reports,* vol. 25, no. 9, pp. 10-17, 2014. [Online]. Available: https://www150.statcan.gc.ca/n1/pub/82-003-x/2014009/article/14087-eng.pdf.

[10] B. R. Deshpande. *et al.*, "The number of persons with symptomatic knee osteoarthritis in the United States: Impact of race/ethnicity, age, sex, and obesity," *Arthritis Care Res (Hoboken),* vol. 68, no. 12, pp. 1743-1750, 2016, doi: 10.1002/acr.22897.

[11] Osteoarthritis Research Society International, "Osteoarthritis: A Serious Disease," *Osteoarthritis Research Society International,* pp. 1-103, 2016. [Online]. Available: https://www.oarsi.org/sites/default/files/library/2018/pdf/oarsi_white_paper_oa_serious_disease121416_1.pdf.

[12] "Osteoarthritis: Structural Endpoints for the Development of Drugs, Devices, and Biological Products for Treatment Guidance for Industry, Food and Drug Administration, 2018.." [Online]. Available: https://www.fda.gov/media/71132/download

[13] "Priority diseases and reasons for inclusion: Osteoarthritis. Priority Medicines for Europe and the World 2013 Update. World Health Organization, 2013, https://www.who.int/medicines/areas/priority_medicines/Ch6_12Osteo.pdf (accessed on Oct. 5, 2020)."

[14] *Food and drugs, 21 C.F.R 312.300 (2019).*

[15] I. L. A. Araujo, M. C. Castro, C. Daltro, and M. A. Matos, "Quality of Life and Functional Independence in Patients with Osteoarthritis of the Knee," *Knee Surgery & Related Research,* vol. 28, no. 3, pp. 219-224, 2016, doi: 10.5792/ksrr.2016.28.3.219.

[16] A. Sharma., P. Kudesia., Q. Shi., and R. Gandhi., "Anxiety and depression in patients with osteoarthritis: impact and management challenges," *Open Access Rheumatol.,* vol. 8, pp. 103-113, 2016, doi: 10.2147/OARRR.S93516.

[17] S. E. Hardy, Y. Kang, S. A. Studenski, and H. B. Degenholtz, "Ability to Walk 1/4 Mile Predicts Subsequent Disability, Mortality, and Health Care Costs," *Journal of General Internal Medicine,* vol. 26, no. 2, pp. 130-135, 2011, doi: 10.1007/s11606-010-1543-2.

[18] B. Sharif, J. A. Kopec, H. Wong, and A. H. Anis, "Distribution and Drivers of Average Direct Cost of Osteoarthritis in Canada from 2003 to 2010," *Arthritis Care & Research,* vol. 69, no. 2, pp. 243-251, 2017, doi: 10.1002/acr.22933.

[19] E. Losina *et al.*, "Lifetime medical costs of knee osteoarthritis management in the United States: Impact of extending indications for total knee arthroplasty," *Arthritis Care Res (Hoboken),* vol. 67, no. 2, pp. 203-215, 2015, doi: 10.1002/acr.22412.

[20] A. Migliore *et al.*, "It Is the Time to Think About a Treat-to-Target Strategy for Knee Osteoarthritis," *Ther Clin Risk Manag. ,* vol. 15, pp. 1479-1482, 2019, doi: 10.2147/TCRM.S221562.

[21] A. M. Malfait and T. J. Schnitzer, "Towards a mechanism-based approach to pain management in osteoarthritis," *Nat Rev Rheumatol,* vol. 9, no. 11, pp. 654-64, Nov 2013, doi: 10.1038/nrrheum.2013.138.

[22] A. Dray and S. J. Read, "Arthritis and pain. Future targets to control osteoarthritis pain," *Arthritis Research & Therapy,* vol. 9, no. 3, p. 212, 2007, doi: 10.1186/ar2178.

[23] E. Ayhan, "Intraarticular injections (corticosteroid, hyaluronic acid, platelet rich plasma) for the knee osteoarthritis," *World Journal of Orthopedics,* vol. 5, no. 3, p. 351, 2014, doi: 10.5312/wjo.v5.i3.351.

[24] O. Sibila, G. Suarez-Cuartin, A. Rodrigo-Troyano, and A. Anzueto, "Corticosteroids and Pneumonia in Chronic Obstructive Pulmonary Disease: A Dual Effect?," *BRN Rev.,* vol. 1, pp. 105-15, 2015, doi: 10.23866/BRNRev:2015-0010.

[25] V. B. Kraus, "Pathogenesis and treatment of osteoarthritis," *Medical Clinics of North America,* vol. 81, no. 1, pp. 85-112, 1997, doi: 10.1016/s0025-7125(05)70506-x.

[26] J. C. Mora., R. Przkora., and Y. Cruz-Almeida., "Knee osteoarthritis: pathophysiology and current treatment modalities," *J Pain Res.,* vol. 11, pp. 2189-2196, 2018, doi: 10.2147/JPR.S154002.

[27] A. C. Gelber, D. Cotton, J. K. Rao, D. Taichman, and S. Williams, "Osteoarthritis," *Annals of Internal Medicine,* vol. 161, no. 1, 2014, doi: https://doi.org/10.7326/0003-4819-161-1-201407010-01001.

[28] S. L. Kolasinski *et al.*, "2019 American College of Rheumatology/Arthritis Foundation Guideline for the Management of Osteoarthritis of the Hand, Hip, and Knee," *Arthritis Rheumatol,* vol. 72, no. 2, pp. 220-233, Feb 2020, doi: 10.1002/art.41142.

[29] D. J. Hunter and F. Eckstein, "Exercise and osteoarthritis," *J Anat,* vol. 214, no. 2, pp. 197-207, Feb 2009, doi: 10.1111/j.1469-7580.2008.01013.x.

[30] E. Thijssen, A. Van Caam, and P. M. Van Der Kraan, "Obesity and osteoarthritis, more than just wear and tear: pivotal roles for inflamed adipose tissue and dyslipidaemia in obesity-induced osteoarthritis," *Rheumatology,* vol. 54, no. 4, pp. 588-600, 2015, doi: 10.1093/rheumatology/keu464.

[31] E. Yusuf, "Pharmacologic and Non-Pharmacologic Treatment of Osteoarthritis," *Current Treatment Options in Rheumatology,* vol. 2, no. 2, pp. 111-125, 2016, doi: 10.1007/s40674-016-0042-y.

[32] R. Christensen, E. M. Bartels, A. Astrup, and H. Bliddal, "Effect of weight reduction in obese patients diagnosed with knee osteoarthritis: a systematic review and meta-analysis," *Ann Rheum Dis,* vol. 66, no. 4, pp. 433-9, Apr 2007, doi: 10.1136/ard.2006.065904.

[33] J. Charlesworth, J. Fitzpatrick, N. K. P. Perera, and J. Orchard, "Osteoarthritis- a systematic review of long-term safety implications for osteoarthritis of the knee," *BMC Musculoskeletal Disorders,* vol. 20, no. 1, 2019, doi: 10.1186/s12891-019-2525-0.

[34] S. R. Smith, B. R. Deshpande, J. E. Collins, J. N. Katz, and E. Losina, "Comparative pain reduction of oral non-steroidal anti-inflammatory drugs and opioids for knee osteoarthritis: systematic analytic review," *Osteoarthritis and Cartilage,* vol. 24, no. 6, pp. 962-972, 2016, doi: 10.1016/j.joca.2016.01.135.

[35] A. W. S. Rutjes, P. Jüni, B. R. d. Costa, S. Trelle, E. Nüesch, and S. Reichenbach, "Viscosupplementation for osteoarthritis of the knee: a systematic review and meta-analysis," *Ann Intern Med,* vol. 157, no. 3, pp. 180-91, 2012, doi: 10.7326/0003-4819-157-3-201208070-00473.

[36] E. G. Matzkin, E. J. Curry, Q. Kong, M. J. Rogers, M. Henry, and E. L. Smith, "Efficacy and Treatment Response of Intra-articular Corticosteroid Injections in Patients With Symptomatic Knee Osteoarthritis," *Journal of the American Academy of Orthopaedic Surgeons,* vol. 25, no. 10, pp. 703-714, 2017, doi: 10.5435/jaaos-d-16-00541.

[37] E. Nüesch, A. Rutjes, S. Trelle, S. Reichenbach, and P. Jüni, "Doxycycline for osteoarthritis of the knee or hip (Review)," *Cochrane Database of Systematic Reviews,* no. 4, 2009, Art no. CD007323, doi: 10.1002/14651858.CD007323.pub2.

[38] J. Lin, W. Zhang, A. Jones, and M. Doherty, "Efficacy of topical non-steroidal anti-inflammatory drugs in the treatment of osteoarthritis: meta-analysis of randomised controlled trials," *BMJ,* vol. 329, no. 7461, p. 324, 2004, doi: 10.1136/bmj.38159.639028.7c.

[39] J. Sousa-Valente, L. Calvo, V. Vacca, R. Simeoli, J. C. Arevalo, and M. Malcangio, "Role of TrkA signalling and mast cells in the initiation of osteoarthritis pain in the monoiodoacetate model," *Osteoarthritis Cartilage,* vol. 26, no. 1, pp. 84-94, Jan 2018, doi: 10.1016/j.joca.2017.08.006.

[40] B. R. Da Costa *et al.*, "Effectiveness of non-steroidal anti-inflammatory drugs for the treatment of pain in knee and hip osteoarthritis: a network meta-analysis," *The Lancet,* vol. 390, no. 10090, pp. e21-e33, 2017, doi: 10.1016/s0140-6736(17)31744-0.

[41] M. Wehling, "Non-steroidal anti-inflammatory drug use in chronic pain conditions with special emphasis on the elderly and patients with relevant comorbidities: management and mitigation of risks and adverse effects," *European Journal of Clinical Pharmacology,* vol. 70, no. 10, pp. 1159-1172, 2014, doi: 10.1007/s00228-014-1734-6.

[42] O. Vostinaru, "Adverse Effects and Drug Interactions of the Non-Steroidal Anti-Inflammatory Drugs," in *Nonsteroidal Anti-Inflammatory Drugs*, 2017, ch. Chapter 3.

[43] "Statistics Canada. 2009. “Prevalence of osteoarthritis, by age group and site of joint pain, household population aged 20 or older diagnosed with arthritis, Canada excluding territories, 2009” (table). *2009 Survey on living with chronic diseases in Canada - arthritis.* Health reports. Statistics Canada Catalogue no. 82-003-X. Statistics Canada," ed.

[44] T. E. McAlindon *et al.*, "OARSI guidelines for the non-surgical management of knee osteoarthritis," *Osteoarthritis and Cartilage,* vol. 22, no. 3, pp. 363-388, 2014, doi: 10.1016/j.joca.2014.01.003.

[45] N. Fuggle *et al.*, "Safety of Opioids in Osteoarthritis: Outcomes of a Systematic Review and Meta-Analysis," *Drugs Aging,* vol. 36, no. Suppl 1, pp. 129-143, Apr 2019, doi: 10.1007/s40266-019-00666-9.

[46] M. A. R. Iban. *et al.*, "Use of strong opioids for chronic pain in osteoarthritis: an insight into the Latin American reality," *Expert Review of Clinical Pharmacology* vol. 11, no. 8, pp. 47-59, 2018, doi: https://doi.org/10.1080/17512433.2018.1381556.

[47] D. J. Haleem, "Serotonin-1A receptor dependent modulation of pain and reward for improving therapy of chronic pain," *Pharmacol Res,* vol. 134, pp. 212-219, Aug 2018, doi: 10.1016/j.phrs.2018.06.030.

[48] Wilson N, Kariisa M, S. H. I. Seth P, and Davis NL, "Drug and Opioid-Involved Overdose Deaths — United States, 2017–2018. ," *MMWR Morb Mortal Wkly Rep,* vol. 69, pp. 290-297, 2020, doi: http://dx.doi.org/10.15585/mmwr.mm6911a4.

[49] J. A. J. Martyn, J. Mao, and E. A. Bittner, "Opioid Tolerance in Critical Illness," *The New England Journal of Medicine,* vol. 380, no. 4, pp. 365-378, 2019, doi: 10.1056/NEJMra1800222.

[50] L. W. Moreland, "Intra-articular hyaluronan (hyaluronic acid) and hylans for the treatment of osteoarthritis: mechanisms of action," *Arthritis Research & Therapy,* vol. 5, no. 2, p. 54, 2003, doi: 10.1186/ar623.

[51] C.-T. Wang, J. Lin, C.-J. Chang, Y.-T. Lin, and S.-M. Hou, "Therapeutic Effects of Hyaluronic Acid on Osteoarthritis of the Knee

A Meta-Analysis of Randomized Controlled Trials," *The Journal of Bone & Joint Surgery,* vol. 86, no. 3, pp. 538-545, 2004. [Online]. Available: https://journals.lww.com/jbjsjournal/Abstract/2004/03000/Therapeutic_Effects_of_Hyaluronic_Acid_on.12.aspx.

[52] S.-H. Liu, C. E. Dubé, C. B. Eaton, J. B. Driban, T. E. McAlindon, and K. L. Lapane, "Longterm Effectiveness of Intraarticular Injections on Patient-reported Symptoms in Knee Osteoarthritis," *The Journal of Rheumatology,* vol. 45, no. 9, pp. 1316-1324, 2018, doi: 10.3899/jrheum.171385.

[53] D. Jevsevar, P. Donnelly, G. A. Brown, and D. S. Cummins, "Viscosupplementation for Osteoarthritis of the Knee," *The Journal of Bone and Joint Surgery-American Volume,* vol. 97, no. 24, pp. 2047-2060, 2015, doi: 10.2106/jbjs.n.00743.

[54] P. Creamer, "Intra-articular corticosteroid treatment in osteoarthritis," *Current Opinion in Rheumatology,* vol. 11, no. 5, pp. 417-421, 1999, doi: 10.1097/00002281-199909000-00016.

[55] A. E. Coutinho and K. E. Chapman, "The anti-inflammatory and immunosuppressive effects of glucocorticoids, recent developments and mechanistic insights," *Mol Cell Endocrinol,* vol. 335, no. 1, pp. 2-13, Mar 15 2011, doi: 10.1016/j.mce.2010.04.005.

[56] S. Sakaguchi, K. Wing, and M. Miyara, "Regulatory T cells - a brief history and perspective," *Eur J Immunol,* vol. 37 Suppl 1, pp. S116-23, Nov 2007, doi: 10.1002/eji.200737593.

[57] N. Bellamy, J. Campbell, V. Robinson, R. B. T Gee, and G. Wells, "Intraarticular corticosteroid for treatment of osteoarthritis of the knee," *Cochrane Database Syst Rev. ,* no. 2, p. CD005328, 2006, doi: 10.1002/14651858.CD005328.pub2.

[58] T. E. McAlindon *et al.*, "Effect of Intra-articular Triamcinolone vs Saline on Knee Cartilage Volume and Pain in Patients With Knee Osteoarthritis," *JAMA,* vol. 317, no. 19, p. 1967, 2017, doi: 10.1001/jama.2017.5283.

[59] D. A. Cardone. and A. F. Tallia., "Joint and Soft Tissue Injection," *Am Fam Physician.,* vol. 66, no. 2, pp. 283-289, 2002. [Online]. Available: https://www.aafp.org/afp/2002/0715/p283.html.

[60] W. M. Oo, X. Liu, and D. J. Hunter, "Pharmacodynamics, efficacy, safety and administration of intra-articular therapies for knee osteoarthritis," *Expert Opinion on Drug Metabolism & Toxicology,* vol. 15, no. 12, pp. 1021-1032, 2019, doi: 10.1080/17425255.2019.1691997.

[61] C. Wernecke, H. J. Braun, and J. L. Dragoo, "The Effect of Intra-articular Corticosteroids on Articular Cartilage: A Systematic Review," *Orthop J Sports Med,* vol. 3, no. 5, p. 2325967115581163, May 2015, doi: 10.1177/2325967115581163.

[62] A. J. Kompel., F. W. Roemer., A. M. Murakami., L. E. Diaz., M. D. Crema., and A. Guermazi., "Intra-articular Corticosteroid Injections in the Hip and Knee: Perhaps Not as Safe as We Thought?," *Radiology,* vol. 293, no. 2, 2019, doi: https://doi.org/10.1148/radiol.2019190341.

[63] K. Grzela, A. Strzelak, W. Zagórska, and T. Grzela, "Matrix Metalloproteinases in Asthma-Associated Airway Remodeling – Dr. Jekyll or Mr. Hyde ?," in *Asthma - From Childhood Asthma to ACOS Phenotypes*, 2016, ch. Chapter 3.

[64] G. Man and G. Mologhianu, "Osteoarthritis pathogenesis – a complex process that involves the entire joint," *J Med Life.,* vol. 7, no. 1, pp. 37-41, 2014. [Online]. Available: https://www.ncbi.nlm.nih.gov/pmc/articles/PMC3956093/.

[65] B. R. Da Costa, E. Nüesch, S. Reichenbach, P. Jüni, and A. W. Rutjes, "Doxycycline for osteoarthritis of the knee or hip," *Cochrane Database of Systematic Reviews,* 2012, doi: 10.1002/14651858.CD007323.pub3.

[66] K. D. Brandt and S. A. Mazzuca, "Experience with a placebo-controlled randomized clinical trial of a disease-modifying drug for osteoarthritis: the doxycycline trial," *Rheum Dis Clin North Am,* vol. 32, no. 1, pp. 217-34, xi-xii, Feb 2006, doi: 10.1016/j.rdc.2005.11.002.

[67] D. A. Walsh and J. Stocks, "New Therapeutic Targets for Osteoarthritis Pain," *SLAS DISCOVERY: Advancing the Science of Drug Discovery,* vol. 22, no. 8, pp. 931-949, 2017, doi: 10.1177/2472555217716912.

[68] S. E. Harte, R. E. Harris, and D. J. Clauw, "The neurobiology of central sensitization," *Journal of Applied Biobehavioral Research,* vol. 23, no. 2, p. e12137, 2018, doi: 10.1111/jabr.12137.

[69] A. Latremoliere and C. J. Woolf, "Central Sensitization: A Generator of Pain Hypersensitivity by Central Neural Plasticity," *The Journal of Pain,* vol. 10, no. 9, pp. 895-926, 2009, doi: 10.1016/j.jpain.2009.06.012.

[70] H. A. Ashmawi and G. M. G. Freire, "Peripheral and central sensitization," *Revista Dor,* vol. 17, 2016, doi: 10.5935/1806-0013.20160044.

[71] T. Graven-Nielsen, T. Wodehouse, R. M. Langford, L. Arendt-Nielsen, and B. L. Kidd, "Normalization of widespread hyperesthesia and facilitated spatial summation of deep-tissue pain in knee osteoarthritis patients after knee replacement," *Arthritis & Rheumatism,* vol. 64, no. 9, pp. 2907-2916, 2012, doi: 10.1002/art.34466.

[72] C. J. Woolf, "Central sensitization: Implications for the diagnosis and treatment of pain," *Pain,* vol. 152, no. Supplement, pp. S2-S15, 2011, doi: 10.1016/j.pain.2010.09.030.

[73] S.-Q. Wei, Z.-Y. Tao, Y. Xue, and D.-Y. Cao, "Peripheral Sensitization," IntechOpen, 2019.

[74] G. Musumeci, F. Aiello, M. Szychlinska, M. Di Rosa, P. Castrogiovanni, and A. Mobasheri, "Osteoarthritis in the XXIst Century: Risk Factors and Behaviours that Influence Disease Onset and Progression," *International Journal of Molecular Sciences,* vol. 16, no. 12, pp. 6093-6112, 2015, doi: 10.3390/ijms16036093.

[75] G. Jiménez., J. Cobo-Molinos., C. A. ., and E. López-Ruiz., "Osteoarthritis: Trauma vs Disease.," *Adv Exp Med Biol. ,* vol. 1059, pp. 63-83, 2018. [Online]. Available: https://www.unboundmedicine.com/medline/citation/29736569/Osteoarthritis:_Trauma_vs_Disease_.

[76] P. I. Mapp and D. A. Walsh, "Mechanisms and targets of angiogenesis and nerve growth in osteoarthritis," *Nature Reviews Rheumatology,* vol. 8, no. 7, pp. 390-398, 2012, doi: 10.1038/nrrheum.2012.80.

[77] T. W. O'Neill and D. T. Felson, "Mechanisms of Osteoarthritis (OA) Pain," *Current Osteoporosis Reports,* vol. 16, no. 5, pp. 611-616, 2018, doi: 10.1007/s11914-018-0477-1.

[78] D. A. Walsh and C. Pearson, "Angiogenesis in the pathogenesis of inflammatory joint and lungdiseases," *Arthritis Research,* vol. 3, no. 3, p. 147, 2001, doi: 10.1186/ar292.

[79] I. Macdonald, S.-C. Liu, C.-M. Su, Y.-H. Wang, C.-H. Tsai, and C.-H. Tang, "Implications of Angiogenesis Involvement in Arthritis," *International Journal of Molecular Sciences,* vol. 19, no. 7, p. 2012, 2018, doi: 10.3390/ijms19072012.

[80] K. Fu, S. R. Robbins, and J. J. McDougall, "Osteoarthritis: the genesis of pain," *Rheumatology,* vol. 57, no. suppl_4, pp. iv43-iv50, 2018, doi: 10.1093/rheumatology/kex419.

[81] D. Ribatti, "Inflammation and Angiogenesis," Springer International Publishing, 2017, pp. 25-26.

[82] H. K. Eltzschig and P. Carmeliet, "Hypoxia and Inflammation," *New England Journal of Medicine,* vol. 364, no. 7, pp. 656-665, 2011, doi: 10.1056/nejmra0910283.

[83] Y. Henrotin, L. Pesesse, and C. Lambert, "Targeting the synovial angiogenesis as a novel treatment approach to osteoarthritis," vol. 6, no. 1, pp. 20-34, 2014, doi: 10.1177/1759720x13514669.

[84] M. Klagsbrun and M. A. Moses, "Molecular angiogenesis," *Chemistry & Biology* vol. 6, pp. R217-R224, 1999, doi: .

[85] D. A. Walsh, "Angiogenesis and arthritis," *Rheumatology,* vol. 38, no. 2, pp. 103-112, 1999, doi: https://doi.org/10.1093/rheumatology/38.2.103.

[86] D. Walsh, "Angiogenesis and arthritis," *Rheumatology,* vol. 38, no. 2, pp. 103-112, 1999, doi: 10.1093/rheumatology/38.2.103.

[87] J. L. Hamilton, M. Nagao, B. R. Levine, D. Chen, B. R. Olsen, and H.-J. Im, "Targeting VEGF and Its Receptors for the Treatment of Osteoarthritis and Associated Pain," *Journal of Bone and Mineral Research,* vol. 31, no. 5, pp. 911-924, 2016, doi: 10.1002/jbmr.2828.

[88] T. L. Khong, H. Larsen, Y. Raatz, and E. Paleolog, "Angiogenesis as a therapeutic target in arthritis: learning the lessons of the colorectal cancer experience," *Angiogenesis,* vol. 10, no. 4, pp. 243-258, 2007, doi: 10.1007/s10456-007-9081-1.

[89] N. Thairu, S. Kiriakidis, P. Dawson, and E. Paleolog, "Angiogenesis as a therapeutic target in arthritis in 2011: learning the lessons of the colorectal cancer experience," *Angiogenesis,* vol. 14, no. 3, pp. 223-234, 2011, doi: 10.1007/s10456-011-9208-2.

[90] S. Donell, "Subchondral bone remodelling in osteoarthritis," *EFORT Open Rev,* vol. 4, no. 6, pp. 221-229, Jun 2019, doi: 10.1302/2058-5241.4.180102.

[91] C. S. Bonnet and D. A. Walsh, "Osteoarthritis, angiogenesis and inflammation," *Rheumatology,* vol. 44, no. 1, pp. 7-16, 2005, doi: 10.1093/rheumatology/keh344.

[92] S. Ashraf, H. Wibberley, P. I. Mapp, R. Hill, D. Wilson, and D. A. Walsh, "Increased vascular penetration and nerve growth in the meniscus: a potential source of pain in osteoarthritis," *Annals of the Rheumatic Diseases,* vol. 70, no. 3, pp. 523-529, 2011, doi: 10.1136/ard.2010.137844.

[93] A. Thambyah, A. Nather, and J. Goh, "Mechanical properties of articular cartilage covered by the meniscus," *Osteoarthritis and Cartilage,* vol. 14, no. 6, pp. 580-588, 2006, doi: 10.1016/j.joca.2006.01.015.

[94] A. J. S. Fox, A. Bedi, and S. A. Rodeo, "The Basic Science of Articular Cartilage: Structure, Composition, and Function," *Sports Health: A Multidisciplinary Approach,* vol. 1, no. 6, pp. 461-468, 2009, doi: 10.1177/1941738109350438.

[95] E. A. Makris, P. Hadidi, and K. A. Athanasiou, "The knee meniscus: Structure–function, pathophysiology, current repair techniques, and prospects for regeneration," *Biomaterials,* vol. 32, no. 30, pp. 7411-7431, 2011, doi: 10.1016/j.biomaterials.2011.06.037.

[96] D. Syx, P. B. Tran, R. E. Miller, and A.-M. Malfait, "Peripheral Mechanisms Contributing to Osteoarthritis Pain," *Current Rheumatology Reports,* vol. 20, no. 2, 2018, doi: 10.1007/s11926-018-0716-6.

[97] A. I. Basbaum, D. M. Bautista, G. Scherrer, and D. Julius, "Cellular and Molecular Mechanisms of Pain," *Cell,* vol. 139, no. 2, pp. 267-284, 2009, doi: 10.1016/j.cell.2009.09.028.

[98] L. A. Stoppiello, P. I. Mapp, D. Wilson, R. Hill, B. E. Scammell, and D. A. Walsh, "Structural Associations of Symptomatic Knee Osteoarthritis," *Arthritis & Rheumatology,* vol. 66, no. 11, pp. 3018-3027, 2014, doi: 10.1002/art.38778.

[99] R. E. Miller *et al.*, "CCR2 chemokine receptor signaling mediates pain in experimental osteoarthritis," *Proceedings of the National Academy of Sciences,* vol. 109, no. 50, pp. 20602-20607, 2012, doi: 10.1073/pnas.1209294110.

[100] R. E. Miller, R. J. Miller, and A.-M. Malfait, "Osteoarthritis joint pain: The cytokine connection," *Cytokine,* vol. 70, no. 2, pp. 185-193, 2014, doi: 10.1016/j.cyto.2014.06.019.

[101] J. Sokolove and C. M. Lepus, "Role of inflammation in the pathogenesis of osteoarthritis: latest findings and interpretations," *Therapeutic Advances in Musculoskeletal Disease,* vol. 5, no. 2, pp. 77-94, 2013, doi: 10.1177/1759720x12467868.

[102] J. Massier, A. Eitner, G. Segond Von Banchet, and H.-G. Schaible, "Effects of Differently Activated Rodent Macrophages on Sensory Neurons: Implications for Arthritis Pain," *Arthritis & Rheumatology,* vol. 67, no. 8, pp. 2263-2272, 2015, doi: 10.1002/art.39134.

[103] R.-R. Ji, Z.-Z. Xu, and Y.-J. Gao, "Emerging targets in neuroinflammation-driven chronic pain," *Nature Reviews Drug Discovery,* vol. 13, no. 7, pp. 533-548, 2014, doi: 10.1038/nrd4334.

[104] Y. Okuno, A. M. Korchi, T. Shinjo, and S. Kato, "Transcatheter Arterial Embolization as a Treatment for Medial Knee Pain in Patients with Mild to Moderate Osteoarthritis," *CardioVascular and Interventional Radiology,* vol. 38, no. 2, pp. 336-343, 2015, doi: 10.1007/s00270-014-0944-8.

[105] S. Bagla, R. Piechowiak, T. Hartman, J. Orlando, D. D. Gaizo, and A. Isaacson, "Genicular Artery Embolization for the Treatment of Knee Pain Secondary to Osteoarthritis," *Journal of Vascular and Interventional Radiology,* vol. 31, no. 7, pp. 1096-1102, 2020, doi: 10.1016/j.jvir.2019.09.018.

[106] L. J. Van Baardewijk, Y. L. Hoogeveen, I. C. M. Van Der Geest, and L. J. Schultze Kool, "Embolization of the Geniculate Arteries Is an Effective Treatment of Recurrent Hemarthrosis Following Total Knee Arthroplasty That Can Be Safely Repeated," *The Journal of Arthroplasty,* vol. 33, no. 4, pp. 1177-1180.e1, 2018, doi: 10.1016/j.arth.2017.11.002.

[107] Z. D. Weidner, W. G. Hamilton, J. Smirniotopoulos, and S. Bagla, "Recurrent Hemarthrosis Following Knee Arthroplasty Treated with Arterial Embolization," *The Journal of Arthroplasty,* vol. 30, no. 11, pp. 2004-2007, 2015, doi: 10.1016/j.arth.2015.05.028.

[108] Y. Okuno, A. M. Korchi, T. Shinjo, S. Kato, and T. Kaneko, "Midterm Clinical Outcomes and MR Imaging Changes after Transcatheter Arterial Embolization as a Treatment for Mild to Moderate Radiographic Knee Osteoarthritis Resistant to Conservative Treatment," *Journal of Vascular and Interventional Radiology,* vol. 28, no. 7, pp. P995-1002, 2017, doi: https://doi.org/10.1016/j.jvir.2017.02.033.

[109] "Medication Guide for Non-Steroidal Anti-Inflammatory Drugs (NSAIDs)," U.S. Food and Drug Administration, 2007. [Online]. Available: https://www.fda.gov/media/73092/download

[110] A. Davis and J. Robson, "The dangers of NSAIDs: look both ways," *British Journal of General Practice,* vol. 66, no. 645, pp. 172-173, 2016, doi: 10.3399/bjgp16x684433.

[111] H. A. Elshabrawy, Z. Chen, M. V. Volin, S. Ravella, S. Virupannavar, and S. Shahrara, "The pathogenic role of angiogenesis in rheumatoid arthritis," *Angiogenesis,* vol. 18, no. 4, pp. 433-448, 2015, doi: 10.1007/s10456-015-9477-2.

[112] C. f. D. C. a. Prevention. "About Antibiotic Resistance." https://www.cdc.gov/drugresistance/about.html (accessed April 13, 2021.

[113] C. L. Ventola, "The Antibiotic Resistance Crisis: part 1: causes and threats," *Pharmacy and Therapeutics,* vol. 40, no. 4, pp. 277-283, 2015.

[114] D. J. Swanson, C. Deangelis, I. L. Smith, and J. J. Schentag, "Degradation kinetics of imipenem in normal saline and in human serum," *Antimicrobial Agents and Chemotherapy,* vol. 29, no. 5, pp. 936-937, 1986, doi: 10.1128/aac.29.5.936.

[115] J. Doucet *et al.*, "Multi-modal imageability and degradation characteristics of high-borate glass systems for transient embolization," *Journal of Non-Crystalline Solids,* vol. 510, pp. 26-35, 2019, doi: 10.1016/j.jnoncrysol.2019.01.014.

[116] *FDA 510(k) clearance, CeloNova BioSciences, Inc., Embozene Microspheres, K133447, 2014*. [Online] Available: https://www.accessdata.fda.gov/cdrh_docs/pdf13/K133447.pdf

[117] S. Stampfl *et al.*, "Inflammation and recanalization of four different spherical embolization agents in the porcine kidney model," *J Vasc Interv Radiol,* vol. 19, no. 4, pp. 577-86, Apr 2008, doi: 10.1016/j.jvir.2008.01.011.

[118] V. Verret, S. H. Ghegediban, M. Wassef, J. P. Pelage, J. Golzarian, and A. Laurent, "The Arterial Distribution of Embozene and Embosphere Microspheres in Sheep Kidney and Uterus Embolization Models," vol. 22, no. 2, pp. 220-228, 2011, doi: 10.1016/j.jvir.2010.10.021.

[119] G. Bonomo *et al.*, "Bland embolization in patients with unresectable hepatocellular carcinoma using precise, tightly size-calibrated, anti-inflammatory microparticles: first clinical experience and one-year follow-up," *Cardiovasc Intervent Radiol,* vol. 33, no. 3, pp. 552-9, Jun 2010, doi: 10.1007/s00270-009-9752-y.

[120] U. Stampfl *et al.*, "Experimental Liver Embolization with Four Different Spherical Embolic Materials: Impact on Inflammatory Tissue and Foreign Body Reaction," *CardioVascular and Interventional Radiology,* vol. 32, no. 2, pp. 303-312, 2009, doi: 10.1007/s00270-008-9495-1.

[121] A. Medsinge, A. Zajko, P. Orons, N. Amesur, and E. Santos, "A case-based approach to common embolization agents used in vascular interventional radiology," *AJR Am J Roentgenol,* vol. 203, no. 4, pp. 699-708, Oct 2014, doi: 10.2214/AJR.14.12480.

[122] J. Doucet *et al.*, "Advances in Degradable Embolic Microspheres: A State of the Art Review," *J Funct Biomater,* vol. 9, no. 1, Jan 26 2018, doi: 10.3390/jfb9010014.

[123] T. Health, "Geniculate Artery Embolization: Interventional Radiologists Qualitative Research Report," Philadelphia, 2019.

[124] S. K. Gupta and R. P. Nayak, "Off-label use of medicine: Perspective of physicians, patients, pharmaceutical companies and regulatory authorities," *J Pharmacol Pharmacother,* vol. 5, no. 2, pp. 88-92, Apr 2014, doi: 10.4103/0976-500X.130046.

[125] *Biological evaluation of medical devices — Part 1: Evaluation and testing within a risk management process, ISO 10993-1*, 2018.

[126] S. Kehoe, S. Amensag, M. Looney, R. J. Abraham, and D. Boyd, ""Imageable" Zinc-Silicate Glass Microspheres For Transarterial Embolization: A Renal Artery Embolization Study," *Biomedical glasses,* vol. 1, no. 1, 2015, doi: 10.1515/bglass-2015-0007.

[127] R. J. Owen, P. N. Nation, R. Polakowski, J. A. Biliske, P. B. Tiege, and I. J. Griffith, "A Preclinical Study of the Safety and Efficacy of Occlusin™ 500 Artificial Embolization Device in Sheep," vol. 35, no. 3, pp. 636-644, 2012, doi: 10.1007/s00270-011-0218-7.

[128] M. Caine, D. Carugo, X. Zhang, M. Hill, M. R. Dreher, and A. L. Lewis, "Review of the Development of Methods for Characterization of Microspheres for Use in Embolotherapy: Translating Bench to Cathlab," *Advanced Healthcare Materials,* vol. 6, no. 9, p. 1601291, 2017, doi: 10.1002/adhm.201601291.

[129] *Sterilization of health care products — Radiation — Part 2: Establishing the sterilization dose, ISO 11137-2*, 2012.

[130] *Sterilization of health care products — Radiation — Part 1: Requirements for development, validation and routine control of a sterilization process for medical devices, ISO 11137-1*, 2006.

[131] *ICH Q3D. ICH guideline Q3D (R1) on elemental impurities*, 2019. [Online]. Available: https://www.ema.europa.eu/en/documents/scientific-guideline/international-conference-harmonisation-technical-requirements-registration-pharmaceuticals-human-use_en-21.pdf

[132] S. Kehoe, E. Tonkopi, R. J. Abraham, and D. Boyd, "Predicting the thermal responses and radiopacity of multicomponent zinc–silicate bioglasses: A focus on ZnO, La2O3, SiO2 and TiO2," *Journal of Non-Crystalline Solids,* vol. 358, no. 23, pp. 3388-3395, 2012, doi: https://doi.org/10.1016/j.jnoncrysol.2012.08.024.

[133] N. Maeda *et al.*, "Targeting and Recanalization after Embolization with Calibrated Resorbable Microspheres versus Hand-cut Gelatin Sponge Particles in a Porcine Kidney Model," *Journal of Vascular and Interventional Radiology,* vol. 24, no. 9, pp. 1391-1398, 2013, doi: 10.1016/j.jvir.2013.05.058.

[134] V. Verret *et al.*, "A Novel Resorbable Embolization Microsphere for Transient Uterine Artery Occlusion: A Comparative Study with Trisacryl-Gelatin Microspheres in the Sheep Model," vol. 25, no. 11, pp. 1759-1766, 2014, doi: 10.1016/j.jvir.2014.06.025.

[135] R. Duran *et al.*, "A Novel Inherently Radiopaque Bead for Transarterial Embolization to Treat Liver Cancer - A Pre-clinical Study," *Theranostics,* vol. 6, no. 1, pp. 28-39, 2016, doi: 10.7150/thno.13137.

[136] R. Pow, B. Fritsch, R. Waugh, and C. Rogan, "Endovascular management of recurrent hemarthrosis of the knee: a case series," *CVIR Endovasc,* vol. 3, no. 1, p. 43, Aug 30 2020, doi: 10.1186/s42155-020-00135-0.

[137] M. S. Hasan, U. Werner-Zwanziger, and D. Boyd, "Composition-structure-properties relationship of strontium borate glasses for medical applications," vol. 103, no. 7, pp. 2344-2354, 2015, doi: 10.1002/jbm.a.35361.

[138] A. C. Wright, "My Borate Life: An Enigmatic Journey," *International Journal of Applied Glass Science,* vol. 6, no. 1, pp. 45-63, 2015, doi: 10.1111/ijag.12113.

[139] A. K. Varshneya, *Fundamentals of inorganic glasses.* . Geneva: Academic Press Limited, 1994.

[140] J. L. George and R. K. Brow, "In-situ characterization of borate glass dissolution kinetics by μ-Raman spectroscopy," *Journal of Non-Crystalline Solids,* vol. 426, pp. 116-124, 2015, doi: 10.1016/j.jnoncrysol.2015.07.003.

[141] J. Biscoe and B. E. Warren, "X-RAY DIFFRACTION STUDY OF SODA-BORIC OXIDE GLASS *," *Journal of the American Ceramic Society,* vol. 21, no. 8, pp. 287-293, 1938, doi: 10.1111/j.1151-2916.1938.tb15777.x.

[142] A. R. Boccaccini, D. S. Brauer, and L. H. Hupa, *Introduction to the structure of silicate, phosphate and borate glasses.* (Bioactive glasses: Fundamentals, technology and applications). Cambridge: Royal Society of Chemistry, 2016.

[143] Q. Fu, M. N. Rahaman, H. Fu, and X. Liu, "Silicate, borosilicate, and borate bioactive glass scaffolds with controllable degradation rate for bone tissue engineering applications. I. Preparation and in vitro degradation," *Journal of Biomedical Materials Research Part A,* vol. 95A, no. 1, pp. 164-171, 2010, doi: 10.1002/jbm.a.32824.

[144] M. Ouis, A. Abdelghany, and H. Elbatal, "Corrosion mechanism and bioactivity of borate glasses analogue to Hench's bioglass," *Processing and Application of Ceramics,* vol. 6, no. 3, pp. 141-149, 2012, doi: 10.2298/pac1203141o.

[145] A. Yao, D. Wang, W. Huang, Q. Fu, M. N. Rahaman, and D. E. Day, "In Vitro Bioactive Characteristics of Borate-Based Glasses with Controllable Degradation Behavior," *Journal of the American Ceramic Society,* vol. 90, no. 1, pp. 303-306, 2007, doi: 10.1111/j.1551-2916.2006.01358.x.

[146] Y. D. Yiannopoulos, G. D. Chryssikos, and E. I. Kamitsos, "Structure and properties of alkaline earth borate glasses," *Phys. Chem. Glasses,* vol. 42, no. 3, pp. 164-172, 2001. [Online]. Available: https://www.ingentaconnect.com/content/sgt/pcg/2001/00000042/00000003/4203164.

[147] H. Doweidar, "Consideration of the boron oxide anomaly," vol. 25, no. 1, pp. 253-258, 1990, doi: 10.1007/bf00544216.

[148] K. Macdonald, M. A. Hanson, and D. Boyd, "Modulation of strontium release from a tertiary borate glass through substitution of alkali for alkali earth oxide," vol. 443, pp. 184-191, 2016, doi: 10.1016/j.jnoncrysol.2016.04.024.

[149] D. Fortin and M. A. Vargas, "The spectrum of composites: new techniques and materials," *The Journal of the American Dental Association,* vol. 131, pp. 26S-30S, 2000, doi: 10.14219/jada.archive.2000.0399.

[150] L. Tian, L. Lu, J. Feng, and M. P. Melancon, "Radiopaque nano and polymeric materials for atherosclerosis imaging, embolization and other catheterization procedures," *Acta Pharmaceutica Sinica B,* vol. 8, no. 3, pp. 360-370, 2018, doi: 10.1016/j.apsb.2018.03.002.

[151] S. Ni, R. Du, and S. Ni, "The Influence of Na and Ti on the In Vitro Degradation and Bioactivity in 58S Sol-Gel Bioactive Glass," vol. 2012, pp. 1-7, 2012, doi: 10.1155/2012/730810.

[152] M. Al Qaysi *et al.*, "Strontium- and calcium-containing, titanium-stabilised phosphate-based glasses with prolonged degradation for orthopaedic tissue engineering," vol. 30, no. 3, pp. 300-310, 2015, doi: 10.1177/0885328215588898.

[153] "Density of Elements Chart. Angstrom Sciences, https://www.angstromsciences.com/density-elements-chart (accessed Oct. 5, 2020)." (accessed.

[154] H. Doweidar, G. M. El-Damrawi, Y. M. Moustafa, and R. M. Ramadan, "Density of Mixed Alkali Borate Glasses: A Structural Analysis," *Physica B Condensed Matter,* vol. 362, no. 1-4, pp. 123-132, May 2005, doi: 10.1016/j.physb.2005.02.001.

[155] S. Kojima, "Mixed-Alkali Effect in Borate Glasses: Thermal, Elastic, and Vibrational Properties," *Solids,* vol. 1, no. 1, pp. 16-30, 2020, doi: https://doi.org/10.3390/solids1010003.

[156] J. Zhong and P. J. Bray, "Change in boron coordination in alkali borate glasses, and mixed alkali effects, as elucidated by NMR," *Journal of Non-Crystalline Solids,* vol. 111, no. 1, pp. 67-76, 1989, doi: 10.1016/0022-3093(89)90425-0.

[157] N. P. Lower *et al.*, "Physical properties of alkaline-earth and alkali borate glasses prepared over an extended range of compositions," *Journal of Non-Crystalline Solids,* vol. 293-295, pp. 669-675, 2001, doi: 10.1016/S0022-3093(01)00768-2.

[158] A. Vegiri, C.-P. E. Varsamis, and E. I. Kamitsos, "Molecular dynamics investigation of mixed-alkali borate glasses: Short-range order structure and alkali-ion environments," *Physical Review B,* vol. 80, no. 18, p. 184202, 2009, doi: 10.1103/PhysRevB.80.184202.

[159] E. I. Kamitsos, Y. D. Yiannopoulos, C. P. Varsamis, and H. Jain, "Structure-property correlation in glasses by infrared reflectance spectroscopy," *Journal of Non-Crystalline Solids,* vol. 222, pp. 59-68, 1997, doi: https://doi.org/10.1016/S0022-3093(97)90097-1.

[160] Z. Ding *et al.*, "Topological understanding of the mixed alkaline earth effect in glass," *Journal of Non-Crystalline Solids,* vol. 527, p. 119696, 2020, doi: 10.1016/j.jnoncrysol.2019.119696.

[161] M. Bengisu, "Borate glasses for scientific and industrial applications: a review," *Journal of Materials Science* vol. 51, no. 5, pp. 2199-2242, 2016, doi: 10.1007/s10853-015-9537-4.

[162] A. C. Profeta and C. Huppa, "Bioactive-glass in Oral and Maxillofacial Surgery," *Craniomaxillofac Trauma Reconstruction,* vol. 9, no. 1, pp. 1-14, 2016, doi: http://dx.doi.org/10.1055/s-0035-1551543.

[163] T. Mehrabi, A. S. Mesgar, and Z. Mohammadi, "Bioactive glasses: a promising therapeutic ion release strategy for enhancing wound healing," *ACS Biomaterials Science & Engineering,* vol. 6, no. 10, pp. 5399-5430, 2020, doi: https://dx.doi.org/10.1021/acsbiomaterials.0c00528.

[164] I. Izquierdo-Barba, A. J. Salinas, and M. Vallet-Regí, "Bioactive glasses: from macro to nano," *International Journal of Applied Glass Science,* vol. 4, no. 2, pp. 149-161, 2013, doi: 10.1111/ijag.12028.

[165] M. T. Mubarak, I. Ozsahin, and D. U. Ozsahin, "Evaluation of Sterilization Methods for Medical Devices," *Advances in Science and Engineering Technology International Conferences (ASET),* pp. 1-4, 2019, doi: 10.1109/ICASET.2019.8714223.

[166] N. P. Tipnis and D. J. Burgess, "Sterilization of implantable polymer-based medical devices: A review," *International Journal of Pharmaceutics,* vol. 544, no. 2, pp. 455-460, 2018, doi: 10.1016/j.ijpharm.2017.12.003.

[167] P. J. Bray and J. G. O'Keefe, "Nuclear Magnetic Resonance Investigations of the Structure of Alkali Borate Glasses," *Phys. Chem. Glasses,* vol. 4, no. 2, pp. 37-46, 1963.

[168] K. O'Connell, M. Hanson, H. O'Shea, and D. Boyd, "Linear release of strontium ions from high borate glasses via lanthanide/alkali substitutions," *Journal of Non-Crystalline Solids,* vol. 430, pp. 1-8, 2015, doi: 10.1016/j.jnoncrysol.2015.09.017.

[169] *ASTM Standard E1356, 2014, "Standard Test Method for Assignment of the Glass Transition Temperatures by Differential Scanning Calorimetry," ASTM International*, A. S. E1356, West Conshohocken, PA, 2014, 2014.

[170] D. Boyd, S. Murphy, M. R. Towler, A. W. Wren, and S. Hayakawa, "Analysis of γ-irradiated synthetic bone grafts by 29Si MAS-NMR spectroscopy, calorimetry and XRD," *Journal of Non-Crystalline Solids,* vol. 355, no. 45-47, pp. 2285-2288, 2009, doi: 10.1016/j.jnoncrysol.2009.07.014.

[171] Subhashini, H. D. Shashikala, and N. K. Udayashankar, "Investigation of mixed alkali effect on mechanical, structural and thermal properties of three-alkali borate glass system," *Journal of Alloys and Compounds,* vol. 658, pp. 996-1002, 2016, doi: 10.1016/j.jallcom.2015.11.014.

[172] A. Li, M. Wang, M. Li, Z. Liu, Y. Hu, and X. Zhang, "The effect of mixed alkali on structural changes and ionic migration characteristics in zinc borate glasses," *Materials Chemistry and Physics,* vol. 217, pp. 519-526, 2018, doi: 10.1016/j.matchemphys.2018.07.013.

[173] J. E. Shelby, *"Structural Models for Borate Glasses," in Introduction to Glass Science and Technology, 2nd ed.* Cambridge: Royal Society of Chemistry, 2005.

[174] Y. Tokuda *et al.*, "Local structure of alkalis in mixed-alkali borate glass to elucidate the origin of mixed-alkali effect," *Journal of Asian Ceramic Societies,* vol. 3, no. 4, pp. 412-416, 2015, doi: 10.1016/j.jascer.2015.09.002.

[175] P. K. Gupta and J. C. Mauro, "Composition dependence of glass transition temperature and fragility. I. A topological model incorporating temperature-dependent constraints," *The Journal of Chemical Physics,* vol. 130, no. 9, p. 094503, 2009, doi: 10.1063/1.3077168.

[176] M. M. Smedskjaer, J. C. Mauro, R. E. Youngman, C. L. Hogue, M. Potuzak, and Y. Yue, "Topological Principles of Borosilicate Glass Chemistry," *The Journal of Physical Chemistry B,* vol. 115, no. 44, pp. 12930-12946, 2011, doi: 10.1021/jp208796b.

[177] J. C. Mauro, P. K. Gupta, and R. J. Loucks, "Composition dependence of glass transition temperature and fragility. II. A topological model of alkali borate liquids," *The Journal of Chemical Physics,* vol. 130, no. 23, p. 234503, 2009, doi: 10.1063/1.3152432.

[178] F. Berkemeier, S. Voss, Á. W. Imre, and H. Mehrer, "Molar volume, glass-transition temperature, and ionic conductivity of Na- and Rb-borate glasses in comparison with mixed Na–Rb borate glasses," *Journal of Non-Crystalline Solids,* vol. 351, no. 52-54, pp. 3816-3825, Dec 2005, doi: 10.1016/j.jnoncrysol.2005.10.010.

[179] C. Fild, D. F. Shantz, R. F. Lobo, and H. Koller, "Cation-induced transformation of boron-coordination in zeolites," *Physical Chemistry Chemical Physics,* vol. 2, no. 13, pp. 3091-3098, 2000, doi: 10.1039/b002134m.

[180] S.-J. Hwang, C.-Y. Chen, and S. I. Zones, "Boron Sites in Borosilicate Zeolites at Various Stages of Hydration Studied by Solid State NMR Spectroscopy," *The Journal of Physical Chemistry B,* vol. 108, no. 48, pp. 18535-18546, 2004, doi: 10.1021/jp0476904.

[181] R. de Ruiter, A. P. M. Kentgens, J. Grootendorst, J. C. Jansen, and H. van Bekkum, "Calcination and deboronation of [B]-MFI single crystals," *Zeolites,* vol. 13, no. 2, pp. 128-138, 1993, doi: 10.1016/0144-2449(93)90072-B.

[182] H. Othman *et al.*, "Spectroscopic study of the role of alkaline earth oxides in mixed borate glasses - site basicity, polarizability and glass structure," *Journal of Non-Crystalline Solids,* vol. 533, p. 119892, 2020, doi: 10.1016/j.jnoncrysol.2020.119892.

[183] N. Mascaraque, K. Januchta, K. F. Frederiksen, R. E. Youngman, M. Bauchy, and M. M. Smedskjaer, "Structural dependence of chemical durability in modified aluminoborate glasses," *Journal of the American Ceramic Society,* vol. 102, no. 3, pp. 1157-1168, 2019, doi: 10.1111/jace.15969.

[184] M. S. Gaafar, S. Y. Marzouk, H. A. Zayed, L. I. Soliman, and A. H. Serag El-Deen, "Structural studies and mechanical properties of some borate glasses doped with different alkali and cobalt oxides," *Current Applied Physics,* vol. 13, no. 1, pp. 152-158, 2013, doi: 10.1016/j.cap.2012.07.007.

[185] S. Kapoor, H. Bola George, A. Betzen, M. Affatigato, and S. Feller, "Physical properties of barium borate glasses determined over a wide range of compositions," *Journal of Non-Crystalline Solids,* vol. 270, no. 1-3, pp. 215-222, 2000, doi: 10.1016/S0022-3093(00)00061-2.

[186] M. A. Marzouk, F. H. ElBatal, W. H. Eisa, and N. A. Ghoneim, "Comparative spectral and shielding studies of binary borate glasses with the heavy metal oxides SrO, CdO, BaO, PbO or Bi2O3 before and after gamma irradiation," *Journal of Non-Crystalline Solids,* vol. 387, pp. 155-160, 2014, doi: 10.1016/j.jnoncrysol.2014.01.002.

[187] N. A. El-Alaily, F. M. Ezz-Eldin, and H. A. El-Batal, "Durability of some Gamma-Irradiated Alkali Borate Glasses," *Radiation Physics and Chemistry,* vol. 44, no. 1-2, pp. 45-51, 1994, doi: https://doi.org/10.1016/0969-806X(94)90101-5.

[188] N. A. El-Alaily and R. M. Mohamed, "Effect of irradiation on some optical properties and density of lithium borate glass," *Materials Science and Engineering: B,* vol. 98, no. 3, pp. 193-203, 2003, doi: 10.1016/s0921-5107(02)00587-1.

[189] R. Kaur, S. Singh, and O. P. Pandey, "FTIR structural investigation of gamma irradiated BaO–Na2O–B2O3–SiO2 glasses," *Physica B Condensed Matter,* vol. 407, no. 24, pp. 4765-4769, 2012, doi: 10.1016/j.physb.2012.08.031.

[190] D. J. Hunter and S. Bierma-Zeinstra, "Osteoarthritis," *The Lancet,* vol. 393, no. 10182, pp. 1745-1759, 2019, doi: 10.1016/S0140-6736(19)30417-9.

[191] J. Doucet, K. MacDonald, C. Lee, R. A. Hana, G. Soulez, and B. Boyd, "The feasibility of degradable glass microspheres as transient embolic medical devices," *Journal of Biomaterials Applications,* vol. 35, no. 6, pp. 615-632, 2021, doi: 10.1177/0885328220944871.

[192] S. Kehoe *et al.*, "Effects of γ-irradiation and accelerated aging on composition-structure–property relationships for radiopaque embolic microspheres," *Journal of Non-Crystalline Solids,* vol. 402, pp. 84-90, 2014, doi: https://doi.org/10.1016/j.jnoncrysol.2014.05.016.

[193] A. L. Lewis *et al.*, "Comparative in vitro evaluation of microspherical embolisation agents," *Journal of Materials Science: Materials in Medicine,* vol. 17, no. 12, pp. 1193-1204, 2006, doi: 10.1007/s10856-006-0592-x.

[194] A. H. Negussie *et al.*, "Synthesis, characterization, and imaging of radiopaque bismuth beads for image-guided transarterial embolization," *Scientific Reports,* vol. 11, no. 1, p. 533, 2021, doi: 10.1038/s41598-020-79900-z.

[195] K. Ashrafi *et al.*, "Characterization of a novel intrinsically radiopaque Drug-eluting Bead for image-guided therapy: DC Bead LUMI^{TM}," *Journal of Controlled Release,* vol. 250, pp. 36-47, 2017, doi: 10.1016/j.jconrel.2017.02.001.

[196] K. V. Sharma *et al.*, "Development of "Imageable" beads for transcatheter embolotherapy," *Journal of Vascular and Interventional Radiology,* vol. 21, no. 6, pp. 865-876, 2010, doi: 10.1016/j.jvir.2010.02.031.

[197] J. Hu *et al.*, "Advances in Biomaterials and Technologies for Vascular Embolization," *Advanced Materials,* vol. 31, no. 33, p. 1901071, 2019, doi: 10.1002/adma.201901071.

[198] C. G. Johnson *et al.*, "Preparation of Radiopaque Drug-Eluting Beads for Transcatheter Chemoembolization," *Journal of Vascular and Interventional Radiology,* vol. 27, no. 1, pp. 117-126.e3, 2016, doi: 10.1016/j.jvir.2015.09.011.

[199] M. M. Kawano, I. L. Araujo, M. C. Castro, and M. A. Matos, "Assessment of quality of life in patients with knee osteoarthritis," *Acta Ortop Bras,* vol. 23, no. 6, pp. 307-10, Nov-Dec 2015, doi: 10.1590/1413-785220152306150596.

[200] G. Zhang, M. Wang, F. Duan, K. Yuan, J. Yan, and Z. Chang, "Early- and intermediate-term outcome of transarterial embolization for symptomatic hepatic focal nodular hyperplasia," *Journal of Interventional Medicine,* vol. 1, no. 2, pp. 86-91, 2018, doi: https://doi.org/10.19779/j.cnki.2096-3602.2018.02.05.

[201] C. M. Phan *et al.*, "MR imaging findings in the follow-up of patients with different stages of knee osteoarthritis and the correlation with clinical symptoms," *European Radiology,* vol. 16, pp. 608-618, 2006, doi: https://doi.org/10.1007/s00330-005-0004-5.

[202] M. Shymka, "A Toxicological Risk Assessment (TRA): Examining the Toxicological Hazards of the Inorganic Components of a Degradable Microsphere for Genicular Artery Embolization," BSc Honours Thesis, Medical Sciences, Dalhousie University, Halifax, NS, 2021.

[203] *Biological evaluation of medical devices - Part 1: Evaluation and testing within a risk managment process, ISO 10993-1*, 2020.

[204] U.S. Food and Drug Administration. (2004). *Class II special controls guidance document: vascular and neurovascular embolization devices – guidance for industry and FDA staff*. [Online] Available: www.fda.gov/regulatory-information/search-fda-guidancedocuments/class-ii-special-controls-guidance-document-vascular-and-neurovascular-embolization-devices-guidance

APPENDIX A

This appendix is included in this thesis work to provide users with the calculations (mol% to gram) and the mass (g) of each reagent for all BKSA1-16 compositions characterized in this work.

BKSA	Mol% B_2O_3	Mol% K_2O	Mol% SrO	1/3 mole B_2O_3 (g)	1/3 mole K_2CO_3 (g)	1/3 mole $SrCO_3$ (g)
1	69.00	30.00	1.00	15.85	13.68	0.49
2	75.79	8.74	15.47	17.41	3.99	7.53
3	90.00	8.28	1.73	20.68	3.77	0.84
4	83.55	15.45	1.00	19.20	7.05	0.49
5	69.00	15.53	15.47	15.85	7.09	7.53
6	69.00	1.00	30.00	15.85	0.46	14.62
7	69.00	15.53	15.47	15.85	7.09	7.53
8	83.55	15.45	1.00	19.20	7.05	0.49
9	79.37	1.00	19.63	18.23	0.46	9.57
10	79.37	1.00	19.63	18.23	0.46	9.57
11	69.00	8.24	22.76	15.85	3.76	11.09
12	69.00	1.00	30.00	15.85	0.46	14.62
13	69.00	30.00	1.00	15.85	13.68	0.49
14	82.72	8.93	8.35	19.00	4.07	4.07
15	90.00	1.00	9.00	20.68	0.46	4.38
16	73.91	20.40	5.69	16.98	9.30	2.77

Figure A.1: Calculation from mol% to gram for boron, potassium and strontium in each composition. Molecular weights used for the calculation are B_2O_3 69.62 g/mol, K_2CO_3 138.205 g/mol, and $SrCO_3$ 147.63 g/mol.

APPENDIX B

The following data is being provided for completeness of the residual mass data (seen in chapter 4) and provides the model and data for residual mass in contrast media at 2 hrs.

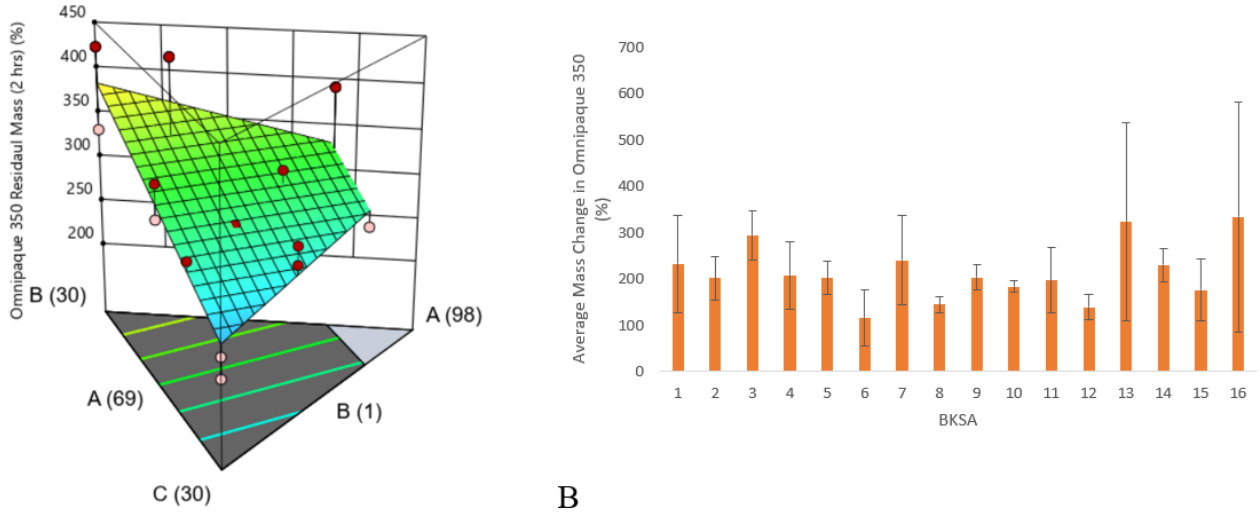

Figure A.2. (A) A contour plot displaying residual mass in 100% contrast media at 2 hrs for varying mol% B_2O_3, K_2O, and SrO. As seen in the plot 'A', 'B', and 'C' signifies the mol% of B_2O_3, K_2O, and SrO respectively. (B) A bar graph displaying the average mass change for each BKSA glass composition in 100% Omnipaque 350 for 2 hrs. A positive value for average mass change represents a gain in mass from the original mass weighed.

APPENDIX C

The following data is being included as it was excluded from chapter 4; however, demonstrates the average mass loss of BKSA16 in two physiologically representative media and provides completeness to the residual mass/mass loss data in this thesis work. Mass loss was assessed in two physiologically representative media in (100% bovine calf serum (BCS) and 10% BCS/90% Dulbecco's Modified Eagle Medium (DMEM)) to assess which media is most representative of *in vivo* mass loss and to gain insight into the anticipated dissolution behaviour of BKSA16 *in vivo* as seen in Figure A.3. Data for the dissolution (residual mass) of the BKSA16 irregular particles at 72 hrs in 10% BCS/90% DMEM is also reported in chapter four [1].

Methods

A preferred glass (BKSA16) was assessed for mass loss in two physiologically representative media; (i) 10 mL of 100% BCS and (ii) 10 mL of 10% BCS/90% DMEM (Sigma Aldrich, USA) at 0.25, 1, 12, 24, 36, 72 hrs. To assess mass loss, 0.1 g of BKSA16 (100-300 μm) was placed into individual Corning® 15 ml centrifuge tubes (n=3 per media) [1]. The falcon tubes were then placed into a shaking incubator at 120 RPM and 37 °C for 2 hrs. Following incubation, the falcon tubes were then immediately centrifuged at 3.0 RCF / 4.4 RPM for 15 mins. The supernatant was then decanted from the pellet, and the original test tube with the pellet was then dried at 50 °C for 96 hrs. Following drying, the tube with the pellet was then weighed to determine the mass loss [1].

Results

BKSA16 was selected for mass loss evaluations in simulated physiological media. Mass loss for this composition in 100% BCS and 10% BCS/90% DMEM are provided in Figure A.3. Complete mass loss of BKSA16 was not observed in either media at 72 hrs.

Discussion

Following the selection of BKSA16, dissolution in 100% BCS and 10% BCS/90% DMEM was conducted to better characterize the dissolution behaviour of the glass *in vivo*. Mass loss was lower in 100% BCS (Fig. A.3A) at all time points compared to 10% BCS/90% DMEM (Fig. A.3B). These results are anticipated due to the higher protein content in the 100% BCS which may increase the number of

available proteins to interact and absorb to the surface of the particles. As such these protein interactions may lead to reduced dissolution rates *(short-term)* of the glass by reducing the wear due to friction [2] and/or by acting as a barrier to hydrolysis/hydration of the glass network. BKSA16 did not achieve 100% mass loss in <72 hrs in either media however, as discussed in Manchester *et al*. [1] benchtop models in the literature have overestimated mass loss observed *in situ* [3], [4]. As such, future *in vivo* work is required to (i) confirm 100% mass loss of BKSA16 in <72 hrs and (ii) identify which media is most representative of *in vivo* conditions however, it is likely complete dissolution of BKSA16 will occur in <72 hrs *in vivo*.

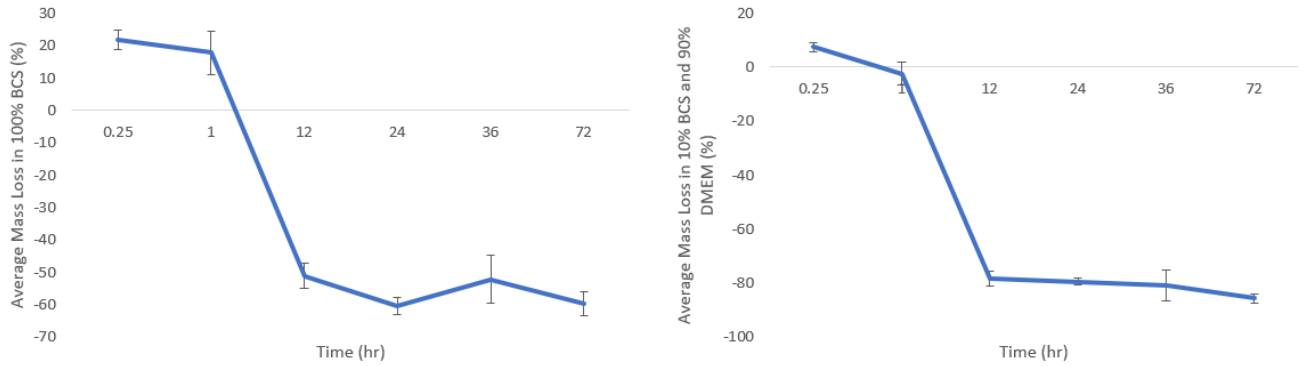

A B

Figure A.3. (A) A line graph displaying the average mass loss for BKSA16 in 100% CBS at 0.25, 1, 12, 24, 36, and 72 hrs. (B) A line graph displaying the average mass loss for BKSA16 in 10% CBS and 90% DMEM 0.25, 1, 12, 24, 36, and 72 hrs. A positive average mass loss value represents a gain in mass and a negative average mass loss represents a loss in mass from the original mass weighed.

References

[1] R. A. Manchester, T. Z. Todorova, E. Tonkopi, B. Kelly, J. Gosse, C. Davis, K. Brewer, M. Shymka, and D. Boyd, "Dissolution Behaviour and Imageability of Ternary Borate Glasses for use in Geniculate Artery Embolization," *under review Discover Materials*.

[2] Y. S. Hedberg, "Role of proteins in the degradation of relatively inert alloys in the human body," *Npj Mater. Degrad.*, vol. 2, no. 1, p. 26, Dec. 2018, doi: 10.1038/s41529-018-0049-y.

[3] J. Doucet *et al.*, "Multi-modal imageability and degradation characteristics of high-borate glass systems for transient embolization," *J. Non-Cryst. Solids*, vol. 510, pp. 26–35, Apr. 2019, doi: 10.1016/j.jnoncrysol.2019.01.014.

[4] J. Doucet, K. MacDonald, C. Lee, R. A. Hana, G. Soulez, and D. Boyd, "The feasibility of degradable glass microspheres as transient embolic medical devices," *J. Biomater. Appl.*, vol. 35, no. 6, pp. 615–632, Jan. 2021, doi: 10.1177/0885328220944871.

APPENDIX D

Both models and data for R1 and R2* slope are included in this work for completeness as they were evaluated and are important preliminary inputs regarding MRI imageability of the BKSA16 irregular particles. The R1 and R2* models produced from the MRI findings were not statistically significant (within DoM) and as such this data was excluded for publication (seen in chapter 4). Below outlines the methods, results, and discussion of the R1 and R2* MRI findings.

Methods

To determine MRI susceptibility for each composition (100-300 μm) the materials were dispersed in a non-aqueous gel made with 1% Evonik Intelimer IPA 13-1 NG polymer in peanut oil (2, 4, 6, 8, 10% w/w, n=5) [1]. After which, 5 mm tubes were used to hold the gels. The gels were then subjected to horizontal rotation, magnetic stirring, and heating and then solidified by cooling on ice. Using an Agilent 3T preclinical MRI, each composition was measured at room temperature to obtain both R2* (spectral linewidth) and R1 (arrayed inversion recovery) MRI relaxometry measurements. To provide values for the particles, an extrapolation to 100% volume fraction and a linear regression analysis was employed [1][2].

Results

Analysis of R1 slope for MRI demonstrated a non-statistically significant linear model (Model F-value: 3.47, Lack of Fit F-value: 1.12, R^2: 0.3482, Adjusted R^2: 0.2480, Predicted R^2: 0.0009, C.V. %: 48.34), with slope values which ranged from -0.2025 to 4.565. While the model is not statistically significant the relationship demonstrated among the factors, which may indicate an important role on increasing radiopacity, is indicated for R1 slope as follows K>Sr>B.

Lastly, the R2* model was assessed and shown to produce a non-statistically significant linear model (Model F-value: 3.88, Lack of Fit F-value: 0.39, R^2: 0.3736, Adjusted R^2: 0.2773, Predicted R^2: 0.0875, C.V. %: 45.81), with slope values which ranged from 748.78 to 5177.5. Analysis of the coefficients for R2* slope indicates the ranking of factors for increased slope as follows Sr>B>K. The ΔX was measured for all samples, however, for half the samples the signal was too weak to measure, and the data is not reported. BKSA3, 7, 8, 14, and 15 were found to be diamagnetic and BKSA6, 9, 11 were found to be paramagnetic.

Discussion

Each of the 16 compositions was assessed for MRI R_1 and R_2* relaxivity. From the data it appears that none of the BKSA compositions have significant R_1 effects. As such, no singular compositions will not be visible on T_1 scans and physicians will be able to examine ligaments and tissues without interference from the particles. For R_2*-weighted scans, the particles were shown to have moderate R_2* contrast (with BKSA6, 10, 12, and 15 exhibiting the strongest R_2* contrast) and may be detectable using a specialized gradient-echo sequence. Yet, within the vasculature the iron content in the blood may overwhelm the contrast from the particles and as a result the particles may not be visible within the blood. Therefore, further studies are required to analyze the visibility of the microspheres within the blood for R_2*-weighted sequences. Additionally, the ΔX values were assessed for each BKSA composition. The ΔX values indicate that the particles are only "mild" perturbers and as a result will not perturb the magnetic field in any strong faction. It is also important to note that half of the samples (BKSA1, 2, 4, 5, 10, 12, 13, 16) were too weak to measure their ΔX value and as a result remain inconclusive. Some of the ΔX values were unattainable and this may be due to the limited volume fraction range utilized (in this work 0-10% was used) and as a result, a larger volume fraction range may have provided more concise values.

Table A.1: Slope values for R_1, R_2*, and ΔX for each BKSA composition.

Composition	R_1	R_2*	ΔX
BKSA1	3.735	1116.7	*
BKSA2	3.29	3098.8	*
BKSA3	3.91	1873.7	-6.755
BKSA4	1.685	748.78	*
BKSA5	4.565	2672.7	*
BKSA6	1.185	3678.1	3.05
BKSA7	2.825	829.52	-4.825
BKSA8	3.575	1240.1	-8.67
BKSA9	1.6075	1404.1	6.575
BKSA10	-0.2025	5177.5	*
BKSA11	2.125	2955	4.77
BKSA12	2.645	3521.7	*
BKSA13	3.195	2210	*
BKSA14	1.185	1212.4	-4.205
BKSA15	0.5125	3911	-9.73
BKSA16	2.195	2419.8	*

*Indicates the sample was too weak to measure

References

[1] R. A. Manchester, T. Z. Todorova, E. Tonkopi, B. Kelly, J. Gosse, C. Davis, K. Brewer, M. Shymka, and D. Boyd, "Dissolution Behaviour and Imageability of Ternary Borate Glasses for use in Geniculate Artery Embolization," *under review Discover Materials*.

[2] J. Doucet *et al.*, "Multi-modal imageability and degradation characteristics of high-borate glass systems for transient embolization," *J. Non-Cryst. Solids*, vol. 510, pp. 26–35, Apr. 2019, doi: 10.1016/j.jnoncrysol.2019.01.014.

APPENDIX E

This figure is incorporated to illustrate the genicular arteries within the knee. These arteries may supply an hypervascular blush (abnormal angiogenesis and perivascular nerves) which are ‘pruned’ or targeted through geniculate artery embolization.

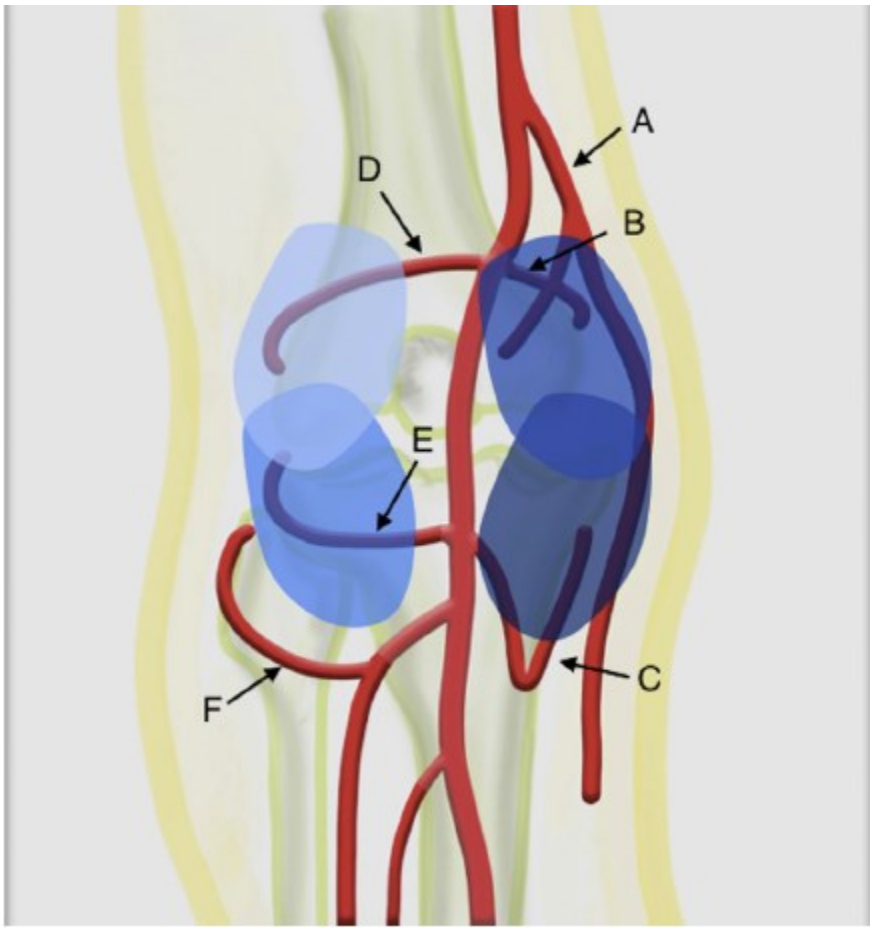

Figure A.4. Image depicting the genicular arteries located in the knee where the corresponding genicular arteries are a) descending, b) superior medial, c) inferior medial, d) superior lateral, e) inferior lateral, and f) recurrent [1].

References

[1] S. Bagla, R. Piechowiak, T. Hartman, J. Orlando, D. D. Gaizo, and A. Isaacson, "Genicular Artery Embolization for the Treatment of Knee Pain Secondary to Osteoarthritis," *Journal of Vascular and Interventional Radiology,* vol. 31, no. 7, pp. 1096-1102, 2020, doi: 10.1016/j.jvir.2019.09.018.

APPENDIX F

Chapter 3 consists of an accepted publication in th Journal of Non-Crystalline Solids (doi: https://doi.org/10.1016/j.jnoncrysol.2021.120982) available online at https://www.sciencedirect.com/science/article/abs/pii/S0022309321003410?via%3Dihub with permission:

https://www.elsevier.com/about/policies/sharing

Article Sharing

Authors who publish in Elsevier journals can share their research in several ways. Researchers who have subscribed access to articles published by Elsevier can share too. There are some simple guidelines to follow, which vary depending on the article version you wish to share. Elsevier is a signatory to the STM Voluntary Principles for article sharing on Scholarly Collaboration Networks and a member of the Coalition for Responsible Sharing.

Preprint

- Authors can share their preprint anywhere at any time.
- If accepted for publication, we encourage authors to link from the preprint to their formal publication via its Digital Object Identifier (DOI). Millions of researchers have access to the formal publications on ScienceDirect, and so links will help your users to find, access, cite, and use the best available version.
- Authors can update their preprints on arXiv or RePEc with their accepted manuscript .

Please note:

- Some society-owned titles and journals that operate double-blind peer review have different preprint policies. Please check the journals Guide for Authors for further information.
- Preprints should not be added to or enhanced in any way in order to appear more like, or to substitute for, the final versions of articles.

Accepted Manuscript

Authors can share their accepted manuscript:

Immediately

- via their non-commercial personal homepage or blog
- by updating a preprint in arXiv or RePEc with the accepted manuscript
- via their research institute or institutional repository for internal institutional uses or as part of an invitation-only research collaboration work-group
- directly by providing copies to their students or to research collaborators for their personal use
- for private scholarly sharing as part of an invitation-only work group on commercial sites with which Elsevier has an agreement

After the embargo period

- via non-commercial hosting platforms such as their institutional repository
- via commercial sites with which Elsevier has an agreement

In all cases accepted manuscripts should:

- link to the formal publication via its DOI
- bear a CC-BY-NC-ND license – this is easy to do
- if aggregated with other manuscripts, for example in a repository or other site, be shared in alignment with our hosting policy
- not be added to or enhanced in any way to appear more like, or to substitute for, the published journal article

Published Journal Article

Policies for sharing published journal articles differ for subscription and gold open access articles:

Subscription articles